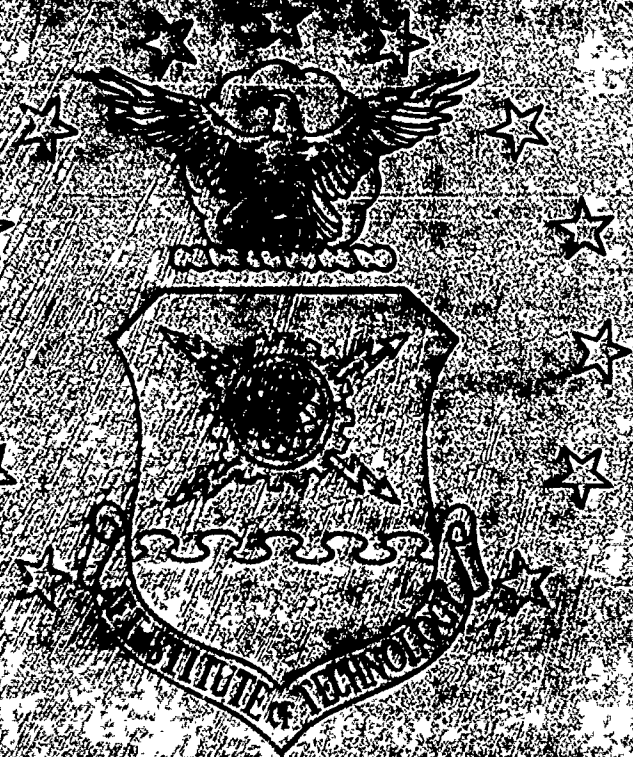


7

AD-A230 465



MULTI-INPUT MULTI-OUTPUT FLIGHT CONTROL
SYSTEM DESIGN FOR THE YF-16 USING
NONLINEAR QFT AND PILOT COMPENSATION

THESIS

Russel B. Miller, Second Lieutenant, USAF

AFIT/GE/ENG/90D-42

DISSEMINATION STATEMENT
Approved for public release
Distribution unlimited

DEPARTMENT OF THE AIR FORCE
AIR UNIVERSITY

AIR FORCE INSTITUTE OF TECHNOLOGY

Wright-Patterson Air Force Base, Ohio

91 1 3 147

AFIT/GE/ENG/90D-42

①

DTIC
ELECTE
JAN 08 1991
S D D

MULTI-INPUT MULTI-OUTPUT FLIGHT CONTROL
SYSTEM DESIGN FOR THE YF-16 USING
NONLINEAR QFT AND PILOT COMPENSATION

THESIS

Russel B. Miller, Second Lieutenant, USAF

AFIT/GE/ENG/90D-42

Approved for public release; distribution unlimited

**Best
Available
Copy**

AFIT/GE/ENG/90D-42

MULTI-INPUT MULTI-OUTPUT FLIGHT CONTROL
SYSTEM DESIGN FOR THE YF-16 USING NONLINEAR
QFT AND PILOT COMPENSATION

THESIS

Presented to the Faculty of the School of Engineering
of the Air Force Institute of Technology
Air University

In Partial Fulfillment of the
Requirements for the Degree of
Master of Science in Electrical Engineering

Russel B. Miller, B.S.E.E.
Second Lieutenant, USAF

December 1990

Approved for public release: distribution unlimited

Accession For	
NTIS CRA&I	<input checked="checked" type="checkbox"/>
DTIC TAB	<input type="checkbox"/>
Unannounced	<input type="checkbox"/>
Justification	
By	
Distribution /	
Availability Codes	
Dist	Avail and/or Special
A-1	



Preface

For reasons unrelated to the design techniques used in this thesis, the focus of the project was significantly redirected in the middle of the research quarter. Additionally, large amounts of time were required to develop new software (SISOTF and MIMOTF) and to modify existing software (YF-16 Simulator). These items placed severe time constraints on the design aspect of the project. As a result, some areas of the problem could not be examined in as much detail as would have been desired. The results of this thesis do, however, show that nonlinear QFT is a very effective Flight Control System design technique capable of providing effective first cut designs in a relatively short period of time.

This thesis is not intended to be a tutorial in QFT or flight control system design. It has been written to describe only the design of this thesis and how nonlinear QFT was used in the project. Although its intent is not to teach any of the methods, it has been written in a manner to significantly assist an individual attempting follow on work.

I would like to express my sincere thanks to all of the professionals of the AFIT faculty and the Flight Dynamics Lab for their guidance and support. Dr. Constantine H. Houppis, Dr. Issac Horowitz, and Mr. Finley Barfield among many others have been instrumental in the completion of this project. Appreciation is also extended to Mr. Tom Cord for his help with the nonlinear simulator. A special thanks to Dr. Horowitz for the "long distance" guidance and encouragement. My fellow QFT thesis students, Dave Wheaton and Ken Crosby were extremely helpful by staying far enough ahead of me to always clue me in on the next step. Most importantly, I would like to thank my wife Linda for her unending support, understanding and encouragement through all of the hills and valleys we have been through, and for putting her life and goals on hold for the past 18 months while we have worked through these trying times together. Also thanks to my kids, Amy, Pamela, Russel, and Raleigh for their patience.

Russel B. Miller

Table of Contents

	Page
Preface	ii
List of Figures	vi
List of Tables	x
Abstract	xi
I. Background	1-1
Introduction	1-1
Problem Statement	1-3
Review of Current Literature	1-4
Quantitative Feedback Theory	1-5
Pilot Modelling	1-8
Assumptions	1-10
Scope	1-11
Standards	1-11
Approach	1-11
Inner Loop Design	1-12
Pilot Compensation	1-12
Simulation	1-13
Documentation	1-13
Summary	1-14
II. Nonlinear QFT	2-1
Introduction	2-1
Overview of Quantitative Feedback Theory	2-1
Thumbprint Specifications	2-2
Equivalent Linear Time Invariant Plant Models	2-3
Nichols Chart	2-4
Plant Templates	2-4
Nominal Plant	2-5
Boundaries	2-5
Loop Transmission Synthesis	2-5
Prefilter	2-6
The 2x2 MIMO Problem	2-6
Summary	2-10
III. Equivalent Linear Time Invariant Plants	3-1

Introduction	3-1
Mathematical Development for the Generation of SISO Equivalent LTI Plants	3-1
SISO Example	3-5
Extension of the Golubev Technique to the MIMO Problem	3-10
MIMO Example	3-12
Generation of Equivalent LTI Plants	3-16
Cautions and Pitfalls	3-20
Summary	3-22
 IV. Inner Loop Design	 4-1
Introduction	4-1
Design Requirements	4-2
Templates	4-2
Loop Shaping	4-4
P Loop Compensator	4-6
C* Loop Compensator	4-9
Prefilters	4-9
Summary	4-13
 V. Simulation of the Inner Loop	 5-1
Introduction	5-1
Linear Simulations	5-1
C* linear simulation	5-1
Roll Linear Simulation	5-1
Nonlinear Simulations	5-2
Nonlinear Simulation of the SISO Systems	5-2
Nonlinear MIMO Simulations Over the Design Range	5-3
Nonlinear MIMO Simulations Over an Extended Input Range	5-4
Additional Simulations	5-8
Summary	5-9
 VI. Pilot Compensation	 6-1
Introduction	6-1
Plant Generation for Pilot Compensation	6-2
Pilot Model	6-4
Longitudinal Pilot Compensation	6-4
Lateral Pilot Compensation	6-6

Simulation of the Pilot Compensation	6-12
Summary	6-14
VII. Conclusions and Recommendations	7-1
Discussion	7-1
Conclusions	7-2
Recommendations	7-3
Appendix A. Thumbprints and Equivalent LTI Plants	A-1
Thumbprint Transfer Functions	A-1
Equivalent LTI Plants for Inner Loop Design	A-2
Equivalent MISO Plants for Inner Loop Design	A-9
Equivalent LTI SISO Plants for the Compensated Inner Loop	A-13
C* equivalent plants	A-13
p equivalent plants	A-14
Appendix B. Equivalent Plant Fits	B-1
Appendix C. Additional Simulations	C-1
Bibliography	BIB-1
Vita	VITA-1

List of Figures

Figure	Page
1.1 Closed Loop Control System	1-2
1.2 Closed Loop Control System Including Man in the Loop	1-3
2.1 Unity Feedback Control System	2-1
2.2 Time Domain Thumbprints	2-2
2.3 Frequency Domain Thumbprints	2-3
2.4 Signal Flow Graph of the MIMO Problem	2-7
2.5 Signal Flow Graphs of the Equivalent MISO Loops	2-8
3.1 Nonlinear System	3-1
3.2 Equivalent Plant Fit for the SISO Example Using 11 Data Points	3-9
3.3 Equivalent Plant Fit for the SISO Example Using 101 Data Points	3-10
3.4 $u_1(t)$ for the MIMO Example	3-13
3.5 Fit and Error for the MIMO Example	3-16
3.6 Modified YF-16 Simulator	3-17
3.7 Effects of Including Trim	3-18
3.8 System Responses Used for Equivalent Plant Generation	3-20
4.1 Inner Loop Compensation	4-1
4.2 Uncertainty of the Uncompensated System	4-3
4.3 Spreadsheet Work Area	4-5
4.4 Uncompensated Roll Loop and Stability Bounds	4-7
4.5 Compensated Roll Loop	4-8
4.6 Uncompensated C^* Loop	4-10
4.7 Compensated C^* Loop and Stability Bounds	4-11
4.8 Compensated Responses Without Prefilters	4-12
4.9 Compensated Responses With Prefilters	4-13

5.1	Linear Simulations of the Inner Loop	5-2
5.2	Nonlinear SISO Simulations of the Completed Design	5-3
5.3	Nonlinear MIMO Responses Over the Design Range	5-4
5.4	Nonlinear MIMO Simulations Over an Extended Input Range	5-5
5.5	Nonlinear MIMO Simulation with the Modified Roll Compensator	5-7
5.6	Template of q_{22} at 30 rad/s	5-8
5.7	Nonlinear MIMO Simulations at 0.6M, 30K with Increased Gain	5-9
6.1	Closed Loop Control System Including Man-in-the-Loop	6-1
6.2	Equivalent Plants for Outer Loop Design	6-2
6.3	Uncertainty of the Equivalent Plants for Pilot Compensation	6-3
6.4	C* Pilot in the Loop Criteria	6-5
6.5	Compensated C* Loop	6-7
6.6	Pilot in the Loop Roll Criteria	6-10
6.7	Compensated Roll Response	6-11
6.8	Problems Caused by the Pade' Approximation	6-12
6.9	Pilot in the Loop SISO Simulations	6-13
B.1	Fit and Error for C*, Plant 1	B-1
B.2	Fit and Error for p, Plant 1	B-2
B.3	Fit and Error for C*, Plant 2	B-2
B.4	Fit and Error for p, Plant 2	B-3
B.5	Fit and Error for C*, Plant 3	B-3
B.6	Fit and Error for p, Plant 3	B-4
B.7	Fit and Error for C*, Plant 4	B-4
B.8	Fit and Error for p, Plant 4	B-5
B.9	Fit and Error for C*, Plant 5	B-5
B.10	Fit and Error for p, Plant 5	B-6
B.11	Fit and Error for C*, Plant 6	B-6

B.12	Fit and Error for p , Plant 6	B-7
B.13	Fit and Error for C^* , Plant 7	B-7
B.14	Fit and Error for p , Plant 7	B-8
B.15	Fit and Error for C^* , Plant 8	B-8
B.16	Fit and Error for p , Plant 8	B-9
B.17	Fit and Error for C^* , Plant 9	B-9
B.18	Fit and Error for p , Plant 9	B-10
B.19	Fit and Error for C^* , Plant 10	B-10
B.20	Fit and Error for p , Plant 10	B-11
B.21	Fit and Error for C^* , Plant 11	B-11
B.22	Fit and Error for p , Plant 11	B-12
B.23	Fit and Error for C^* , Plant 12	B-12
B.24	Fit and Error for p , Plant 12	B-13
B.25	Fit and Error for C^* , Plant 13	B-13
B.26	Fit and Error for p , Plant 13	B-14
B.27	Fit and Error for C^* , Plant 14	B-14
B.28	Fit and Error for p , Plant 14	B-15
B.29	Fit and Error for C^* , Plant 15	B-15
B.30	Fit and Error for p , Plant 15	B-16
B.31	Fit and Error for C^* , Plant 16	B-16
B.32	Fit and Error for p , Plant 16	B-17
B.33	Fit and Error for C^* , Plant 17	B-17
B.34	Fit and Error for p , Plant 17	B-18
B.35	Fit and Error for C^* , Plant 18	B-18
B.36	Fit and Error for p , Plant 18	B-19
B.37	Fit and Error for C^* , Plant 19	B-19
B.38	Fit and Error for p , Plant 19	B-20

B.39	Fit and Error for C^* , Plant 20	B-20
B.40	Fit and Error for p , Plant 20	B-21
B.41	Fit and Error for C^* , Plant 21	B-21
B.42	Fit and Error for p , Plant 21	B-22
B.43	Fit and Error for C^* , Plant 22	B-22
B.44	Fit and Error for p , Plant 22	B-23
C.1 (a)	Commanded Outputs for 3 Cases from Ch 5	C-2
C.1 (b)	Elevator and Aileron Deflections for 3 Cases from Ch 5	C-2
C.1 (c)	Rudder and Leading Edge Flap Deflections for 3 Cases from Ch 5	C-3
C.1 (d)	Angle of Attack and Pitch Attitude for 3 Cases from Ch 5	C-3
C.1 (e)	Roll and Sideslip Angles for 3 Cases from Ch 5	C-4
C.1 (f)	Pitch and Yaw Rates for 3 Cases from Ch 5	C-4
C.1 (g)	Velocity and Altitude for 3 Cases from Ch 5	C-5
C.2 (a)	C^* and p for a Roll Out of a 2g Turn	C-5
C.2 (b)	Surface Deflections and Angles for a Roll Out of a 2g Turn	C-6
C.2 (c)	Roll Angle and Misc Rates for a Roll Out of a 2g Turn	C-6
C.3 (a)	Commanded Outputs for a 120°/s Roll Rate Command	C-7
C.3 (b)	Surface Deflections and Roll Angle for a 120°/s Roll Rate Command	C-7
C.3 (c)	Altitude and Velocity for a 120°/s Roll Rate Command	C-8
C.4 (a)	MIMO Outer Loop Simulations at 0.9M, 20K	C-8
C.4 (b)	MIMO Outer Loop Simulations at 0.6M, 30K	C-9

List of Tables

Table	Page
3.1 Numerical Data for SISO Example	3-7

Abstract

Nonlinear Quantitative Feedback Theory (QFT) and pilot compensation techniques are used to design a 2x2 flight control system for the YF-16 aircraft over a large range of plant uncertainty. The design is based on numerical input-output time histories generated with a FORTRAN implemented nonlinear simulation of the YF-16. The first step of the design process is the generation of a set of equivalent linear time-invariant (LTI) plant models to represent the actual nonlinear plant. It has been proven that the solution to the equivalent plant problem is guaranteed to solve the original nonlinear problem. Standard QFT techniques are then used in the design synthesis based on the equivalent plant models. A detailed mathematical development of the method used to develop these equivalent LTI plant models is provided. After this inner loop design, pilot compensation is developed to reduce the pilot's workload. This outer loop design is also based on a set of equivalent LTI plant models. This is accomplished by modelling the pilot with parameters that result in good handling qualities ratings, and developing the necessary compensation to force the desired system responses.

MULTI-INPUT MULTI-OUTPUT FLIGHT CONTROL SYSTEM DESIGN FOR THE YF-16 USING NONLINEAR QFT AND PILOT COMPENSATION

I. Background

Introduction

Requirements placed on modern high-performance aircraft have resulted in inherently unstable airframe designs. Increased speed and altitude among other causes have led to larger aerodynamic forces and moments which cannot be physically controlled by the pilot alone. Roskam points out that the trend toward the design of unstable airframes is expected to continue, with design emphasis placed primarily on performance as opposed to stability [16:10.5]. As a result, modern flight control systems (FCS) must be designed to account for these instabilities and to provide satisfactory dynamic responses while minimizing the pilot's workload.

This thesis is part of a continuing effort to assert the validity and value of both nonlinear QFT and man-in-the-loop modelling to the application of aircraft flight control system design. In a previous thesis, Kobylarz [13] used nonlinear QFT for a single-input single-output (SISO) design and developed a technique to design pilot compensation for tracking tasks with the goal of reducing the pilot's workload. This workload reduction provides the pilot with the opportunity to focus maximum attention on mission accomplishment as opposed to simply maintaining stable flight. This technique was applied and validated for a nonlinear SISO design for the YF-16 aircraft. Kobylarz's method is extended in this thesis for a multi-input multi-output (MIMO) design on the same plant.

A basic control system consists of a plant, various types of compensation, and feedback as shown in Figure 1.1. One purpose of a control system is to provide acceptable outputs for specified inputs. Further, the system should not react to unwanted inputs and disturbances. In FCS design, the aircraft represents the plant, and the control engineer is tasked to design the necessary compensation to ensure a stable system and acceptable outputs for the appropriate commanded inputs in the presence of disturbances and plant parameter variation. At this stage, the airframe, or plant, is fixed and unalterable. Therefore, the control engineer's only tools are compensation and feedback.

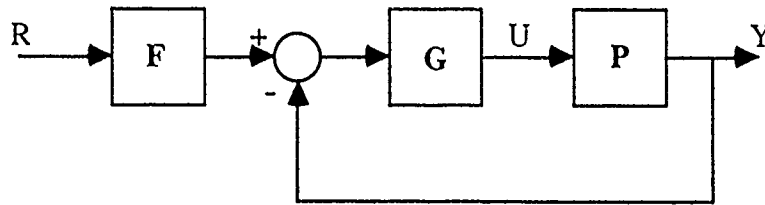


Figure 1.1. Closed Loop Control System

The design of aircraft and their flight control systems is dependant on mathematical representations of physical systems. An aircraft can be represented by a mathematical equation set, or *model*. These models, however, are not constant for all time. They are based on *stability derivatives* and other aerodynamic coefficients that are dependant on flight conditions. Additionally, flight control problems are highly nonlinear, as are most real-world problems.

Dr. Isaac Horowitz has developed a unified theory for control system design that can account for nonlinearities and large parameter uncertainty [9]. The inherent nonlinearities and parameter uncertainties associated with various flight scenarios make nonlinear quantitative feedback theory (QFT) an appropriate design technique for application in the area of flight control systems. QFT is a frequency domain graphical design technique that was developed specifically for systems with parameter uncertainty. The basic objective of QFT is

to develop a single compensator function that can be used to guarantee satisfactory system performance over the entire range of parameter uncertainty. If it is not possible to obtain the desired responses with fixed compensation because of nonminimum phase (nmp) plants or loop bandwidth restrictions, QFT provides insight to the appropriate mix of scheduling and feedback [4].

Based on his observations or perceptions of the current situation, the pilot adjusts his inputs to the system resulting in an additional outer loop as shown in Figure 1.2. The darker feedback path symbolizes this unique human interaction, and F_p represents the pilot compensation proposed to reduce the pilot's workload.

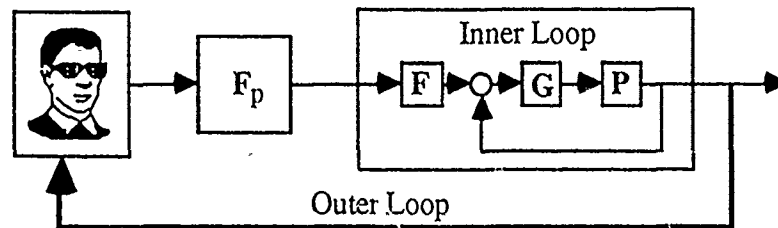


Figure 1.2. Closed Loop Control System Including Man in the Loop

For certain scenarios, models have been developed to account for the pilot's role in the total closed loop operation. Additionally, "optimal" parameters for these models have been determined which result in good pilot ratings of operational systems. These models and desirable parameters lay the foundation for the design of pilot compensation to ensure satisfactory pilot ratings of the completed operational system.

Problem Statement

The need exists for a MIMO systematic design technique for aircraft flight control systems that accounts for nonlinearities and guarantees first cut satisfactory designs. The successful design of many existing flight control systems was made possible only because

of the "ingenuity of practical designers" [8:1]. Most existing flight control systems have been designed on the basis of approximated linearized aircraft models, and neglect the inherent nonlinearities associated with the FCS problem. This approach has resulted in designs which require a great deal of trial and error synthesis. Additionally, the neglect of the human operator in the design process has resulted in the requirement of expensive and time consuming modifications based on real-time simulations with the nonlinear plant.

Review of Current Literature

Aircraft can be adequately modelled by mathematical equations which include nonlinearities and parameter uncertainty. Because of these characteristics, a quantitative synthesis technique such as QFT can be a valuable tool in flight control system design. It has been applied to several Air Force problems where other techniques have failed. Nonlinear QFT lends itself directly to these types of highly nonlinear and uncertain systems, and its use results in first cut robust designs through a straightforward and systematic approach. QFT has been shown to be quantitatively superior to many modern control synthesis techniques and preserves many frequency domain insights which are lost in many modern control methods. Dr. C. H. Houppis has provided a unified document [12] to guide the QFT user smoothly through the process.

Pilot modelling in early stages of the design process may result in more efficient and less expensive designs. The simulation results of Kobylarz's design provide a specific example of the value of pilot modelling. Kobylarz performed both linear and nonlinear simulations on his design which gave excellent results. Additionally, his design was later simulated in real-time on a SIMSTAR hybrid computer. In this simulation, a dual trace oscilloscope was used to display a tracking task and the control system response to a pilot's force stick. The systems tracking performance was significantly improved with the pilot compensation.

Horowitz states that, "The problems of designing adequate (stability) augmentation systems is further complicated by the rapidly expanding flight envelope, nonlinear aerodynamic regions, ... and increased mission requirements," and that "What is needed is a unified theory of flight control design that recognizes the multivariable nature of aircraft control, the plant uncertainties, the wide variations of the plant, the emphasis on robustness, the nonlinear aerodynamic regions, ..." [6:1]. He also points out *The Neglect of Quantitative Synthesis in Feedback Control Theory* [8:Ch 1], in which he states that, "The flight control problem is one of regulation and control despite parameter uncertainty and disturbances". Highly nonlinear mathematical relationships exist between the input and output quantities of interest, and different flight conditions result in variations among dynamic aircraft parameters. Currently there is no complete synthesis technique for this flight control problem, and many current designs "...have worked because of the ingenuity of practical designers and the inherent power of feedback, but a great deal of cut and try design is essential" [8:1]. Theory has fallen behind practice in this field "...due to the almost total neglect of a quantitative feedback synthesis theory" [8:2]. Essentially, the purpose of feedback is to achieve the desired system response despite parameter uncertainty and disturbances. Therefore, it only makes sense to incorporate a design methodology which provides a quantitative relationship between the amounts of uncertainty and feedback [4].

Quantitative Feedback Theory. Quantitative feedback theory was introduced in 1959 by Dr. Isaac Horowitz. The QFT method "...consists of a steadily growing body of design techniques for achieving prespecified system performance tolerances, despite prespecified large plant parameter and disturbance uncertainties" [18:945]. The theory has been developed for linear time-invariant systems as well as nonlinear and time varying systems. It has also been extended to systems with output feedback and internal variable feedback and lumped and distributed parameter plants [18:945]. QFT has been successfully applied and demonstrated on problems of all of the aforementioned classes. The beauty of QFT lies in the fact that "...this technique guarantees a satisfactory design for a large plant uncertainty

class by a comparatively straightforward systematic procedure" [18:946]. Most modern techniques require some sort of trial and error design, but QFT results in an acceptable design on the first (and only) trial. Yaniv and Horowitz presented an improved version of QFT for MIMO systems in 1986, which simplified the design procedure and improved feedback economy [19] by incorporating the designed compensation of the first loops in subsequent compensation synthesis. In 1988, Yaniv further extended the MIMO QFT to a method that results in the diagonal elements of the closed loop transfer function matrix to be not only dominant, but also minimum phase [17:519]. The advantage of this improvement was that it allowed the transformation of time domain specifications into equivalent frequency domain specifications by the methods developed by Krishman and Cruickshanks (1977) and Horowitz (1976) [17:519]. In quantitative comparisons of QFT designs to other modern robustness methods, QFT has consistently proven to be more economical in loop compensation gain and bandwidth [18:959]. Despite its well demonstrated advantages, QFT has been to a large extent ignored by modern control theorists [18:945]. Yaniv pointed out that the lack of extensive computer aided design (CAD) packages for QFT has prevented its use in industry and that most work is currently being done by graduate students [13:1-5]. One such CAD package, ICECAP QFT is currently being developed under the supervision of Dr. Constantine H. Houpis and Dr. Gary B. Lamont at the Air Force Institute of Technology (AFIT).

Houpis [12] has provided AFWAL-TR-86-3107, "Quantitative Feedback Theory Technique for Designing Multivariable Control Systems", as a unified document for practicing engineers and students. This technical report was written for the Air Force Wright Aeronautical Laboratories, and is based on the technical articles and unpublished lecture notes of Dr. Horowitz and the theses of AFIT MS students. Houpis [12:1-1] states that,

Quantitative feedback theory is a unified theory using the available measurable states that is applied to the design of multiple-input multiple-output systems, and incorporates

- a. multivariable nature of control systems
- b. plant uncertainties
- c. wide variations vs time of plant parameters
- d. robustness performance requirements
- e. disturbance attenuation requirements
- f. nonlinearities in the plant model
- g. requirements for decoupled outputs

This design technique is applicable to the following problem classes:

- 1. SISO linear time invariant (LTI) systems
- 2. SISO nonlinear systems. These are rigorously converted to equivalent class 1 systems whose solutions are guaranteed to work for a large problem class.
- 3. MIMO LTI systems. The performance specifications on each individual closed-loop system transfer function and on all the disturbance functions must be specified.
- 4. MIMO nonlinear systems. They are rigorously converted to equivalent class 3 systems whose solutions are guaranteed to work for a large class.

This technical report is used as the primary reference for application of the QFT techniques in this thesis.

Current flight control designs are usually based on the approximate linearized time invariant aircraft model about a fixed point (nominal flight condition). These models are valid only for small perturbations about this nominal point. Models must be generated to approximate the many flight conditions which the aircraft will experience while in flight, and a separate controller is designed for each flight condition. On-board computers are used to determine the appropriate controller to be implemented at any given time [13:1-3]. This multiple controller requirement is the result of flight control designs being performed for fixed deterministic aircraft models. QFT on the other hand is based on systems with parameter uncertainty, not deterministic models. For a given model, ranges are placed on the system parameters which cover all possible variations. Boundaries are developed based on these parameter ranges, tracking requirements and the disturbance attenuation specifications. An algorithmic approach to computing these boundaries has been presented by East [3] which eliminates some of the graphical aspects of the boundary generation and provides a tool for CAD development. Open-loop transfer function and compensator synthesis is

then performed in the frequency domain. By developing an open-loop transfer function that does not violate any of the boundaries, QFT will result in an acceptable controller over the entire range of uncertainty. Thus, robustness is inherent with a QFT design, and the robustness tests of modern control synthesis techniques are not required [4]. Horowitz [10] presented a paper in 1975 that compares transfer function and state space methods of LTI feedback system design. He concluded that the transfer function methods are superior in many respects. Several examples have been provided that clearly place QFT above modern techniques. One such example was given by Walke and Horowitz in which they successfully applied LTI QFT techniques to the X-29 aircraft. Because of right-half plane poles and zeros in the plant determinant, contracted designers, using other design methods, had abandoned an attempt to independently control two of the output variables [5:534]. An example of a nonlinear QFT success is the case where Golubev used QFT to control a modified F-4 to an angle of attack up to 35 degrees, which is a highly nonlinear condition [13:1-6].

Pilot Modelling. Because the complex pilot dynamics play an important role in the operation of an aircraft, they must be considered as part of the closed-loop flight control system. Paschall [15] has stated that even though a designer may produce a highly efficient design, it has not passed the final test until it is deemed acceptable by the pilots who will fly it. He also stated that even though Roskam's [16] presentation on pilot modelling and handling qualities is about ten years old, his views are still current and have not been significantly expanded. Barfield pointed out that current practice in flight control design is to adjust for the pilot dynamics in the advanced simulation and testing phase [13:1-6]. The problem with this practice is that in the later stages of design, adjustments are expensive and time consuming. If pilot models are included in the design process, fine tuning of the design parameters in later stages can be greatly reduced or even eliminated [13:1-6], thereby reducing the design cost considerably [11].

Roskam stated that total human interaction with the flight control system can be described by two quantities: "The first, that portion of the output linearly correlated with the forcing function, characterizes the human's actions in terms of quasi-linear random input describing functions. The second, that portion of the output which is not linearly correlated with the system forcing function is called the remnant" [16:10.9]. Pilot models have been generated basically in the form of a lead-lag filter and time delay. Additionally, Roskam [16:10.12-10.15] has provided some important insights into pilot modelling. They are as follows:

1. The pilot adjusts his gain and filter characteristics to obtain good low frequency closed-loop system response and maintain system stability.
2. Although the internal pilot dynamics are not all well known, insight into their practical implications can be obtained by an examination of past human operator data.
3. Dependable correlations exist between pilot ratings of handling qualities and the amount of gain, lead or lag that has to be generated by the pilot.
4. Pilot gain is inversely proportional to the forcing function bandwidth.
5. The system crossover frequency is approximately constant.

Roskam [16:12.4] also pointed out some specific values for pilot gain, lag, lead and short period damping coefficients which generally result in satisfactory pilot ratings. For instance, he stated that pilot ratings generally deteriorate as the required pilot input departs from the ideal input of pure gain. Also, Cooper-Harper ratings given by pilots typically decrease by 2.5 for each second of input lead required. Similarly, ratings decrease as more input lag is required, and in general, pilots do not like systems that require a lag input. He further said that pilots generally adjust their response to obtain an open-loop phase margin of roughly 50 to 110 degrees, and that pilots prefer constant frequency response

characteristics in the low frequency range. Acceptable bounds on short period damping were also specified to be between 0.35 and 0.55. Roskam concluded his discussions on pilot modelling with "The lesson to be derived here is that variable stability airplane and simulator methods can be used to predict how well pilot plus airframe will behave" [16:12.10]. One intent of this thesis is to show that in particular, pilot simulations and compensation in the early phase of the design process can be of great value.

Kobylarz [13] used the Neal-Smith pilot model for compensatory tracking. Specifically, the Neal-Smith model is given by

$$K_p e^{-\tau s} \left(\frac{\tau_{p1}s + 1}{\tau_{p2}s + 1} \right) \quad (1.1)$$

In the pilot model, K_p represents the pilot gain factor, and τ_{p1} and τ_{p2} represent the pilot's adaptive compensation coefficients. For implementation of the pilot model, a fourth order Pade' approximation was used for the exponential term, which represents the pilot's reaction delay. Simulations of Kobylarz's design with and without pilot compensation were performed on a SIMSTAR hybrid computer. The simulation included a pilot's control stick for input and an oscilloscope to display a tracking task. The method of simulation was such that an arbitrary tracking task was displayed on the oscilloscope, and by use of the control stick the "pilot" attempted to track the task. The results were that with pilot compensation the task was simple, but without the compensation the task proved to be somewhat difficult [11].

Assumptions

The following assumptions are incorporated into this thesis project:

1. Only the modelled inputs are of interest for final performance.
2. All inputs and outputs are Laplace transformable.

Assumption #1 is required to reduce the workload involved with the design. A sufficiently large number of inputs are used to ensure that this is a reasonable assumption. The second assumption does not place any real limitations on the analysis since all smooth functions that are continuous and bounded, and a very large class of unbounded functions for which there exists a δ such that $\int_0^\infty f(t)e^{-\delta t} dt$ exists, are Laplace transformable.

Scope

This project involves the design of a pitch and roll control system for which the only independent commanded controls are symmetric horizontal tail (elevator) deflection and aileron deflection. The original control system for rudder control and the leading edge flaps are left intact. The rudder controls are required for lateral stability, but the decision to leave in the flap controls is rather arbitrary. The intent of this thesis is to apply the design technique to a given model. As long as the design model is the same as the simulation model, treatment of additional control surfaces is not a significant issue.

Standards

The thesis sponsor has provided response specifications for the system based on the guidelines presented in MIL-STD-1797A, *Flying Qualities of Piloted Aircraft*.

Approach

Nonlinear QFT is used to design a 2x2 flight controller for the YF-16. The controller outputs, elevator and aileron command, are used to control C^* and roll rate, where C^* is a blend of normal acceleration and pitch rate as felt at the pilot station, given by

$$C^* = N_{zp} + 12.4q \quad (1.2)$$

The design is based on obtaining satisfactory responses for step commands in both C^* and roll at the two flight conditions 0.9 mach, 20 thousand feet (0.9M,20K) and 0.6M,30K. The maximum commands on which the design is based are 2.2 g's for C^* and 30°/s for roll rate.

Inner Loop Design. The inner loop design consists of the development of the stability augmentation system (SAS) compensator, designated G in Figure 1.1. For this design, G is a 2x2 diagonal compensator given by

$$G = \begin{bmatrix} g_c & 0 \\ 0 & g_p \end{bmatrix} \quad (1.3)$$

The purpose of this compensator is to stabilize the aircraft and ensure appropriate outputs to pilot inputs. Following the completion of the SAS compensator design, a diagonal pre-filter given by

$$F = \begin{bmatrix} f_{11} & 0 \\ 0 & f_{22} \end{bmatrix} \quad (1.4)$$

is developed for simulation and verification of the inner loop design.

Pilot Compensation. The outer loop design consists of choosing a pilot compensation filter, F_p in Figure 1.2, to provide satisfactory system response with minimal pilot workload. The outer loop design is based on the Neal-Smith pilot model of (1.1) which consists of a gain, a time delay, and a lead-lag filter characteristic. Strong correlations have been shown to exist between pilot ratings of aircraft handling qualities and the amounts of gain, delay, lead and lag that the pilots must input to a system [16:10.15]. The basic design strategy is to model the pilot by parameters which have been shown to result in satisfactory pilot ratings, and synthesize pilot compensation that results in the appropriate system response while it is being driven by these optimal pilot characteristics.

In other words, the pilot model simulates an actual human pilot in the loop, "flying" the system in a manner which he would consider to be acceptable. Designs which do not consider the pilot may be capable of producing the appropriate aircraft responses, but if the pilots do not like the way they "feel", time consuming and expensive modifications must be made. These modifications can be avoided by the development of a design technique that considers the pilot-aircraft interaction in the early design phase so that the completed product will always be satisfactory to the pilots who will fly it.

Simulation. Two simulations on the inner loop are performed. First, a linear MATRIXx simulation is performed, followed by the full nonlinear simulation on the FDL VAX with the FORTRAN nonlinear YF-16 simulator. Comparison of the two simulations indicate the validity of the equivalent LTI design models. Finally, the outer loop design is simulated on the nonlinear FORTRAN simulator.

Documentation

This thesis consists of seven chapters. Chapter 2 provides a very basic overview of nonlinear QFT theory as applied to this project. The first part of Chapter 3 mathematically develops the method for deriving a set of equivalent LTI plants that represent the nonlinear system. This development is followed by a detailed description of the equivalent plant generation used for this design. The fourth chapter details the inner loop designs on both channels, which includes the SAS compensator, G , and the prefilter, F . Chapter 5 provides the results of both linear MATRIXx and nonlinear simulations on the completed inner loop designs. Chapter 6 covers the entire pilot compensation portion of the thesis, from method to simulation. The final chapter includes an overall discussion on the project, presents conclusions based on the work, and provides some recommendations for future work in this area. There are three appendices. Appendix A contains all of the important transfer functions used in the design, from the boundary models to the equivalent plants. Appendix B gives the equivalent plant time responses and their respective errors. Finally,

Appendix C provides additional simulations of both the inner and outer loops. Additionally, a supplement is available which includes all computer programs and MATRIXx executables which were used in the design process. Requests for the supplement should be directed to Mr. Finley Barfield at WRDC/FIGX.

Summary

A unified theory for control system design that can account for nonlinearities and large parameter uncertainty has been developed by Dr. Isaac Horowitz. The development of a systematic design procedure that incorporates this theory, combined with pilot compensation techniques, to flight control problems would be of great interest and value to the Air Force. Development of this theory into a systematic design procedure can only be accomplished by applying it to real flight control problems, modifying it as required, and validating the results. This thesis is part of a continuing effort to assert the validity and value of both nonlinear QFT and man-in-the-loop modelling to the application of aircraft flight control system design. Nonlinear QFT has been applied to a single-input single-output flight control problem and the extension to a multi-input multi-output design constitutes an important stepping stone toward the development of a systematic FCS design technique. The Wright Research and Development Center's Flight Dynamics Laboratory at Wright-Patterson AFB, Ohio is the sponsor this ongoing research.

II. Nonlinear QFT

Introduction

This chapter provides a very basic introduction to nonlinear QFT. Emphasis is placed primarily on the particulars of the nonlinear aspect, and the discussion is oriented toward the 2x2 MIMO problem of this thesis. The basic design equations of QFT are given with minimal development, and the reader is referred to references [2,12] for a more detailed and general case investigation.

Overview of Quantitative Feedback Theory

Quantitative Feedback Theory is a control system design technique developed by Dr. Isaac Horowitz to develop single, fixed compensation despite large plant uncertainty. The technique is founded in the frequency domain and preserves many of the insights which are lost in many of the modern control methods. The technique utilizes a Nichols chart and involves the direct loop shaping of the open loop system to obtain the desired closed loop response. The development in this chapter is based on a unity feedback system of the form shown in Figure 2.1, where all of the blocks may represent scalar (SISO), or matrix (MIMO) system transfer functions. For the MIMO problem of order m , the system is rigorously converted to m^2 equivalent multi-input single-output (MISO) loops. The plant $\mathbf{P} = [p_{ij}]$ is assumed to contain bounded uncertainty and can be represented by a set of plants \mathbf{P}

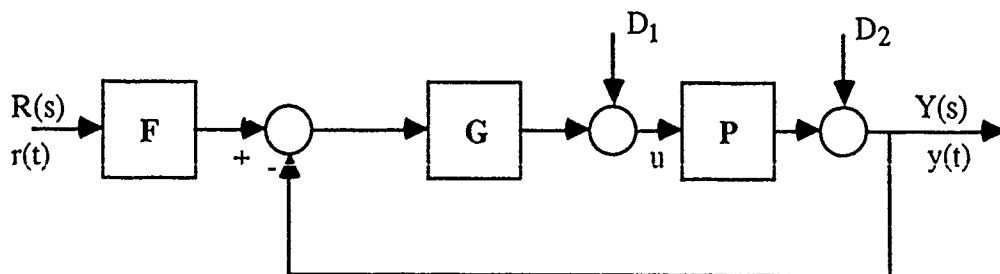


Figure 2.1. Unity Feedback Control System

$= \{P\}$. G represents the cascade compensation to stabilize and shape the output, y , and D_1 and D_2 represent disturbance inputs. Finally, F represents a prefilter to fine tune the system response. The procedure is implemented by deriving frequency domain boundaries and specifications based on the desired system outputs.

Thumbprint Specifications. Thumbprint specifications, which represent a window of acceptable responses for the compensated closed loop system, can be synthesized based on figures of merit such as settling time, rise time, peak overshoot, etc. These specifications are described by upper and lower response functions, $T_{RU}(s)$ and $T_{RL}(s)$ respectively. The thumbprint specifications used in this design are based on general guidelines provided by the sponsor. Transfer functions that satisfy these guidelines are provided in Appendix A, and a plot of their time response is the thumbprint specification for the design, as shown in Figure 2.2.

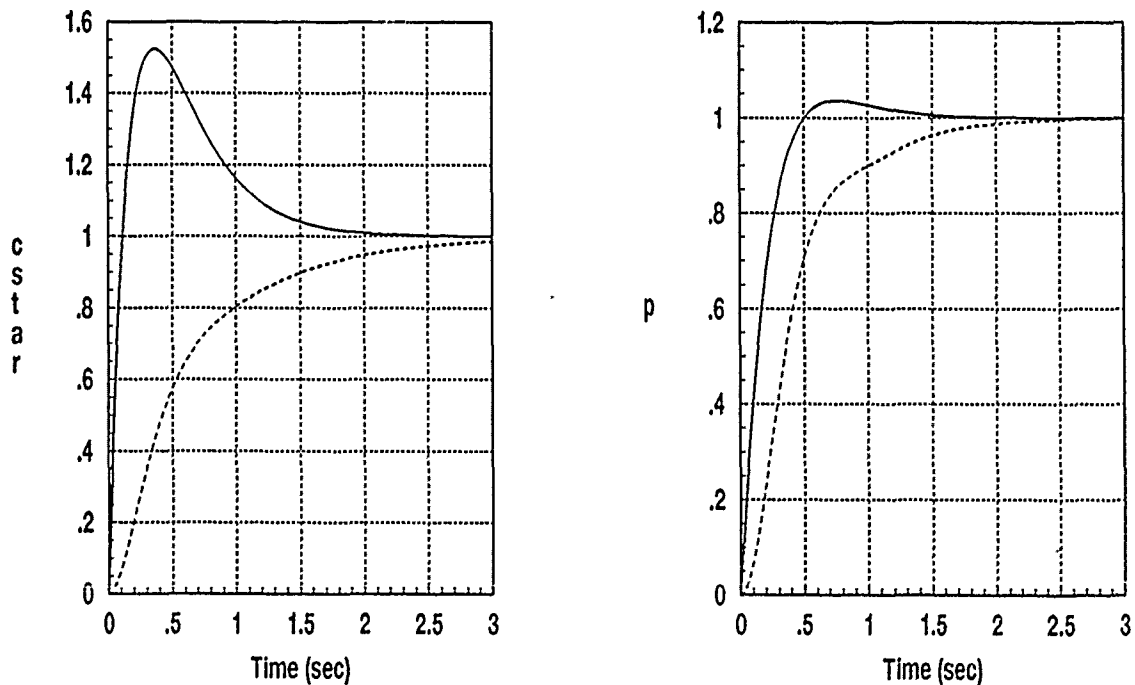


Figure 2.2. Time Domain Thumbprints

The frequency domain thumbprint is then determined by simply plotting the frequency response of the transfer functions which are generated to satisfy the time domain requirements. An important design parameter that comes from the frequency domain thumbprint is the quantity

$$|\delta_T(j\omega)| \equiv |T_{RU}(j\omega)| - |T_{RL}(j\omega)| \quad (2.1)$$

$|\delta_T(j\omega)|$ represents the maximum allowable variation in the frequency response of the closed loop system, and it is desirable that $|\delta_T(j\omega)|$ always increases with frequency. The frequency domain thumbprints for the design in this thesis are shown in Figure 2.3.

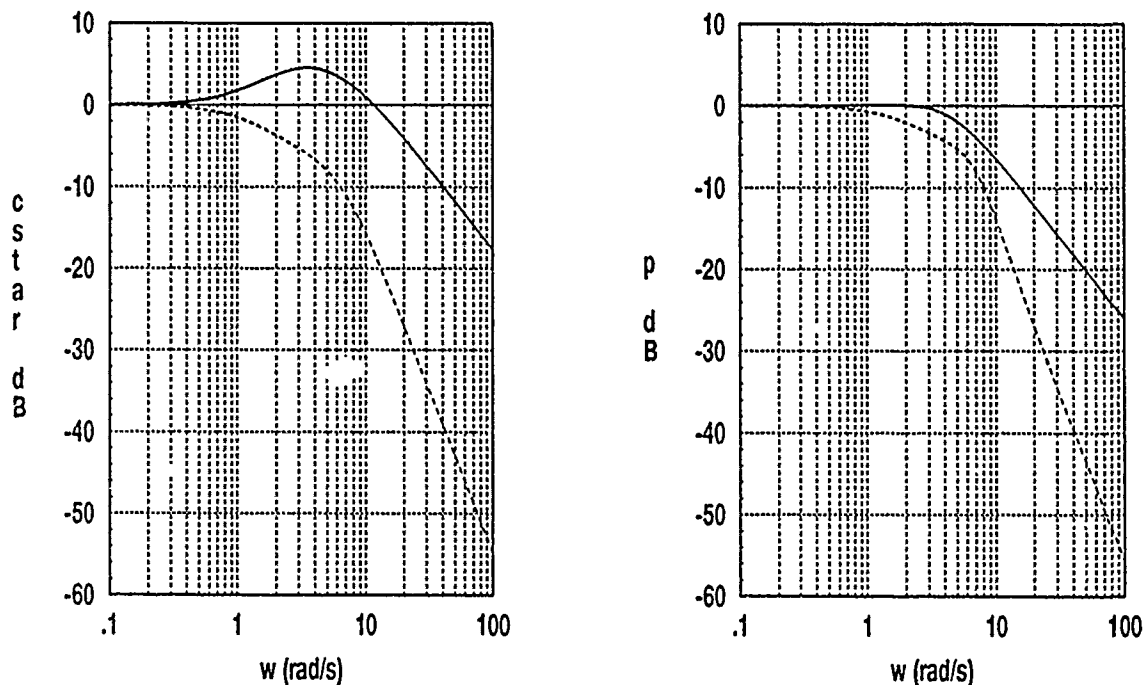


Figure 2.3. Frequency Domain Thumbprints

Equivalent Linear Time Invariant Plant Models. For the nonlinear problem, a set of equivalent linear time invariant (LTI) plant models that rigorously represent the nonlinear plant, in this case the YF-16 aircraft, must be generated. A graduate student under Horowitz, Boris Golubev, wrote a FORTRAN program which given a SISO input-output time history data file, can generate a plant equivalent to the one from which the data file

was obtained. This program was provided by Horowitz, and a detailed analysis of that program and conversations with Horowitz revealed its mathematical basis as described in Chapter 3. A MATRIXx program based on the method proposed by Golubev and extended to the MIMO case is explained in detail in Chapter 3. This program, given an input-output time history of a 2x2 MIMO plant can generate an equivalent LTI transfer function set that represents the nonlinear plant used to generate the time history. This equivalent plant is valid for the specified inputs only. Therefore, given a nonlinear model, by generating input-output time histories for all realistic inputs into the plant, a set of equivalent LTI transfer functions, $\mathbf{P}_e = \{\mathbf{P}(s)\}$, can be developed which represent the single nonlinear plant. This set of plants represents the type of parameter uncertainty for which the QFT design method was developed. It has been proven that for a very large problem class the solution to the \mathbf{P}_e uncertainty problem is guaranteed to solve the original nonlinear uncertainty problem [9].

Nichols Chart. The Nichols chart is an invaluable frequency domain design tool. The linear vertical and horizontal axes represent the open loop magnitude and phase of a unity feedback control system. Superimposed on this linear graph paper are M and α contours that represent the closed loop system magnitude and phase. Therefore, the Nichols chart can be used to shape the open loop transfer function with full knowledge of the resulting closed loop system response characteristics.

Plant Templates. Assuming that the LTI equivalent $\mathbf{P}_e = \{\mathbf{P}(s)\}$ set has been obtained, the plant template at any given frequency ω_i , consists of the set of complex frequency values $\mathbf{P}_e(\omega) = \{\mathbf{P}(j\omega)\}$. A reasonable number of ω values are selected, with ω sufficiently large that $\mathbf{P}_e(\omega)$ approaches the shape of a vertical line (no uncertainty in phase), because as $\omega \rightarrow \infty$, each $p \rightarrow k_p/s^e$ where e is the excess number of $P(s)$ poles over zeros, and e is constant for most problems. Each template represents the entire range of plant magnitude and phase uncertainty for a specific frequency. It is convenient to plot the plant templates on clear plastic sheets so they can be easily manipulated on the Nichols chart.

Nominal Plant. One of the plants in the set \mathcal{P} is conveniently chosen as the nominal plant, designated P_0 . This plant is simply a reference plant on which the boundaries discussed below and the compensator design are based. Then by developing the required compensation, G , such that the nominal loop, $L_0 = GP_0$, satisfies the stability, tracking, and disturbance bounds, all plants in $\{\mathcal{P}\}$ are guaranteed to result in the desired response with the same compensator.

Boundaries. Stability bounds are formed by sliding the templates around a prespecified open loop stability contour on the Nichols chart in a manner such that no part of the template penetrates the stability region. By tracing out the trajectory of the nominal plant as the template is slid about this stability contour, a boundary is formed such that if it is not violated by the nominal loop, all plant cases are guaranteed to satisfy the stability requirements.

Next, tracking boundaries are drawn by placing the templates on the Nichols chart at various phase angles and sliding them in a vertical direction until the total closed loop magnitude variation covered by the template is equal to the magnitude variation specified by $|\delta_r(j\omega)|$ of Equation (2.1). These bounds ensure that the maximum variation in the closed loop frequency response does not exceed the maximum allowable variation as specified by the frequency thumbprint, making it possible to design a prefilter which "pulls" the closed loop frequency responses within the thumbprint for all plant cases. Because there is a significant correlation between the frequency and time domains, satisfying the frequency domain thumbprint generally results in a set of satisfactory system outputs.

Disturbance rejection boundaries are then computed by either graphic or analytic means. The reader is referred to [2] for the specific procedure. Finally, a composite boundary is dictated at each frequency by the most restrictive of the tracking and disturbance boundaries.

Loop Transmission Synthesis. After all of the boundaries have been determined, a nominal loop transmission function, $L_0 = GP_0$, is synthesized by building a transfer

function with poles and zeros so that L_0 falls as close as possible to the boundaries but does not violate them. A certain level of engineering ingenuity and some trial and error is required for this loop synthesis, but with some experience, the loop can be readily shaped with the aid of a simple calculator. In this thesis, a spreadsheet is used to track the magnitude and phase characteristics of the loop as it is built. More details on this procedure are provided in Chapter 4. The resultant transfer function, L_0 , is then divided by the nominal plant transfer function, P_0 , which yields the compensator, G , which can be implemented to guarantee system response variations which do not exceed those allowed by the thumbprint specifications, for the entire range of plant uncertainty.

Prefilter. The final stage in the QFT design process is the development of the prefilter, F of Figure 2.1, to position the closed-loop frequency responses within the thumbprint. With the aid of a Bode magnitude plot, the prefilter can generally be designed by inspection, if the responses are not too complex, using straight line magnitude approximations. Kobylarz used an interesting technique for prefilter design. He plotted a log magnitude plot of the two quantities of the upper frequency bound minus the maximum closed loop frequency response and the lower frequency bound less the minimum closed loop frequency response, resulting in an equivalent set of bounds on the prefilter frequency response. With this set of prefilter bounds, development of the prefilter with straight line magnitude approximations is somewhat simplified.

The 2x2 MIMO Problem. The unity feedback, diagonally compensated 2x2 MIMO problem can be readily described in terms of Figure 2.1 by allowing F , G , and P to represent 2x2 matrices of transfer functions, and \underline{u} and \underline{y} 2x1 input and output vectors respectively. Since external disturbances are not considered in this thesis, D shown in Figure 2.1 for the MIMO system is zero. Analogous to the SISO case where the system transfer function is given by

$$T(s) = \frac{Y(s)}{R(s)} = \frac{FGP}{1 + GP} \quad (2.2)$$

the matrix of closed loop transfer functions for the MIMO system, is described by

$$T = [I + PG]^{-1} PGF \quad (2.3)$$

and can be represented by the signal flow graph (sfg) of Figure 2.4.

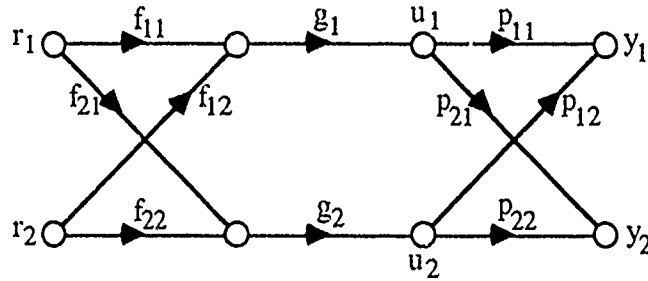


Figure 2.4. Signal Flow Graph of the MIMO Problem

The MIMO QFT design method however, is not based on T of (2.3). Instead, the MIMO system is rigorously converted to four equivalent MISO systems, each having a desired input and a disturbance input. Reference [12] gives a full development of the conversion process and only the design equations are presented here. The MIMO representation of Figure 2.4 can then be further broken down to the equivalent (MISO) loops of Figure 2.5. The system inputs are given by r_i and the plant inputs are represented by the u_{ij} , and the system/plant outputs are given by the y_{ij} . Note that the y_i of Figure 2.4 are given by the sum of y_{ii} and y_{ij} from Figure 2.5. The D_{ij} represent the disturbance inputs associated with cross coupling effects, and they can be precisely modelled in the equivalent MISO systems by a disturbance input of the form of D_1 in Figure 2.1. The input prefilters are represented by the f_{ij} , and the q_{ij} represent the equivalent MISO plants. Note that for a diagonal prefilter, as used in this thesis, $f_{12} = f_{21} = 0$. The q_{ij} are derived from the inverse of the plant matrix, P^{-1} . That is, given

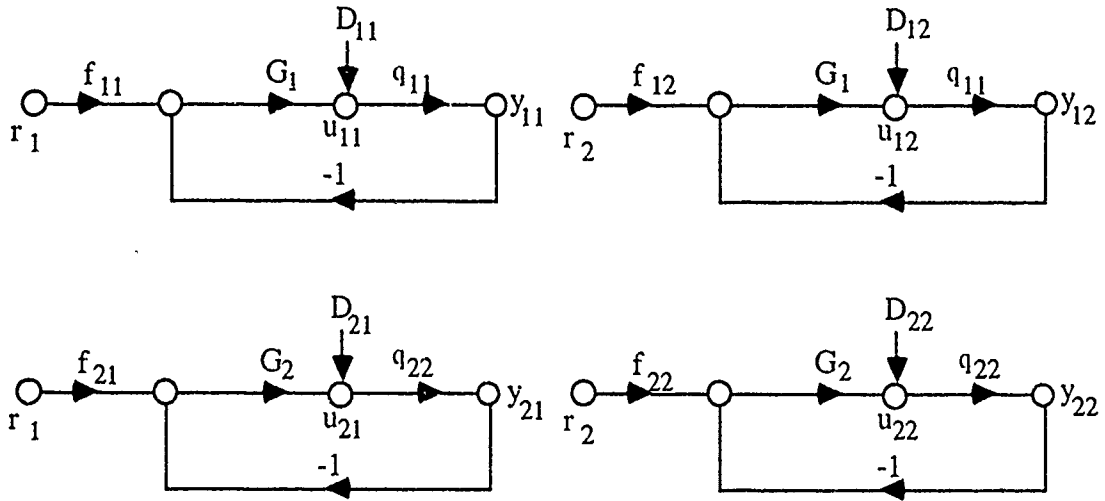


Figure 2.5. Signal Flow Graphs of the Equivalent MISO Loops

$$\mathbf{P}^{-1} = \begin{bmatrix} p_{11}^* & p_{12}^* \\ p_{21}^* & p_{22}^* \end{bmatrix} = \frac{1}{\Delta} \begin{bmatrix} p_{22} & -p_{12} \\ -p_{21} & p_{11} \end{bmatrix} \quad (2.4)$$

where the plant determinant, Δ , is given by

$$\Delta = p_{11}p_{22} - p_{12}p_{21} \quad (2.5)$$

The \mathbf{Q} matrix is then given by

$$\mathbf{Q} = \begin{bmatrix} q_{11} & q_{12} \\ q_{21} & q_{22} \end{bmatrix} = \begin{bmatrix} \frac{1}{p_{11}^*} & \frac{1}{p_{12}^*} \\ \frac{1}{p_{21}^*} & \frac{1}{p_{22}^*} \end{bmatrix} = \begin{bmatrix} \frac{\Delta}{p_{22}} & \frac{-\Delta}{p_{12}} \\ \frac{-\Delta}{p_{21}} & \frac{\Delta}{p_{11}} \end{bmatrix} \quad (2.6)$$

The D_{ij} of Figure 2.5 can be derived by considering the 2x2 sfg of Figure 2.4. For example, D_{11} is determined by considering only the system input r_1 , for which the input-output relationship is given by the following equations:

$$y_{11} = p_{11} u_{11} + p_{12} u_{21} \quad (2.7)$$

$$y_{21} = p_{21} u_{11} + p_{22} u_{21} \quad (2.8)$$

The matrix representation of Equations (2.7) and (2.8) is given by

$$\begin{bmatrix} y_{11} \\ y_{21} \end{bmatrix} = \mathbf{P} \begin{bmatrix} u_{11} \\ u_{21} \end{bmatrix} \quad (2.9)$$

which can be solved for u_{11} and u_{21} as

$$\begin{bmatrix} u_{11} \\ u_{21} \end{bmatrix} = \mathbf{P}^{-1} \begin{bmatrix} y_{11} \\ y_{21} \end{bmatrix} \quad (2.10)$$

Substituting \mathbf{P}^{-1} of Equation (2.4) into Equation (2.10) results in the following expression for u_{11} :

$$u_{11} = \frac{p_{22}}{\Delta} y_{11} - \frac{p_{12}}{\Delta} y_{21} \quad (2.11)$$

This equation can be represented in terms of q_{11} and q_{12} by

$$u_{11} = \frac{y_{11}}{q_{11}} + \frac{y_{21}}{q_{12}} = \frac{y_{11}}{q_{11}} + D_{11} \quad (2.12)$$

Similar developments can be performed with u_{12} , u_{21} , and u_{22} . The complete MISO conversion process is described in reference [12], which results in the MIMO design procedure based on the equivalent MISO systems of Figure 2.4 and the following design equations [12]:

$$t_{1j} = y_{1j} = \frac{f_{1j}L_1 + d_{1j}q_{11}}{1 + L_1} \quad (2.13)$$

$$L_1 = G_1 q_{11} \quad (2.14)$$

$$D_{1j} = \frac{-t_{2j}}{q_{12}} \quad (2.15)$$

The improved QFT method uses the additional information provided by the g_i and f_{ij} of previously designed loops to minimize overdesign. Therefore, the modified equations of the second loop of the 2x2 problem are given by

$$t_{2j} = y_{2j} = \frac{f_{2j}L_{2c} + d_{2j}q_{22}}{1 + L_{2c}} \quad (2.16)$$

$$L_{2c} = G_2 q_{22c} = \frac{G_2 q_{22} (1 + L_1)}{1 - \gamma_{12} + L_1} \quad (2.17)$$

$$\gamma_{ji} = \frac{p_{1j}p_{ji}}{p_{ii}p_{jj}} \quad (2.18)$$

$$D_{2j} = \frac{G_1 f_{1j} p_{21} (1 - \gamma_{12})}{1 - \gamma_{12} + L_1} \quad (2.19)$$

It has been proven that the separate solutions (selection of the appropriate G_i and f_{ij}) which solve the individual MISO uncertainty and disturbance problems are guaranteed to solve the original LTI MIMO uncertainty and disturbance problem [4].

Summary

This chapter presents a very basic overview of nonlinear QFT as applied to the 2x2 MIMO problem of this thesis. Next, the basic design equations and the MISO equivalent representation are given with minimal derivation. Two excellent references [2,12] are also provided for the reader interested in a detailed investigation of the general case method.

III. Equivalent Linear Time Invariant Plants

Introduction

This chapter describes in detail the method in which equivalent linear time invariant plants are generated for this nonlinear QFT design. A nonlinear system can be described by Figure 3.1, in which $y(t) = W(u(t))$.

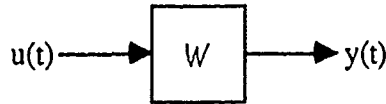


Figure 3.1. Nonlinear System

An equivalent plant as used in this thesis is defined as one which when stimulated with the same input results in the same output achieved from the original plant. The transfer characteristics of W vary with the input, but for any specific input there exists a $P(s)$ such that $Y(s) = P(s)U(s)$, where $Y(s) = \mathcal{L}\{y(t)\}$ and $U(s) = \mathcal{L}\{u(t)\}$. The object of equivalent plant generation is then to determine a LTI $P_e(s)$ which is an approximation to this $P(s)$ when $y(t)$ and $u(t)$ are known only numerically. The method proposed by Golubev, which was used for Kobylarz's SISO design is mathematically detailed, followed by the extension to the MIMO case. Finally, the application of these methods to the design presented in this thesis is fully discussed while some important criteria and possible pitfalls to valid plant generation are pointed out.

Mathematical Development for the Generation of SISO Equivalent LTI Plants.

Given an input-output time history for the nonlinear SISO problem, Golubev proposed the method described below to determine equivalent LTI plants, $P_e(s)$, such that $Y(s) = P_e(s)U(s)$.

Let $P_e(s)$ be represented by a rational function consisting of a polynomial numerator of order m , $N(s)$, and a polynomial denominator of order n , $D(s)$. The relationship can now be written in the following form:

$$D(s)Y(s) = N(s)U(s). \quad (3.1)$$

$D(s)$ can be written as a polynomial of s as

$$D(s) = s^n + d_{n-1} s^{n-1} + d_{n-2} s^{n-2} + \dots + d_1 s + d_0, \quad (3.2)$$

and similarly $N(s)$ can be written in the form

$$N(s) = q_m s^m + q_{m-1} s^{m-1} + \dots + q_1 s + q_0. \quad (3.3)$$

By substituting (3.2) and (3.3) into (3.1) and solving for $Y(s)$, the following is obtained:

$$Y(s) = \frac{1}{s^n} \left[\left(q_m s^m + q_{m-1} s^{m-1} + \dots + q_1 s + q_0 \right) U(s) - \left(d_{n-1} s^{n-1} + \dots + d_1 s + d_0 \right) Y(s) \right] \quad (3.4)$$

This equation in the time domain can then be written as

$$y(t_i) = q_m \int_{t=0}^{t_i} u \, dt + \dots + q_0 \int_{t=0}^{t_i} u \, dt - d_{n-1} \int_{t=0}^{t_i} y \, dt - \dots - d_0 \int_{t=0}^{t_i} y \, dt \quad (3.5)$$

For simplicity in notation, let the n^{th} integral from 0 to t_i of x be represented by $\langle x_i \rangle^n$. By using numerical integration techniques, an input-output time history consisting of k points results in k equations (one for each value of t_i) of the form of (3.5). In matrix notation, this set of equations can be represented by

$$[y(t_i)] = [q_m \langle u_i \rangle^{n-m} + \dots + q_0 \langle u_i \rangle^n - d_{n-1} \langle y_i \rangle - \dots - d_0 \langle y_i \rangle^n] \quad (3.6)$$

where both sides of (3.6) represent column vectors consisting of k rows. Recall that the y 's, u 's, and all of their integrals are known numerically, so the left side of (3.6) is a vector of numbers, while the right side is a vector of polynomials in the unknown q 's and d 's. Note that there are only $n + m + 1$ unknowns, $q_m \dots q_0$ and $d_{n-1} \dots d_0$, but k equations. Provided that $k > n + m + 1$, the system is overdetermined and can be solved using a least squares approach. Element by element multiplications are performed between the column vectors of (3.6) and the $n + m + 1$ column vectors of $[\langle u \rangle^{n-m}] \dots [\langle u \rangle^n]$ and

$[<y>] \dots [<y>^n]$, one at a time. After each vector multiplication, the resulting k equations are then summed to result in a single equation. For example, the first equation is formed as follows. First, recall that (3.6) simply represents a set of k equations. Let j represent an index such that the first equation in (3.6) corresponds to $j = 1$, and the last equation corresponds to $j = k$. The above mentioned multiplications refer to multiplying both sides of the j^{th} equation in (3.6) by the j^{th} element of $[<u>^{n-m}]$ (a numerical value), for all values of j from one to k . This procedure simply consists of multiplying both sides of a linear equation by a constant, which has no effect on the equality of the two sides. Realize, however, that there are k different equations in (3.6), and each is multiplied by a different constant, given by the j^{th} element in $[<u>^{n-m}]$ for the j^{th} equation in (3.6). After this multiplication, there are still k equations, but each has been modified by a constant. These k modified equations are then summed to form a single equation. Note that the addition of two or more linear equations does not affect the equality of the two sides. This procedure is then repeated with the remaining column vectors of the appropriate integrals of u and y mentioned above. Since there are $n + m + 1$ multiplications/summations the result is a linear system of $n + m + 1$ equations with $n + m + 1$ unknowns as given by Equation (3.7) shown on the following page. This relationship can be written as a linear equation of the form $Ax = b$, where x represents a column vector of the unknown coefficients of $N(s)$ and the negative of the coefficients of $D(s)$. The A matrix consists of the terms on the right side of (3.7), (less the unknown coefficients, as shown at the end of this section), and b is the vector on the left of (3.7). Thus the unknown coefficients can be determined by standard linear algebra, $x = A^{-1}b$. In the event that A is ill-conditioned, numerical solution techniques can be used to solve for the unknown coefficients. There are subroutines available for this purpose in both the NAG and IMSL FORTRAN libraries. In this thesis, there are no ill-conditioned matrices, and a relatively simple MATRIXx program is used to compute the exact solution (to working precision) of the linear equations in all cases.

$$\begin{bmatrix} \sum_{i=1}^k \langle y_i | u_i \rangle^{n+m} \\ \cdot \\ \sum_{i=1}^k \langle y_i | u_i \rangle^n \\ \sum_{i=1}^k \langle y_i | y_i \rangle \\ \cdot \\ \sum_{i=1}^k \langle y_i | y_i \rangle^n \end{bmatrix} = \begin{bmatrix} \sum_{i=1}^k \left(\left[q_m \langle u_i \rangle^{n+m} + \dots + q_0 \langle u_i \rangle^n - d_{n-1} \langle y_i \rangle - \dots - d_0 \langle y_i \rangle^n \right] \langle u_i \rangle^{n+m} \right) \\ \cdot \\ \sum_{i=1}^k \left(\left[q_m \langle u_i \rangle^{n+m} + \dots + q_0 \langle u_i \rangle^n - d_{n-1} \langle y_i \rangle - \dots - d_0 \langle y_i \rangle^n \right] \langle u_i \rangle^n \right) \\ \sum_{i=1}^k \left(\left[q_m \langle u_i \rangle^{n+m} + \dots + q_0 \langle u_i \rangle^n - d_{n-1} \langle y_i \rangle - \dots - d_0 \langle y_i \rangle^n \right] \langle y_i \rangle \right) \\ \cdot \\ \sum_{i=1}^k \left(\left[q_m \langle u_i \rangle^{n+m} + \dots + q_0 \langle u_i \rangle^n - d_{n-1} \langle y_i \rangle - \dots - d_0 \langle y_i \rangle^n \right] \langle y_i \rangle^n \right) \end{bmatrix} \quad (3.7)$$

For the SISO problem, the A, b and x matrices are given below:

$$x = \begin{bmatrix} q_m \\ \cdot \\ q_0 \\ -d_{n-1} \\ \cdot \\ -d_0 \end{bmatrix}$$

b is given by the left hand side of (3.7), and A is shown on the following page. Note that A is a symmetric matrix with its diagonal elements given by the sums of the squares of the (n-m)th to the nth integrals of u, and the first to nth integrals of y.

$$A = \begin{bmatrix} \sum_{i=1}^k \langle u_i \rangle^{n-m} \langle u_i \rangle^2 & \dots & \sum_{i=1}^k \langle u_i \rangle^n \langle u_i \rangle^{n-m} & \sum_{i=1}^k \langle y_i \rangle \langle u_i \rangle^{n-m} & \dots & \sum_{i=1}^k \langle y_i \rangle^n \langle u_i \rangle^{n-m} \\ \cdot & \cdot & \cdot & \cdot & \cdot & \cdot \\ \sum_{i=1}^k \langle u_i \rangle^{n-m} \langle u_i \rangle^n & \dots & \sum_{i=1}^k \langle u_i \rangle^n \langle u_i \rangle^2 & \sum_{i=1}^k \langle y_i \rangle \langle u_i \rangle^n & \dots & \sum_{i=1}^k \langle y_i \rangle^n \langle u_i \rangle^n \\ \sum_{i=1}^k \langle u_i \rangle^{n-m} \langle y_i \rangle & \dots & \sum_{i=1}^k \langle u_i \rangle^n \langle y_i \rangle & \sum_{i=1}^k \langle y_i \rangle^2 & \dots & \sum_{i=1}^k \langle y_i \rangle^n \langle y_i \rangle \\ \cdot & \cdot & \cdot & \cdot & \cdot & \cdot \\ \sum_{i=1}^k \langle u_i \rangle^{n-m} \langle y_i \rangle^n & \dots & \sum_{i=1}^k \langle u_i \rangle^n \langle y_i \rangle^n & \sum_{i=1}^k \langle y_i \rangle \langle y_i \rangle^n & \dots & \sum_{i=1}^k \langle y_i \rangle^n \langle y_i \rangle^n \end{bmatrix}$$

SISO Example

This section provides a numerical example of SISO equivalent plant generation to clarify the technique. To simplify the presentation, a limited number of data points are used at the expense of accuracy. Additionally, a known linear transfer function is used to generate the input-output time history to provide further insight to the accuracy of the technique. It is important to note that whether or not the time history is generated by a nonlinear plant is of no consequence. The technique is essentially a curve fitting procedure for numerical data, and the actual nonlinearities of the system do not come into play except that a different P_e must be generated for each input to the nonlinear plant. This example is based on the unit step response of the plant

$$P(s) = \frac{5}{(s+5)} = \frac{q_0}{(s+d_0)} \quad (3.8)$$

The time history is from $t = 0$ to $t = 1$ s, incremented by 0.1s for a total of 11 points. From this point on, it is assumed that only the time histories $u(t)$ and $y(t)$ are known. The order of the numerator, m , is equal to zero, and the order of the denominator, n , is one. Since $n - m = 1 - 0 = 1$, Equation 3.7 implies that only the first integrals of u and y are required. These integrals are easily approximated by

$$\int_0^t f(t)dt \approx \sum_{i=0}^k \frac{f(t_i) + f(t_{i+1})}{2} \Delta t \quad (3.9)$$

where $\Delta t = t_{i+1} - t_i$, and k is the number of points in the interval from zero to t_i . Table 3.1 provides all of the numerical values required to apply the technique. From (3.1) to (3.4), $Y(s)$ is solved to be

$$Y(s) = \frac{1}{s} [q_0 U(s) - d_0 Y(s)] \quad (3.10)$$

From the numerical data of Table 3.1, Equation (3.6) can be written as

$$\begin{bmatrix} 0.0000 \\ 0.3935 \\ 0.6321 \\ 0.7769 \\ . \\ . \\ 0.9933 \end{bmatrix} = \begin{bmatrix} 0.0 \\ 0.1q_0 - 0.0197d_0 \\ 0.2q_0 - 0.0710d_0 \\ 0.3q_0 - 0.1414d_0 \\ . \\ . \\ 1.0q_0 - 0.7972d_0 \end{bmatrix} \quad (3.11)$$

The next step is to perform element by element multiplications of (3.11) and the first integral of u , resulting in the equations of (3.12)

Table 3.1. Numerical Data for SISO Example

t	u(t)	y(t)	$\int_0^t u(t) dt$	$\int_0^t y(t) dt$	$\int_0^t u(t) dt \int_0^t y(t) dt$	$\left(\int_0^t u(t) dt\right)^2$	$\int_0^t y(t) dt \int_0^t u(t) dt$	$\int_0^t y(t) dt$	$\left(\int_0^t y(t) dt\right)^2$
0.0	1.0	0.0000	0.0	0.0000	0.0000	0.00	0.0000	0.0000	0.0000
0.1	1.0	0.3935	0.1	0.0393	0.0020	0.01	0.0077	0.0077	0.0004
0.2	1.0	0.6321	0.2	0.1264	0.0142	0.04	0.0449	0.0449	0.0050
0.3	1.0	0.7769	0.3	0.2331	0.0424	0.09	0.1099	0.1099	0.0200
0.4	1.0	0.8647	0.4	0.3459	0.0894	0.16	0.1932	0.1932	0.0499
0.5	1.0	0.9179	0.5	0.4590	0.1563	0.25	0.2869	0.2869	0.0977
0.6	1.0	0.9502	0.6	0.5701	0.2463	0.36	0.3858	0.3858	0.1648
0.7	1.0	0.9698	0.7	0.6789	0.3514	0.49	0.4869	0.4869	0.2520
0.8	1.0	0.9817	0.8	0.7853	0.4797	0.64	0.5886	0.5886	0.3595
0.9	1.0	0.9889	0.9	0.8900	0.6283	0.81	0.6904	0.6904	0.4861
1.0	1.0	0.9933	1.0	0.9933	0.7972	1.00	0.7919	0.7919	0.6356
Sums			5.1213	3.850	2.8045	3.5861	2.0724		

$$\begin{bmatrix} 0.000 \\ 0.0393 \\ 0.1264 \\ 0.2331 \\ \cdot \\ \cdot \\ 0.9933 \end{bmatrix} = \begin{bmatrix} 0 \\ 0.01q_0 - 0.0020d_0 \\ 0.04q_0 - 0.0142d_0 \\ 0.09q_0 - 0.0424d_0 \\ \cdot \\ \cdot \\ 1.0q_0 - 0.7972d_0 \end{bmatrix} \quad (3.12)$$

Note that all of the coefficients of (3.12) come directly from Table 3.1. Now, all of the rows of (3.12) are summed to form a single equation, given by (3.13). This equation is the first of two which form the linear system $\mathbf{Ax} = \mathbf{b}$. Note that again, the coefficients are directly from Table 3.1.

$$5.1213 = 3.850 q_0 - 2.8045 d_0 \quad (3.13)$$

The second equation is formed in the same manner, except that element by element multiplications are performed with (3.11) and the first integral of y . The second equation can be written by inspection from Table 3.1, and is given by

$$3.5861 = 2.8045 q_0 - 2.0724 d_0 \quad (3.14)$$

Hence, (3.13) and (3.14) form a linear system of equations with two unknowns, and can be written in matrix form as

$$\begin{bmatrix} 3.850 & 2.8045 \\ 2.8045 & 2.0724 \end{bmatrix} \begin{bmatrix} q_0 \\ -d_0 \end{bmatrix} = \begin{bmatrix} 5.1213 \\ 3.5861 \end{bmatrix} \quad (3.15)$$

Comparisons of the A matrix here and Table 3.1 show it to be in the general case form given on page 3-5. Note that for this 2x2 example, the A matrix consists of the four corner elements of the generalized form. The solution to (3.15) is given by

$$\begin{bmatrix} q_0 \\ -d_0 \end{bmatrix} = \begin{bmatrix} 3.850 & 2.8045 \\ 2.8045 & 2.0724 \end{bmatrix}^{-1} \begin{bmatrix} 5.1213 \\ 3.5861 \end{bmatrix} = \begin{bmatrix} 4.8984 \\ -4.8984 \end{bmatrix} \quad (3.16)$$

$P_e(s)$ is then given by

$$P_e(s) = \frac{4.8984}{s + 4.8984} \quad (3.17)$$

A comparison of the actual and "equivalent" time responses and the error between them are shown in Figure 3.2. Considering the crude set of data used to represent the plant (a mere 11 points!), the fit is exceptional. Using the same procedure with 101 data points (0.01s time increment) the fit and error of Figure 3.3 and

$$P_e(s) = \frac{4.999}{s + 4.999} \quad (3.18)$$

are obtained.

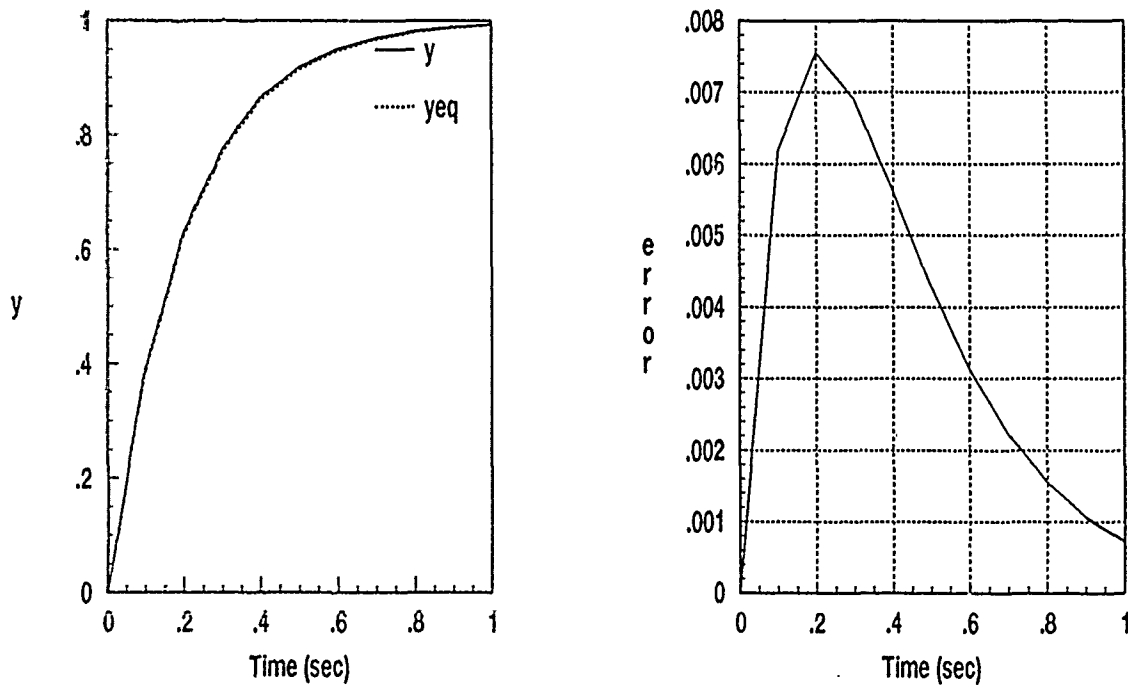


Figure 3.2. Equivalent Plant Fit for the SISO Example Using 11 Data Points

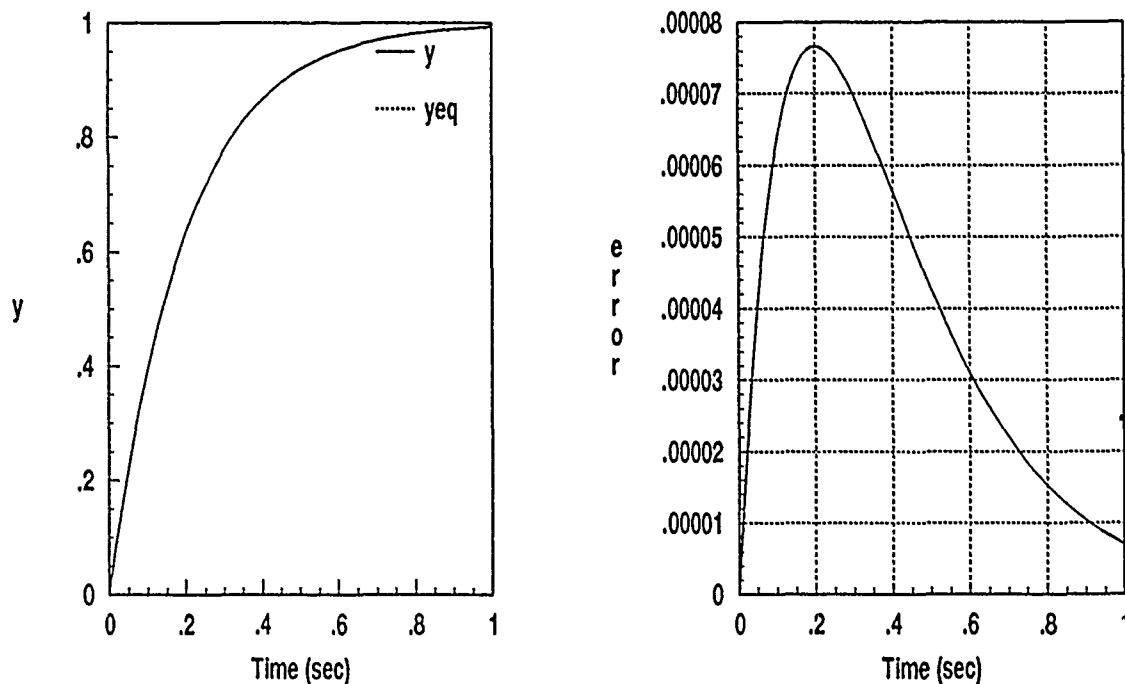


Figure 3.3. Equivalent Plant Fit for the SISO Example Using 101 Data Points

Extension of the Golubev Technique to the MIMO Problem

This technique can be readily extended to the MIMO problem if the individual $p_{ij}(s)$'s in the plant matrix are assumed to have the same denominator. Strictly speaking, the required assumption is that only each of the rows in $P(s)$ have a common denominator. Considering the state space representation, the denominator for all elements of the plant transfer function is determined by $[sI - A]^{-1}$, and one can readily see that this assumption is reasonable. Even if the denominators are different, the requirement can be satisfied by increasing the order of the individual numerators and placing them over a common denominator. In the MIMO problem the Laplace domain input-output relationship is given by $Y(s) = P(s)U(s)$ as in the SISO case, but $Y(s)$ and $U(s)$ are vectors, and $P(s)$ is a matrix. For the 2x2 MIMO problem, the relationship is described by

$$\begin{bmatrix} y_1(s) \\ y_2(s) \end{bmatrix} = \begin{bmatrix} p_{11}(s) & p_{12}(s) \\ p_{21}(s) & p_{22}(s) \end{bmatrix} \begin{bmatrix} u_1(s) \\ u_2(s) \end{bmatrix} \quad (3.19)$$

With the assumption that the denominators on each row are the same, the plants

$$p_{ij}(s) = \frac{N_{ij}(s)}{D_i(s)} \quad (3.20)$$

can be represented in polynomial form by

$$\begin{aligned} D_1(s) &= s^n + d_{n-1} s^{n-1} + \dots + d_1 s + d_0 \\ D_2(s) &= s^h + c_{h-1} s^{h-1} + \dots + c_1 s + c_0 \\ N_{11}(s) &= q_m s^m + q_{m-1} s^{m-1} + \dots + q_1 s + q_0 \\ N_{12}(s) &= r_p s^p + r_{p-1} s^{p-1} + \dots + r_1 s + r_0 \\ N_{21}(s) &= v_x s^x + v_{x-1} s^{x-1} + \dots + v_1 s + v_0 \\ N_{22}(s) &= w_z s^z + w_{z-1} s^{z-1} + \dots + w_1 s + w_0 \end{aligned} \quad (3.21 \text{ a-f})$$

To apply this technique to the MIMO problem, the matrix equation of (3.19) is first broken down into two scalar equations:

$$y_1(s) = p_{11}(s)u_1(s) + p_{12}(s)u_2(s) \quad (3.22)$$

$$y_2(s) = p_{21}(s)u_1(s) + p_{22}(s)u_2(s) \quad (3.23)$$

A method very similar to that for the SISO case is then applied separately to each of (3.22) and (3.23). That is, the technique is applied to (3.22) to compute the coefficients of D_1 , N_{11} , and N_{12} . A second and completely independent application is then used with (3.23) to compute the coefficients of D_2 , N_{21} , and N_{22} . Looking only at the first application, the unknowns are the d_i 's, q_i 's, and r_i 's, and the equation to be solved is

$$D_1(s) y_1(s) = N_{11}(s) u_1(s) + N_{12}(s) u_2(s). \quad (3.24)$$

Similar to the SISO case, the expanded forms of $D_1(s)$, $N_{11}(s)$, and $N_{12}(s)$ are inserted into (3.24) and the resulting equation is solved for $y_1(s)$:

$$y_1(s) = \frac{1}{s^n} \left[(q_m s^m + \dots + q_0) u_1(s) + (r_p s^p + \dots + r_0) u_2(s) - (d_{n-1} s^{n-1} + \dots + d_0) y_1(s) \right] \quad (3.25)$$

A linear equation analogous to the one in the SISO case is formed and solved in the same manner. The only difference here is that additional element by element multiplications of the appropriate integrals of u_2 are also performed, $\langle u_2 \rangle^{n-p} \dots \langle u_2 \rangle^n$, resulting in a total of $n + m + p + 2$ equations and the same number of unknowns. Note that the A matrix is symmetric, and its diagonal elements are given by $\Sigma(\langle u_{1i} \rangle^{n-m})^2, \dots, \Sigma(\langle u_{1i} \rangle^n)^2, \Sigma(\langle u_{2i} \rangle^{n-p})^2, \dots, \Sigma(\langle u_{2i} \rangle^n)^2$, and $\Sigma(\langle y_{1i} \rangle)^2, \dots, \Sigma(\langle y_{1i} \rangle^n)^2$. In this case, the x vector contains the q_i 's, r_i 's, and the negative of the d_i 's. The entire process is then repeated for (3.23) to solve for the v_i 's, w_i 's and c_i 's. In general, the two denominators obtained are not the same. In other words, the resulting equivalent LTI transfer function $P_e(s)$ will have the same denominator only on each row. Since the requirement on $P_e(s)$ is that it be equivalent but not necessarily identical to $P(s)$, this presents no problem.

MIMO Example

Equivalent plant generation for the MIMO problem of order m is broken down into m separate problems with the requirement that all of the elements of the plant matrix on a given row have a common denominator. For the 2×2 problem, the two separate problems consist of:

1. Solving Equation (3.22) for $N_{11}(s)$, $N_{12}(s)$, and $D_1(s)$
2. Solving Equation (3.23) for $N_{21}(s)$, $N_{22}(s)$, and $D_2(s)$

This section looks only at the first part, solving for

$$p_{11e}(s) = \frac{N_{11}(s)}{D_1(s)}, \text{ and } p_{12e}(s) = \frac{N_{12}(s)}{D_1(s)} \quad (3.26)$$

The general form of the A matrix and the b and x vectors are given, as well as the equivalent plants and the plot of the fit and corresponding error. The plants used to generate the time histories are given by

$$p_{11}(s) = \frac{12.8(s+5)}{s^2+8s+64} = \frac{12.8s+64}{s^2+8s+64} = \frac{q_1s+q_0}{s^2+d_1s+d_0}, \text{ and} \quad (3.27)$$

$$p_{12}(s) = \frac{64}{s^2+8s+64} = \frac{r_0}{s^2+d_1s+d_0} \quad (3.28)$$

The first input, $u_1(t)$, consists of a ramped step as shown in Figure 3.4, and $u_2(t)$ is a unit step.

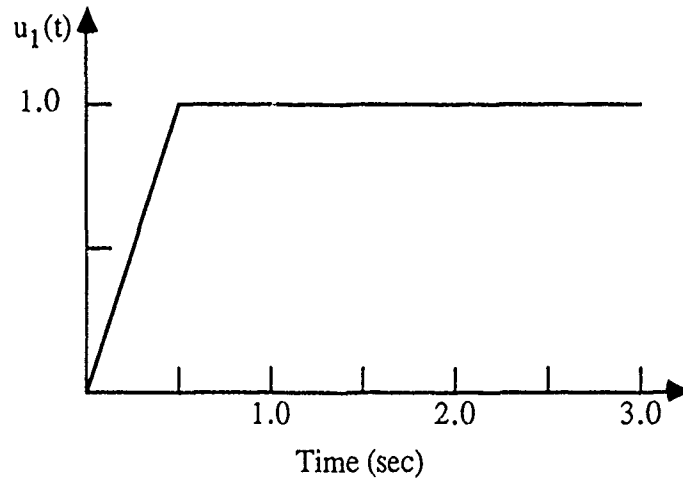


Figure 3.4. $u_1(t)$ for the MIMO Example

The difference in the two inputs brings out an important point for the MIMO problem. All of the inputs to a MIMO plant must be different. That is, for the MIMO problem identical inputs (e.g. simultaneous step commands) are not allowed. The reason for this requirement is clarified later in this example. For this example, Equation (3.25) can be written as

$$y_1(s) = \frac{1}{s^2} \left[(q_1 s + q_0) u_1(s) + r_0 u_2(s) - (d_1 s + d_0) y_1(s) \right] \quad (3.29)$$

In the time domain, (3.29) is given by

$$y_1(t_i) = q_1 \int_0^{t_i} u_1(t) dt + q_0 \int_0^{t_i} \int_0^t u_1(t) dt + r_0 \int_0^{t_i} u_2(t) dt - d_1 \int_0^{t_i} y_1(t) dt - d_0 \int_0^{t_i} \int_0^t y_1(t) dt \quad (3.30)$$

From (3.30) it is apparent that the first and second integrals of $u_1(t)$ and $y_1(t)$ are required, while only the second integral of $u_2(t)$ is needed. These integrals are the "appropriate" integrals mentioned in the previous section that are multiplied with (3.30) (and the resultant k equations summed) to form the $n + m + p + 2 = 2 + 1 + 0 + 2 = 5$ equations required for the linear system of equations represented by A , b , and x . A is given by

$$A = \begin{bmatrix} \sum_{i=1}^k \langle u_{1i} \rangle^2 & \sum_{i=1}^k \langle u_{1i} \rangle^2 \langle u_{1i} \rangle & \sum_{i=1}^k \langle u_{2i} \rangle^2 \langle u_{1i} \rangle & \sum_{i=1}^k \langle y_{1i} \rangle \langle u_{1i} \rangle & \sum_{i=1}^k \langle y_{1i} \rangle^2 \langle u_{1i} \rangle \\ \sum_{i=1}^k \langle u_{1i} \rangle \langle u_{1i} \rangle^2 & \sum_{i=1}^k \langle u_{1i} \rangle^2 & \sum_{i=1}^k \langle u_{2i} \rangle^2 \langle u_{1i} \rangle^2 & \sum_{i=1}^k \langle y_{1i} \rangle \langle u_{1i} \rangle^2 & \sum_{i=1}^k \langle y_{1i} \rangle^2 \langle u_{1i} \rangle^2 \\ \sum_{i=1}^k \langle u_{1i} \rangle \langle u_{2i} \rangle^2 & \sum_{i=1}^k \langle u_{1i} \rangle^2 \langle u_{2i} \rangle^2 & \sum_{i=1}^k \langle u_{2i} \rangle^2 & \sum_{i=1}^k \langle y_{1i} \rangle \langle u_{2i} \rangle^2 & \sum_{i=1}^k \langle y_{1i} \rangle^2 \langle u_{2i} \rangle^2 \\ \sum_{i=1}^k \langle u_{1i} \rangle \langle y_{1i} \rangle & \sum_{i=1}^k \langle u_{1i} \rangle^2 \langle y_{1i} \rangle & \sum_{i=1}^k \langle u_{2i} \rangle^2 \langle y_{1i} \rangle & \sum_{i=1}^k \langle y_{1i} \rangle^2 & \sum_{i=1}^k \langle y_{1i} \rangle^2 \langle y_{1i} \rangle \\ \sum_{i=1}^k \langle u_{1i} \rangle \langle y_{1i} \rangle^2 & \sum_{i=1}^k \langle u_{1i} \rangle^2 \langle y_{1i} \rangle^2 & \sum_{i=1}^k \langle u_{2i} \rangle^2 \langle y_{1i} \rangle^2 & \sum_{i=1}^k \langle y_{1i} \rangle \langle y_{1i} \rangle^2 & \sum_{i=1}^k \langle y_{1i} \rangle^2 \end{bmatrix} \quad (3.31)$$

Note that if $u_1(t)$ and $u_2(t)$ are identical the second and third rows and the second and third columns of A are identical, resulting in a singular matrix. Therefore, in order to solve for the coefficients of $P_c(s)$, the two inputs must be different. If the two inputs represent plant inputs from a closed loop system, as in this thesis, this restriction is not likely to cause a

problem. If the technique is to be used on an open loop plant (as in this example), and step responses are desired, one of the inputs can be ramped as done here. The x vector for this example is given by

$$x = [q_1 \ q_0 \ r_0 \ -d_1 \ -d_0]^T, \quad (3.31)$$

and b is given by

$$b = \begin{bmatrix} \sum_{i=1}^k y_{1i} \langle u_{1i} \rangle \\ \sum_{i=1}^k y_{1i} \langle u_{1i} \rangle^2 \\ \sum_{i=1}^k y_{1i} \langle u_{2i} \rangle^2 \\ \sum_{i=1}^k y_{1i} \langle y_{1i} \rangle \\ \sum_{i=1}^k y_{1i} \langle y_{1i} \rangle^2 \end{bmatrix} \quad (3.32)$$

Solution of the equation $x = A^{-1}b$, using three second time histories with a 0.01s time increment ($k = 301$) gives

$$x = \begin{bmatrix} q_1 \\ q_0 \\ r_0 \\ -d_1 \\ -d_0 \end{bmatrix} = \begin{bmatrix} 12.6555 \\ 64.1198 \\ 62.1678 \\ -7.9482 \\ -63.1424 \end{bmatrix} \quad (3.33)$$

Inserting these coefficients into (3.27) and (3.28) gives

$$p_{11c}(s) = \frac{12.6555s + 64.1198}{s^2 + 7.9482s + 63.1424}, \text{ and } p_{12c}(s) = \frac{62.1678}{s^2 + 7.9482s + 63.1424} \quad (3.34)$$

The fit and error of the equivalent plant are given in Figure 3.5.

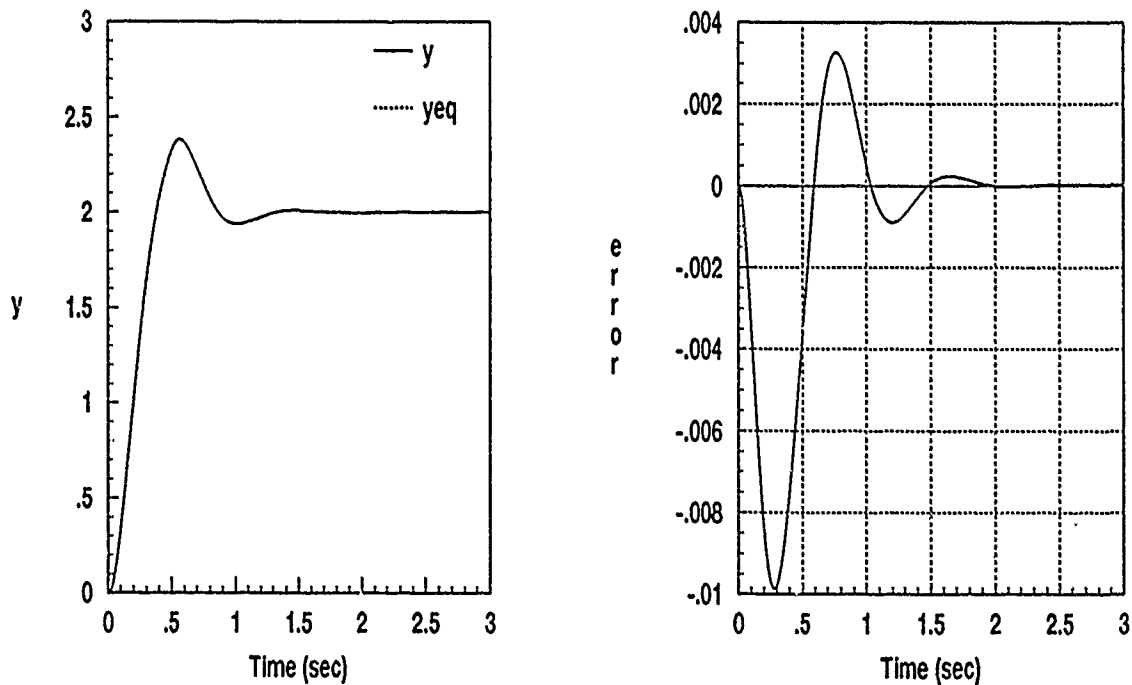


Figure 3.5. Fit and Error for the MIMO Example

Generation of Equivalent LTI Plants

This section explains in detail how the equivalent linear time invariant plants used in this thesis are generated. Both the Golubev technique for SISO systems and the modified technique for MIMO systems are implemented in MATRIXx, and these programs are henceforth referred to as SISOTF and MIMOTF respectively. The two programs have been significantly tested with known transfer functions, and give excellent fits. Fits on the actual equivalent transfer functions used in the design and their errors are shown in Appendix B.

A FORTRAN implemented YF-16 simulator is used to generate sets of input-output time histories for plant generation. The simulator was provided by Tom Cord of WRDC, and it represents the full nonlinear six degree of freedom equations of motion for the YF-16. The original control system in the simulator is significantly modified to ease the task of filling the response envelopes. Since this thesis is limited to a 2x2 system, the original rudder and leading edge flap controls are left intact. In fact, the entire flight control system is left intact, except that the connections to the elevator and ailerons are broken and controlled independently of the original control system. Both loops are closed with pure gain compensators, as shown in Figure 3.6.

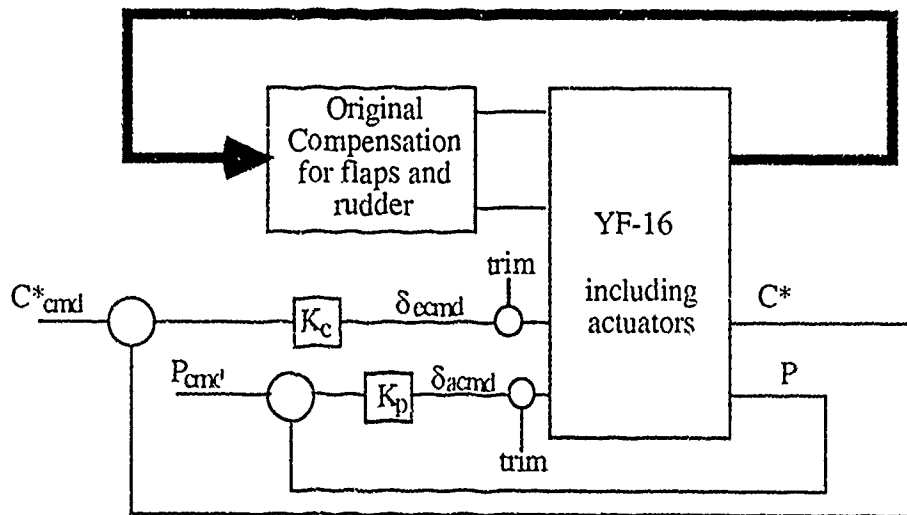


Figure 3.6. Modified YF-16 Simulator

The use of pure gain compensation results in tight loops whose outputs are very similar to the commanded inputs, which makes it a relatively simple task to fill the desired response envelope. Additionally, since the gains K_c and K_p do not affect the equivalent plant, they can be altered from run to run. During the simulator runs, surface commands to the actuators (inputs) and aircraft responses (outputs) are recorded. These input-output histories are

then used with MIMOTF to generate a set of equivalent LTI plants which represent the YF-16 for the full range of desired responses.

The inputs used for plant generation are δ_{ecmd} and δ_{acmd} as shown in Figure 3.6, while the outputs are C^* and p . Notice that the elevator and aileron trim values are not included in the plant input as far as linear plant generation is concerned. Theory requires that the inputs used for equivalent plant generation should include only the inputs which are directly responsible for the obtained outputs [7]. In the case of C^* , the addition of the trim value is enough to make the input appear as a negative step, which results in stable plants for the YF-16's longitudinal axis. Since this axis is well known to be unstable, these plants obviously cannot be equivalent to the actual system. Figure 3.7 clarifies the difference in the plant generation with and without including the trim value. In the figure, "delta de" represents the change in elevator only (no trim), and "de" includes the trim value.

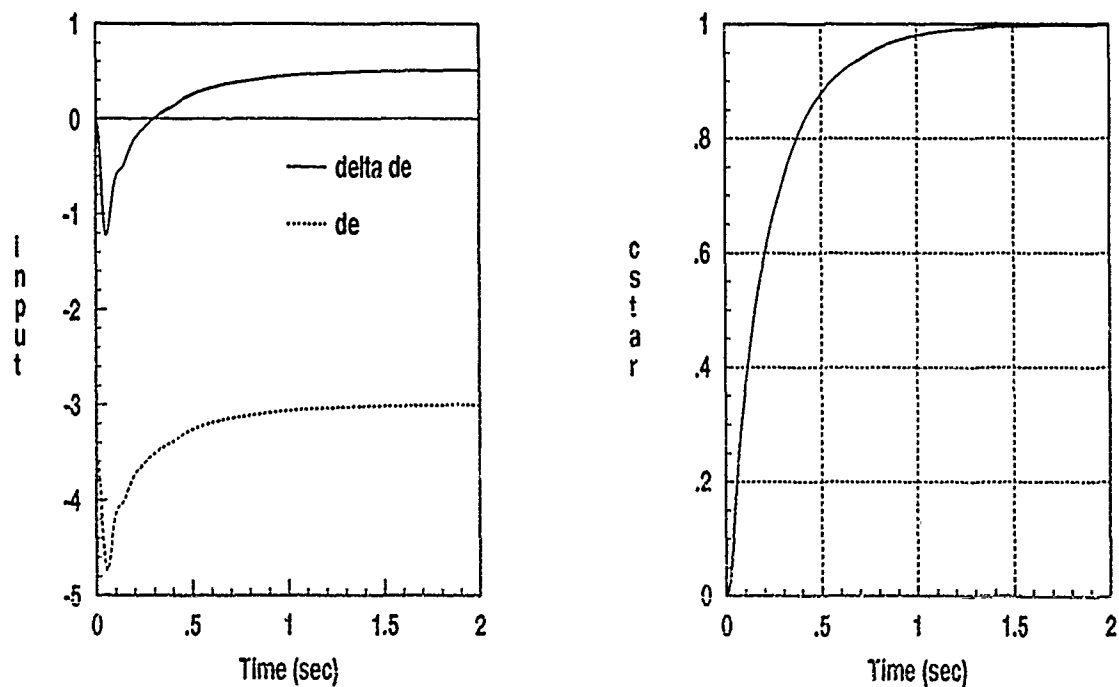


Figure 3.7. Effects of Including Trim

Note that when the trim value is included, the input looks like a negative step with significant overshoot. A relatively slow, stable transfer function could easily be matched to the resulting input-output pair. On the other hand, without the trim value the input has a large negative peak to initiate the response, but a positive final value to maintain the condition. Right half plane poles are required to match this input output pair, as is expected for a longitudinal F-16 transfer function. It should be clarified that the plant used in this design is defined to be the YF-16 with the original rudder and leading edge flap compensation in place, and open-loop simulations verify that the leading edge flap compensation is not sufficient to stabilize the longitudinal axis.

For the C^* loop, an interesting technique is used to drive the system to the desired output set. Since the system outputs closely resemble the commanded inputs, weighted averages of the response envelope are used to drive the system. As a result, the response envelope is filled rather nicely. Problems are encountered, however, in determining equivalent plants for most of the cases with overshoot and no undershoot that do not violate the requirements of $\{q_{ii}\}$ having no phase uncertainty at infinity. Therefore, those responses are not used in the design. Instead, underdamped responses which contain both undershoot and overshoot are used to fill the upper area of the response bounds.

For the roll rate responses, the driving inputs consist of filtered steps. That is, first order filters of varying speeds are formed in MATRIXx, and the step responses of those filters used as inputs to the roll channel.

A total of 22 equivalent LTI plants are developed for the design using MIMOTF with actual simulator responses. These plants represent the YF-16 at the two flight conditions 0.9 M, 20 thousand feet and 0.6 M, 30 thousand feet. The maximum commands are 2.2 g's for C^* and 30°/s for roll rate. At the second flight condition, the system reaches moderately high angles of attack up to approximately 15°. These system responses enclosed in their respective bounds are shown in Figure 3.8, and the plant transfer functions are

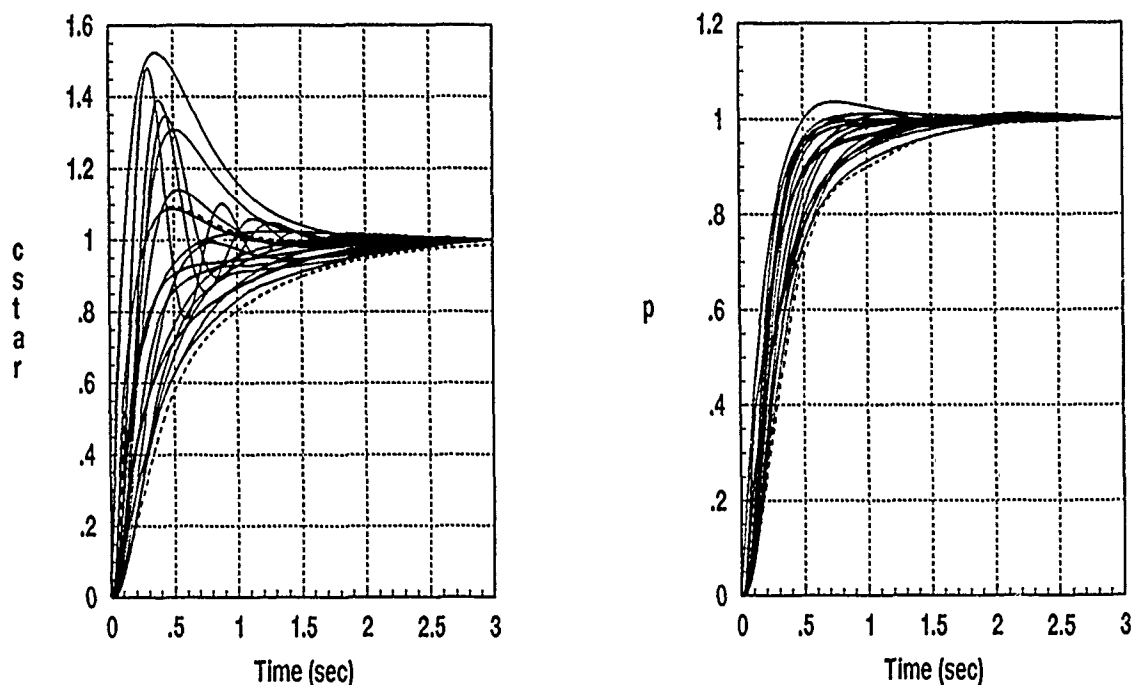


Figure 3.8. System Responses Used for Equivalent Plant Generation

given in appendix A. It should be noted that the original thumbprints were somewhat less severe, but have been tightened around the achieved responses to provide for a more stringent test on the design.

Cautions and Pitfalls

The generation of equivalent plants for the MIMO problem requires an additional consideration. For a response of the form

$$y_1 = y_{11} + y_{12}$$

there exists an infinite number of solutions because of the addition involved. It is not sufficient, however, to get a good fit on only the response y_1 , but it also is important to accurately model the individual components y_{11} and y_{12} . In the nonlinear problem, superposition does not apply, and the individual components of the response are not available.

When using the programs SISOTF and MIMOTF, the user must specify the order of each polynomial numerator and denominator. In general, a good fit on the response can be found with several different combinations. As described above, a good fit on the response does not necessarily imply a valid plant. This issue has not been rigorously resolved, but a possible approach is to check the individual elements of the time response using the "equivalent" plant to ensure that they at least make physical sense. For instance, if one tries to force unrealistic equivalent plant fits (e.g. no rhp poles in the longitudinal axis), the result is a good fit on the overall response, but analysis of the individual components implies that both outputs are primarily a function of aileron deflection. This scenario does not agree with the physical system, so these "equivalent" plant models are obviously invalid and must be discarded. The approach used in this thesis includes an additional measure to ensure that the plants are at least reasonable, by staggering the inputs by one second. That is, for each set of commanded inputs, one is commanded at time $t=0$, while the second input is not applied until $t=1$ s. Some runs have C^* first, while others have C^* as the delayed response. The delay is applied to each of the variables with the intent that the range of plant uncertainty includes the case of simultaneous responses. This staggering effect forces MIMOTF to at least reasonably weight the individual components of the response since during the first second one of the inputs is zero and there exists a substantial response on only one of the outputs. An analysis of the individual components of the responses of the generated plants when simulated with the input with which they were derived shows them to all be reasonable at least for the majority of the run. In some plant cases, toward the end of the run the individual components of y_{11} and y_{12} begin to diverge in opposite directions with a cancelling effect. Horowitz [4] points out that in reality, the control system forces the plant input to contain right half plane zeros to exactly cancel the right half plane poles of the plant, so this apparent divergence from reality is not necessarily a real problem. An additional aid in the generation of the equivalent plants is to run input-output time histories for a longer time period than that on which the design is to be based. In some

cases, the "equivalent" plants are only valid for the first 80 or 90% of the run. That is, three second responses are considered to be sufficient for the desired outputs, but the plant generation runs are extended to five seconds to prevent premature divergence of the unstable longitudinal equivalent plants.

A priori knowledge of the order of the individual plant elements can provide a starting point in the search for equivalent plants. This knowledge can be obtained from preexisting linear models or the nonlinear differential equations if available. Trial and error may also be used, but for a system of order m , there are $m + 1$ orders which must be specified (each numerator and a single denominator for each row of the plant matrix) for each application of the technique to a given problem. The number of permutations of these input parameters grows rapidly with the order of the plant matrix.

Summary

This chapter provides a mathematical development of the methods used to generate a set of equivalent LTI plants that represent a single nonlinear system. The SISO case is developed first, followed by an extension to the MIMO problem. Specific examples are provided for both the SISO and MIMO problems. These methods are implemented in MATRIXx with the programs SISOTF and MIMOTF respectively. Following the mathematical development, the application of these methods to the design of this thesis is described in detail. Finally, some cautions and possible pitfalls to valid plant generation are discussed.

IV. Inner Loop Design

Introduction

This chapter describes the design of the compensation for the two inner loops, f_{11} , f_{22} , g_c , and g_p of Figure 4.1.

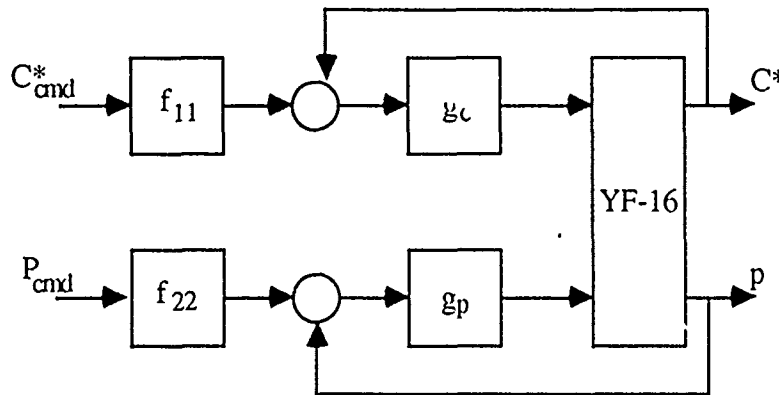


Figure 4.1. Inner Loop Compensation

Since the designs are based on the equivalent MISO systems described in Chapter 2, in this chapter the term 'plant', or P refers to the equivalent MISO plant, q_{ii} . In both designs regard to overdamping is neglected and the only criteria considered is stability and the requirement for a maximum open-loop crossover frequency of 30 rad/s to ensure sufficient attenuation of structural modes. That is, tracking and disturbance bounds are not determined and maximum loop transmission is obtained while meeting the crossover and stability requirements. The reason for neglecting tracking and disturbance boundaries is that Horowitz's experience suggests that the 30 rad/s crossover requirement is the dominant constraint, which means that a detailed QFT design to satisfy the tracking and disturbance requirements with minimum overdamping would result in higher crossover frequencies. The decision is made to design the roll rate compensator first because of lesser uncertainty present.

Design Requirements

There are basically three requirements on the completed design:

1. The time domain responses fall within the specified envelopes.
2. Stability margins of 6 dB and 45 degrees are maintained.
3. A maximum crossover frequency of 30 rad/s is maintained for all plant cases.

As mentioned previously, only the stability and crossover frequency requirements are considered. By obtaining maximum loop transmission, the tracking and disturbance requirements are automatically satisfied if they are obtainable. The expectation that the crossover requirement would be dominant is substantiated by the simulation results in the following chapter. Note that even if this had not been the dominant constraint, the increased loop transmissions are still helpful for gust alleviation and robustness over a larger range of uncertainty.

Templates

Templates which represent the entire plant uncertainty in the frequency domain are formed by plotting the magnitude and phase of each of the plants for each separate frequency of interest. A general rule of thumb is to pick frequencies about an octave apart until the templates become a vertical line (no uncertainty in phase). The approach taken in this thesis however, is to generate a set of frequencies of interest based on the appearance of the composite frequency response plots of Figure 4.2. Areas which contain extreme variations dictate that many frequencies should be looked at while areas where minimal change takes place can be handled with fewer templates. The templates used here are computer generated by MATRIXx and scaled to the size of the Nichols chart used in the design by modifying the header of the MATRIXx postscript output file. Since the templates are easily generated, a large number of them are made. When little variation exists in the templates of a certain frequency range they result in very similar boundaries and only the most restrictive (highest frequency) need be drawn on the Nichols chart.

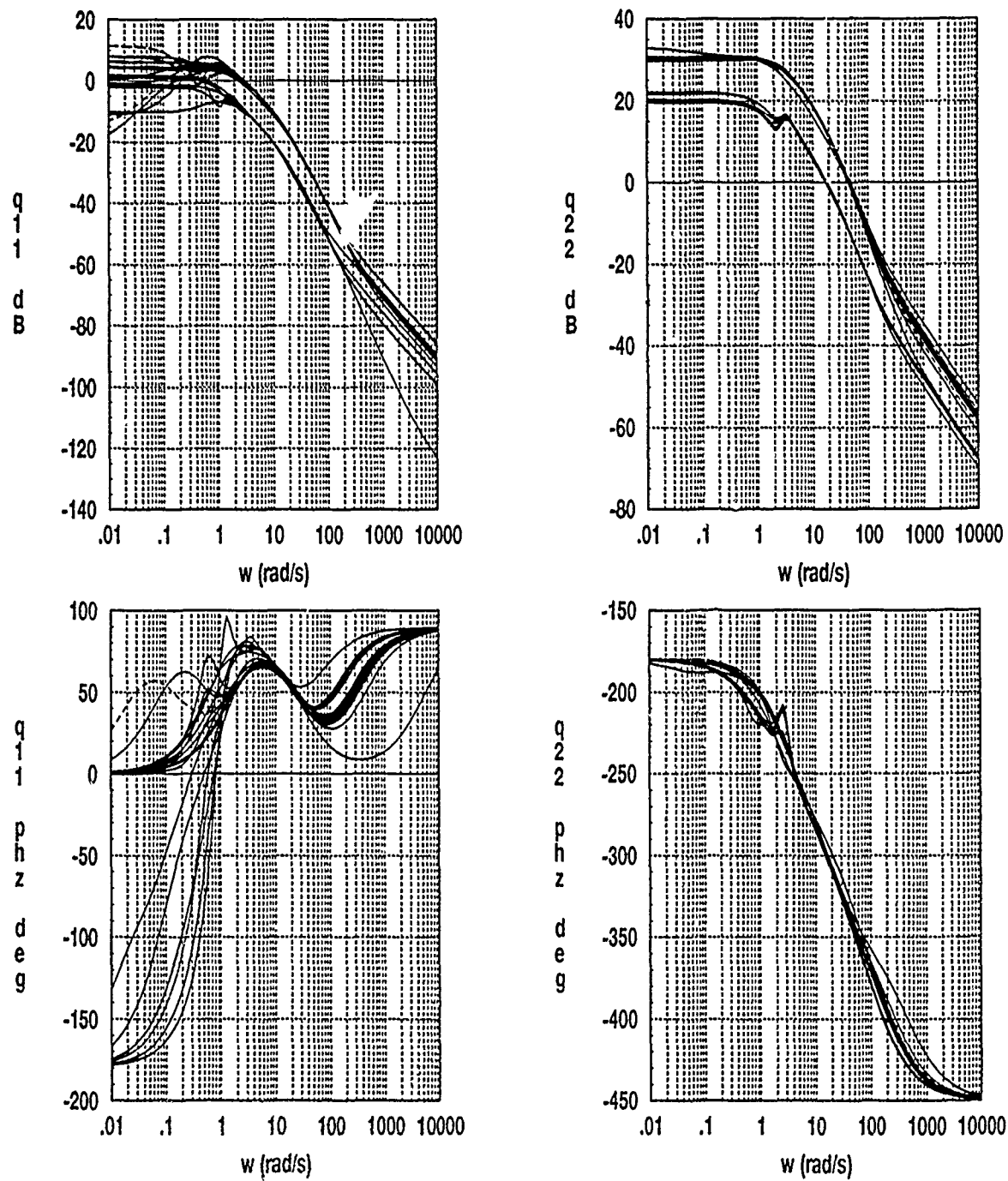


Figure 4.2. Uncertainty of the Uncompensated System

The plots of Figure 4.2 provide insight into the characteristics of q_{11} and q_{22} that are worth mentioning. For instance, they bring out the fact that both q_{11} and q_{22} have an excess of one pole, since all cases have a final slope of -20 dB/decade. One case for q_{11} has a very large zero, and the -20 dB/decade final slope is not entirely obvious from the figure. Also, q_{11} contains two right-half plane poles in some cases, and only one in others. Since q_{22} has a -20 dB/decade final slope, indicating the one excess pole, but 270° of phase change, it can be noted that in all cases q_{22} contains one right-half plane zero.

Loop Shaping

A spread sheet is used to aid in the loop shaping process, that is, synthesizing Equation (4.1).

$$GP_o = L_o = \frac{K_m \left(\frac{s}{z_1} + 1\right) \left(\frac{s}{z_2} + 1\right) \dots \left(\frac{s}{z_m} + 1\right)}{\left(\frac{s}{p_1} + 1\right) \left(\frac{s}{p_2} + 1\right) \dots \left(\frac{s}{p_n} + 1\right)} \quad (4.1)$$

Figure 4.3 shows the spread sheet work area. First, the nominal plant must be entered into the spread sheet. Real poles and zeros are added by their location, with left-half plane roots entered as positive numbers and right-half plane roots negative for convenience, since most of the roots involved are in the left-half plane. Complex pairs are added in terms of ζ and ω_n providing maximum frequency domain insight. The compensator poles and zeros can then be added while the total magnitude and phase response for the entire loop for any frequency of interest can be immediately observed. The loop gain K_m , located in the middle of the spreadsheet, is also an input variable which represents the gain for L of the form of (4.1). The gain K , at the top of the spreadsheet is automatically updated to the value of the numerator constant for L in the standard polynomial form of (4.2).

k= 27742.78891						
Sum Mag	Sum Phz	Frequencies of Interest	poles		zeros	
			mult	location	mult	location
24.71134	-90.96928	0.1	1	origin	-----	-----
1.376842	-104.4903	1.5	1	3.7433	1	8.0405
-0.961021	-109.3418	2	1	48	1	300
-2.682453	-114.2885	2.5	1	13.5335	1	4
-3.994819	-119.4008	3	1	40	0	300
-5.013132	-124.7416	3.5	1	4	0	2
-5.810567	-130.3579	4	0	300	0	15
-6.933162	-142.5149	5	0	48	0	20
-7.633821	-155.9238	6	1	cmplx pole #1	km= 1.72	
-8.073097	-170.484	7	zeta	0.5		
-8.35038	-186.0333	8	wn	100		
			0	cmplx pole #2	1	cmplx z #1
			zeta	0.3591417	zeta	1
			wn	3.007448	wn	5
			0	cmplx pole #3	0	cmplx z #2
			zeta	0.4	zeta	0.3734335
			wn	175	wn	2.585762
			delay	0.3		

Figure 4.3. Spreadsheet Work Area

$$L_o = \frac{K(s^{in} + c_{m-1}s^{m-1} + \dots + c_1s + c_0)}{(s^n + d_{n-1}s^{n-1} + \dots + d_1s + d_0)} \quad (4.2)$$

Additionally, any of the ten frequencies can be changed to any value providing the capability to see the big picture, or zoom in on any specific range. Magnitude and phase contributions of the individual poles and zeros are also available on another area of the spreadsheet, but are of little use since they are generally known. They are useful however for very fine adjustments in the loop shape.

With the aid of a loop shaping tool such as the spread sheet mentioned above, the loop shaping process is relatively straight forward. By beginning the loop with the nominal plant poles and zeros, the complexity of the compensator is reduced since the nominal plant must be divided out of this nominal loop to determine the compensator G. Compensator

poles and zeros are added to bring the loop down the edge of the stability bounds. A high frequency complex pair of poles is generally added at the end to provide maximum attenuation for high frequencies where the design model may no longer be valid. Since $L_0 = GP_0$, the compensator G is calculated by simply dividing the nominal plant out of L_0 .

P Loop Compensator

Plant number 22 is used as the nominal plant for the p loop design. The criteria for choosing the nominal plant primarily is a personal choice, but by choosing a point on the left side of the template the stability bounds are usually closer together and easier to deal with. Figure 4.4 shows the uncompensated Nichols plot along with a few of the stability bounds. The stability contour is determined by the required gain and phase margins. The 3 dB contour corresponds to a 45° phase margin, but to ensure the 6 dB gain margin requirement, it must be extended on the lower half as shown in Figure 4.4. The general idea, is to hug the stability bounds as close as possible, while not violating them. For this thesis, the designs are made as to provide maximum loop transmission at all frequencies while meeting the stability and crossover frequency requirements. Since the template at 30 rad/s is 13 dB in magnitude and the nominal plant is located at the bottom of the template, the nominal loop must fall at -13 dB at 30 rad/s to guarantee a 30 rad/s crossover for all plant cases. The compensator g_p is originally determined to be

$$g_p(s) = \frac{-180(s+4)(s+10)(s+20)}{s(s+6)(s^2+100s+15,625)} \quad (4.3)$$

For reasons which are discussed in detail in the following chapter, the roll compensator used for the final loop shape of Figure 4.5 is modified to

$$g_p(s) = \frac{-259.2(s+4)(s+25)(s+30)}{s(s+10)(s^2+140s+30,625)} \quad (4.4)$$

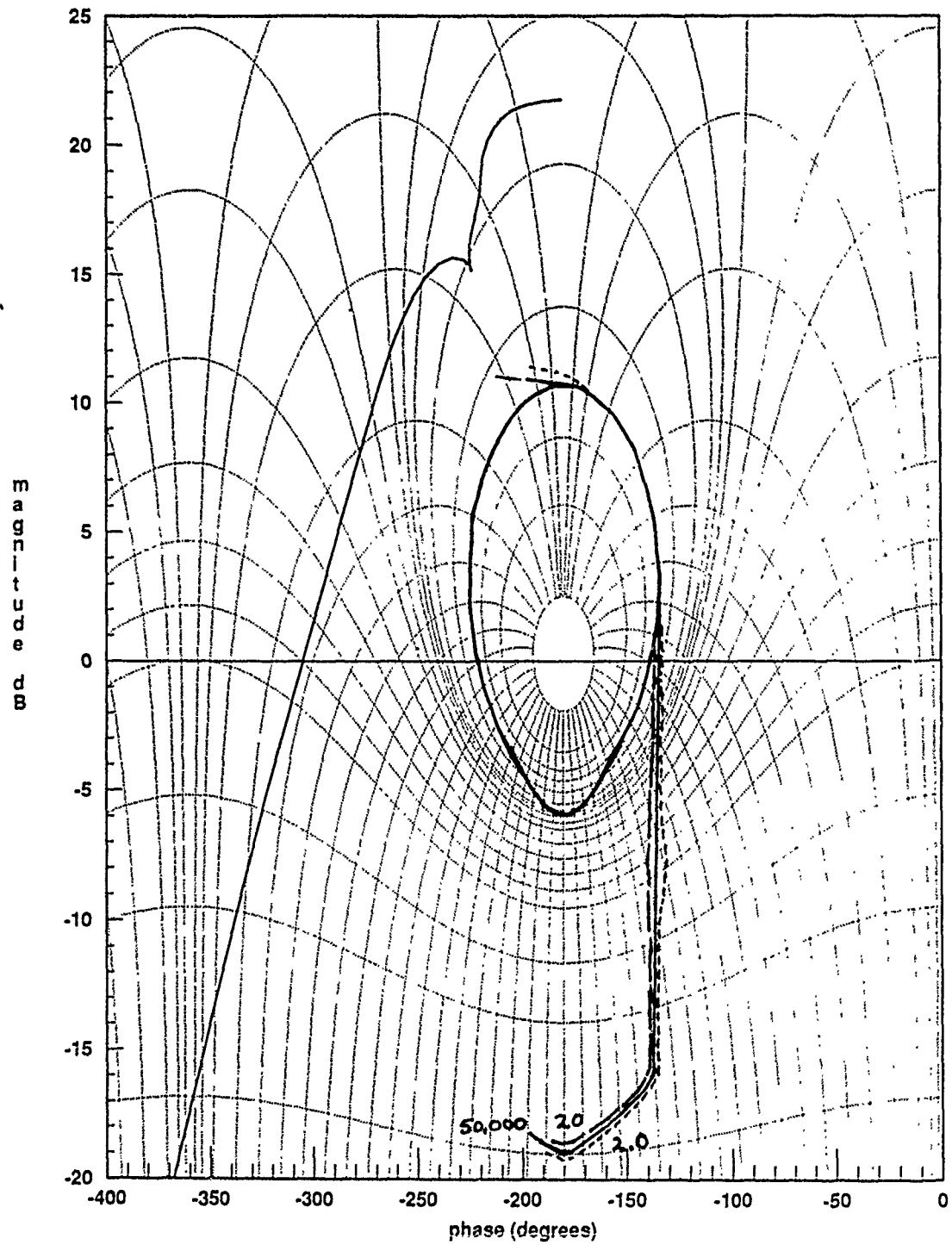


Figure 4.4. Uncompensated Roll Loop and Stability Bounds

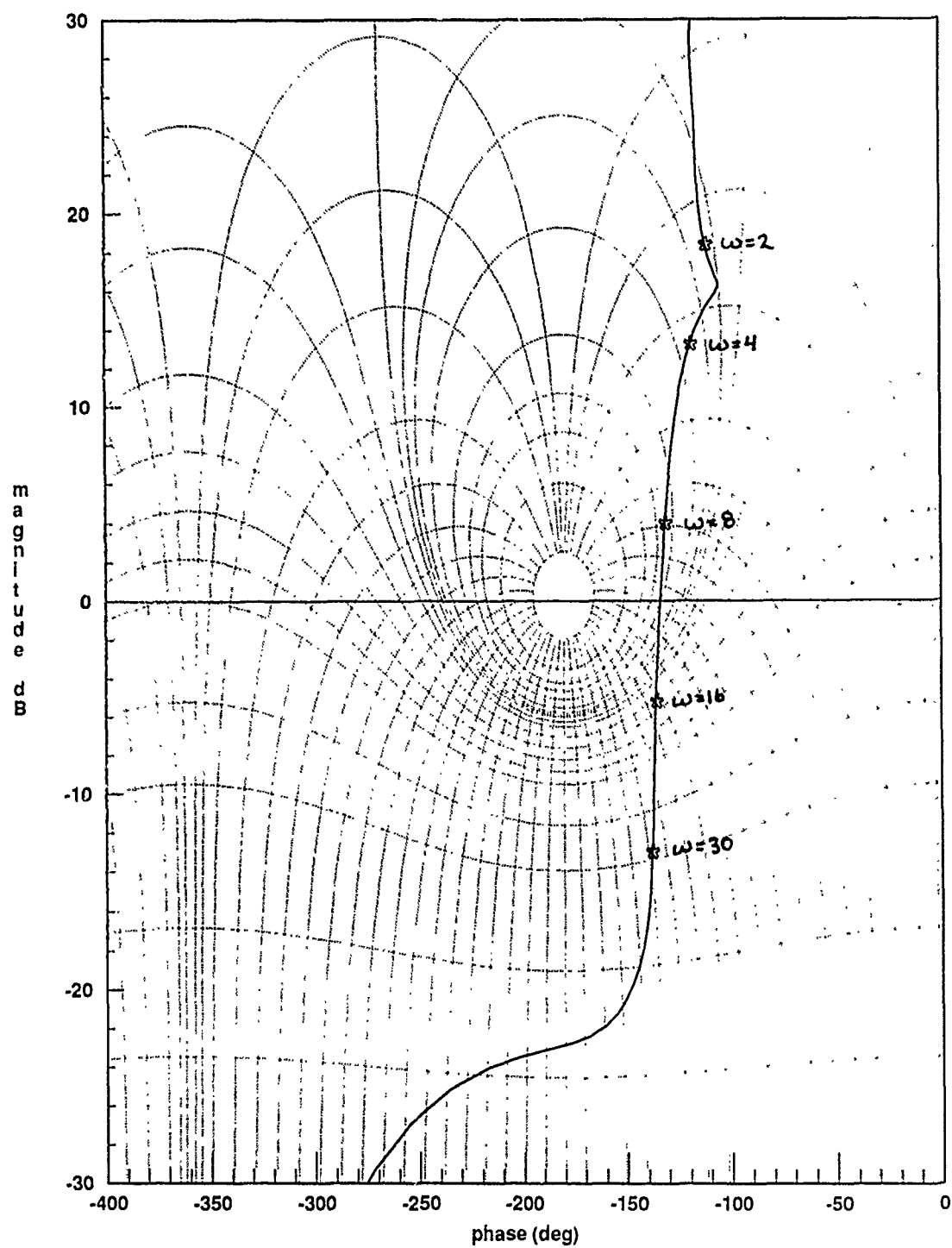


Figure 4.5. Compensated Roll Loop

C Loop Compensator*

Plant 2 is chosen as the nominal plant for the C* loop. The stability requirements for this loop are the same as in the roll channel, 3 dB and 45°. As described in Chapter 2, the second loop design is based on modified design equations involving q_{22eq} . In this design, however; the frequency response for q_{22eq} is identical to that of the original q_{22} , and the second loop design is based on the original equivalent plants derived in Chapter 3. The uncompensated nominal plant is shown on the Nichols chart of Figure 4.6. With the aid of the spreadsheet mentioned above, compensator poles and zeros are added to the nominal plant to end up with the loop shape of Figure 4.7, shown with a few of the stability bounds. In this case, the nominal plant is located at the top of the template, so a 30 rad/s crossover of the nominal loop guarantees the required maximum crossover frequency for all plant cases. The compensator, $g_c(s)$ is then determined to be

$$g_c(s) = \frac{-1665(s+2)(s+15)(s+26)}{s(s+10)(s^2+75s+5625)} \quad (4.4)$$

Prefilters

Figure 4.8 shows the frequency domain thumbprints with the frequency response for the completed inner loop design without prefilters. The prefilters, f_{11} for C*, and f_{22} for roll rate can essentially be determined by inspection from Figure 4.8. For roll rate, the response needs to be lowered by approximately 20 dB/decade starting at roughly 3.5 rad/s. Note that violations of the thumbprint at high frequencies does not present a problem since the desired control ratios can be augmented with nondominant poles to spread the magnitude variation at high frequencies without significantly affecting the time response. Based on the discussion above, f_{22} is determined to be

$$f_{22}(s) = \frac{3.5}{s+3.5} \quad (4.6)$$

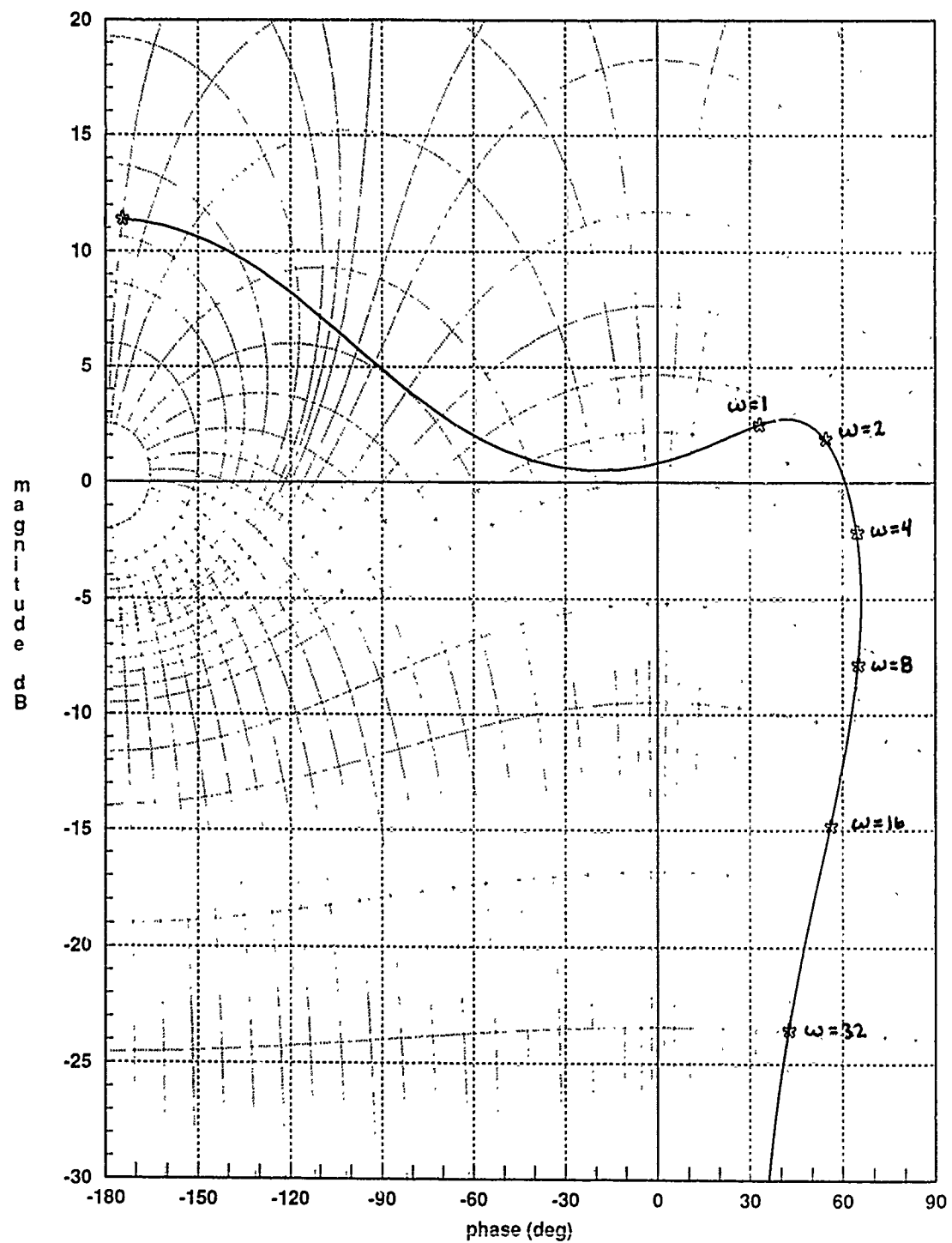


Figure 4.6. Uncompensated C* Loop

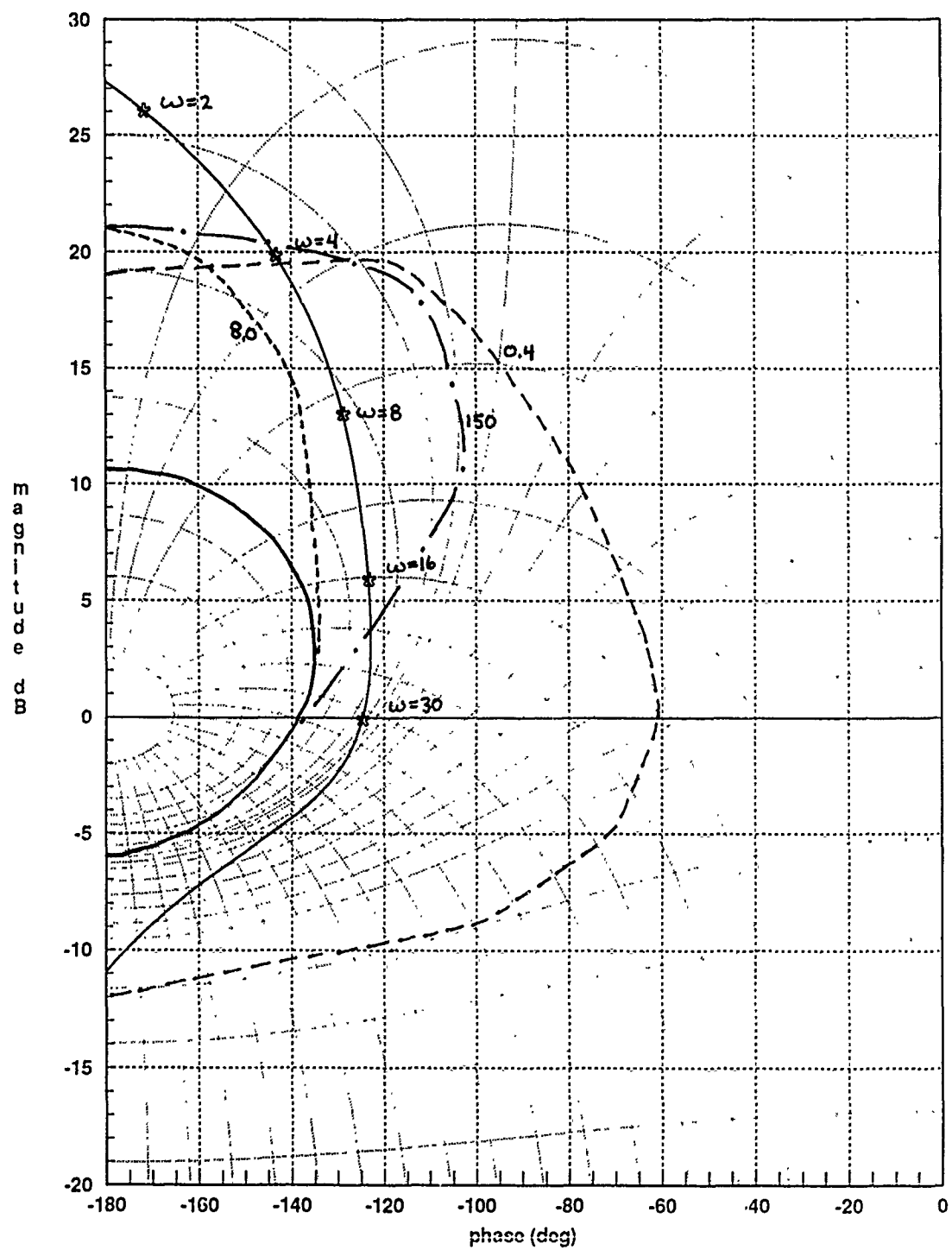


Figure 4.7. Compensated C* Loop and Stability Bounds

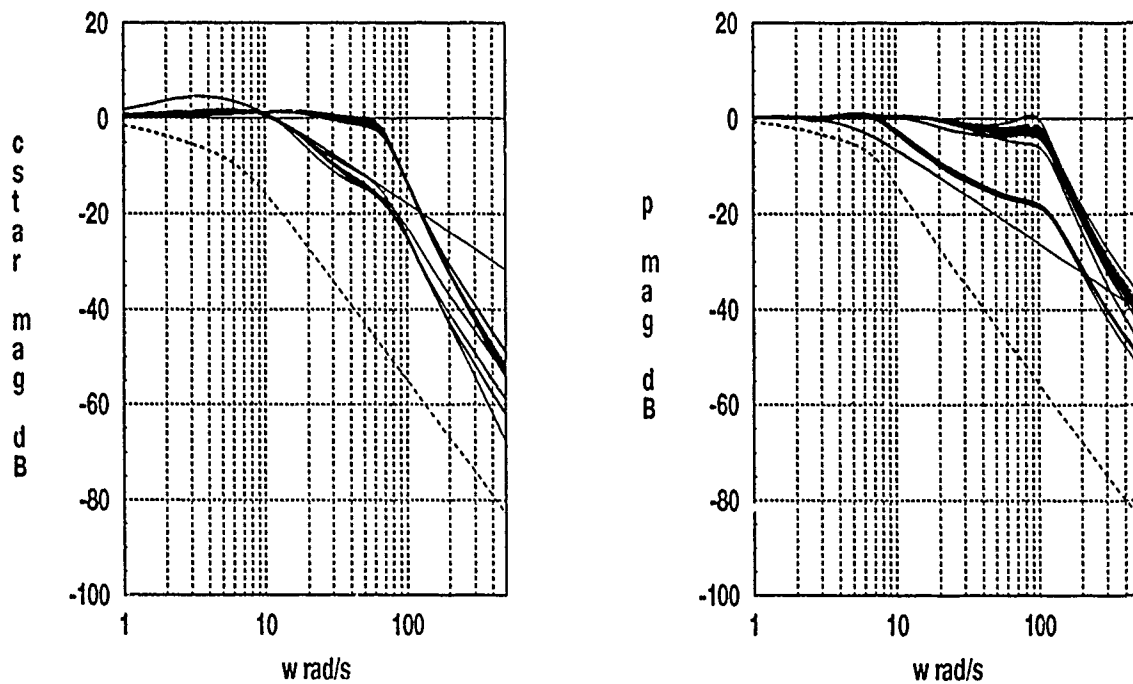


Figure 4.8. Compensated Responses Without Prefilters

The frequency response for the C* loop is slightly more complicated. The response needs to be lowered starting around 4 rad/s, but a single pole there would result in significant violations of the lower bound at later frequencies. A zero is placed at 40 rad/s to prevent these lower bound violations, and finally another pole is placed at 300 for additional high frequency attenuation. The resultant prefilter for C* is therefore chosen to be

$$f_{11}(s) = \frac{30(s + 40)}{(s + 4)(s + 300)} \quad (4.7)$$

The frequency response with prefilters are shown for both cases in Figure 4.9. Note that in both cases the responses are adequately enclosed within the thumbprints. The high frequency violations are not a problem for the reasons discussed above.

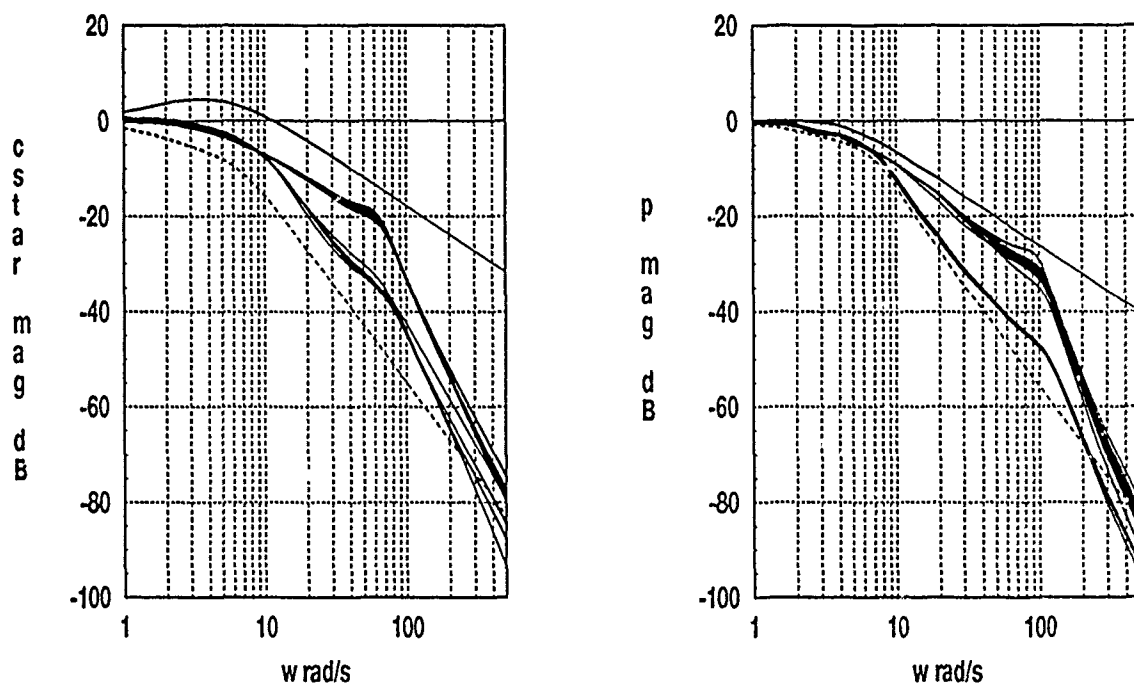


Figure 4.9. Compensated Responses With Prefilters

Summary

This chapter presents the design of the inner loop compensators \mathbf{G} and \mathbf{F} given by Equations (4.8) and (4.9).

$$\mathbf{G} = \begin{bmatrix} g_c & 0 \\ 0 & g_p \end{bmatrix} \quad (4.8)$$

$$\mathbf{F} = \begin{bmatrix} f_{11} & 0 \\ 0 & f_{22} \end{bmatrix} \quad (4.9)$$

Simulations are provided in the following chapter, as well as a discussion on the modifications made to the roll compensator, g_p .

V. *Simulation of the Inner Loop*

Introduction

This chapter describes the simulation of both inner loop compensators. Two simulations are performed: a MATRIXx simulation with the equivalent linear design models, and a full nonlinear simulation with the original FORTRAN simulator used to generate the design models. The first simulation is used to validate the design, while the second is used to determine the validity of the design models. Also, modifications made to the roll compensator to improve the nonlinear performance are detailed.

Linear Simulations

C Linear Simulation.* The first linear simulation is that of the C* compensation with the equivalent LTI design models via MATRIXx system build. For the linear simulations, the response is independent of the input magnitudes and only unit step simulations are performed. The linear simulation of all plant cases is shown in Figure 5.1. The responses are all predominantly within the bounds with only minor excursions toward the end of the run. These excursions are from the plants at flight condition 2 and are due to small complex zeros in the linear plants. These zeros result in nearby closed-loop poles with very large time constants and small residues. These linear responses are judged to be satisfactory, and the simulation phase is continued.

Roll Linear Simulation. Next, linear simulations are performed on the roll loop. The roll channel unit step responses are also shown in Figure 5.1. In this case, more pronounced boundary violations are noted. A small, oscillatory component of the time response prevents the responses from being completely enclosed within the bounds. Note that these oscillations are present only in the cases of flight condition 2. A look at the Bode plots of q_{22} (Figure 4.2) at these conditions indicate a peak at approximately 2.5 rad/s. An

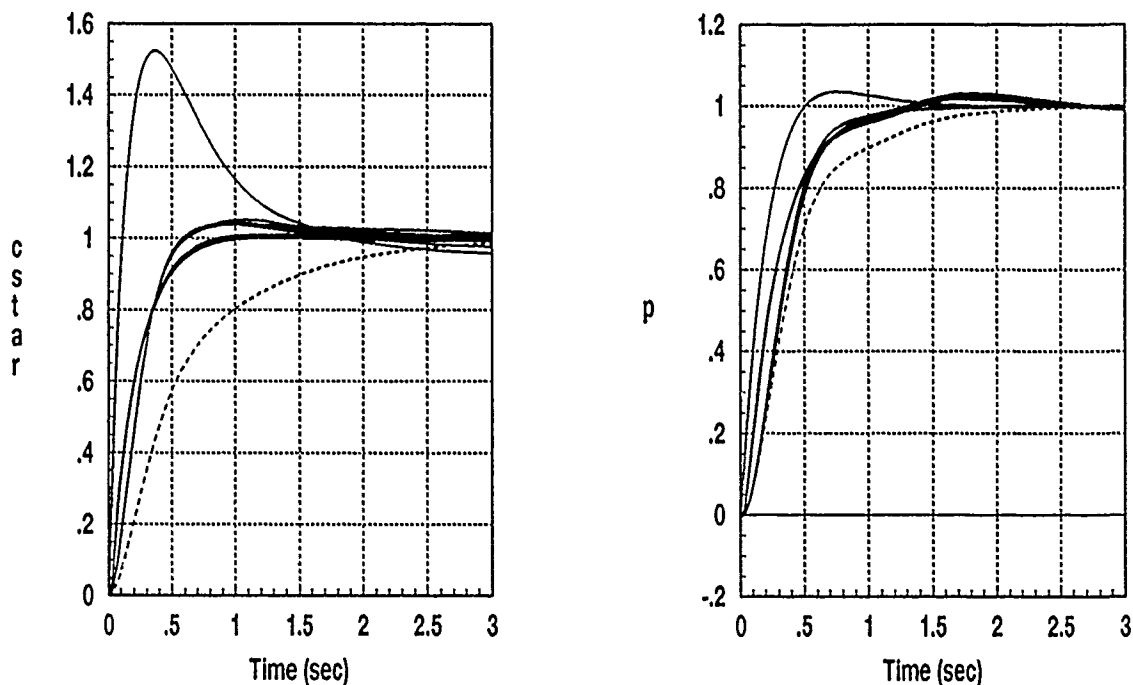


Figure 5.1. Linear Simulations of the Inner Loop

inspection of the q_{22} transfer functions reveals the existence of a pair of complex poles and zeros in this frequency range that nearly cancel, but not completely. Since the final objective is the nonlinear response, the linear simulation is considered acceptable and the nonlinear simulation performed.

Nonlinear Simulations

Once the compensators and prefilters are coded into the FORTRAN simulator, the opportunity for simulations is unlimited. As opposed to the linear simulation where simple step commands are sufficient simulations, the nonlinear system must be evaluated with commands of varying magnitudes.

Nonlinear Simulation of the SISO Systems. First, nonlinear simulations are performed on each channel separately. For the SISO C^* simulation, C^* is commanded from 1 to 5 g's at each flight condition for a total of 10 runs. The response on roll rate for the

SISO C^* simulations is essentially zero for all cases. The SISO simulations for roll rate consist of step commands from 10 to 40°/s in increments of 10°/s. In these simulations, the C^* response is negligible. The normalized responses enclosed in the thumbprints are shown for both cases in Figure 5.2. Both sets of responses are completely satisfactory.

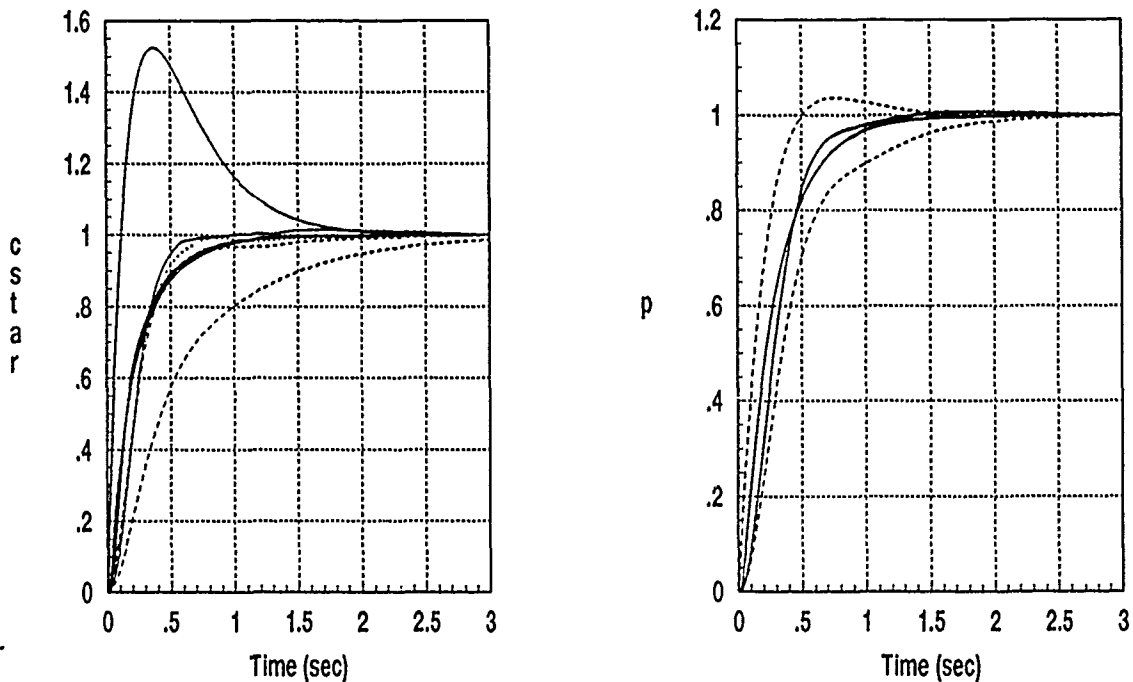


Figure 5.2. Nonlinear SISO Simulations of the Completed Design

Nonlinear MIMO Simulations Over the Design Range. The true test of the nonlinear design consists of simulations over the range of input magnitudes on which the design is based. As mentioned earlier, it is essential that in the equivalent plant generation phase, equivalent plants are generated for the full range of desired outputs. Figure 5.3 shows the normalized responses of the nonlinear plant over the full range of input magnitudes on which the design is based. The only significant boundary violations are in the roll rate response, and are similar to those of the linear simulation. Before attempts are made to eliminate these boundary violations, the nonlinear system is simulated over a wider range of input magnitudes to provide additional insight into corrective measures.

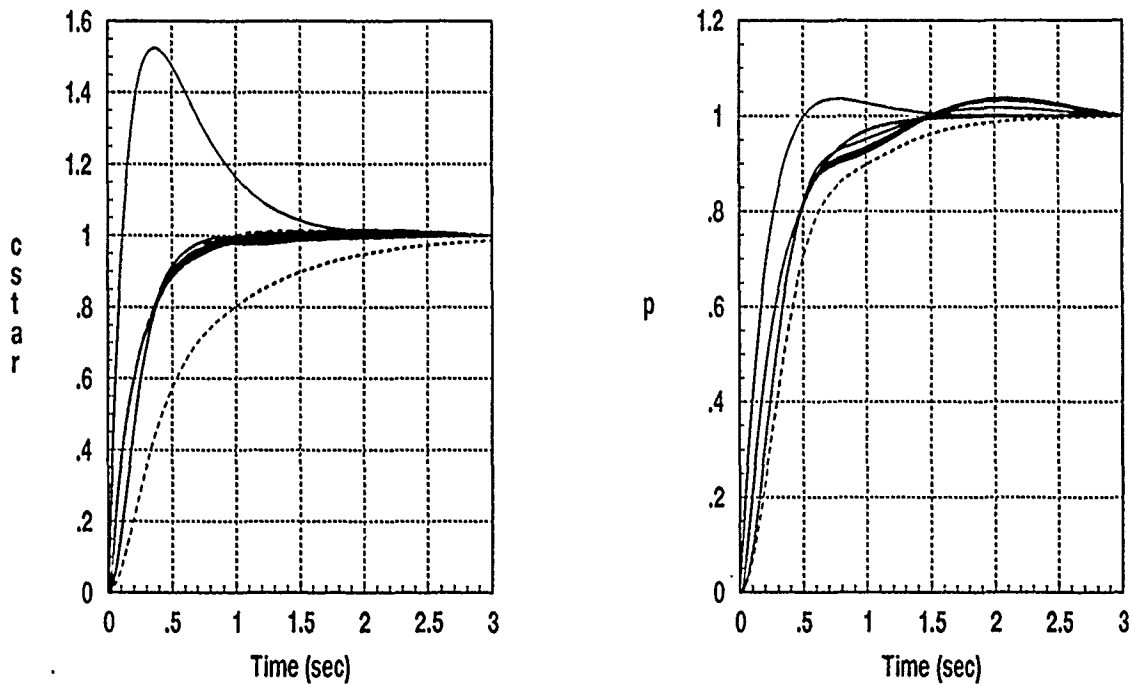


Figure 5.3. Nonlinear MIMO Responses Over the Design Range

Nonlinear MIMO Simulations Over an Extended Input Range. The extended MIMO simulations consist of simultaneous step commands extending various degrees beyond the original design range. C^* is commanded from 1 to 5 g's in increments of 1 g at the first flight condition, while p is simultaneously commanded from 10 to 40°/s in 10°/s increments for each magnitude of C^* . At the second flight condition, C^* is limited to 3 g's while the p commands are the same as in the first case. The composite normalized time responses for all cases are shown in Figure 5.4. The top figures are for the flight condition 0.9M, 20K, and the lower set is for 0.6M, 30K. All responses at the first condition are excellent. There are, however; some problems at the second flight condition. In the C^* response it is noted that there is one case that significantly violates the boundaries. The bad case is for a 3 g C^* command with 40°/sec of roll rate at the second flight condition, which is outside the range of responses used in the design process.

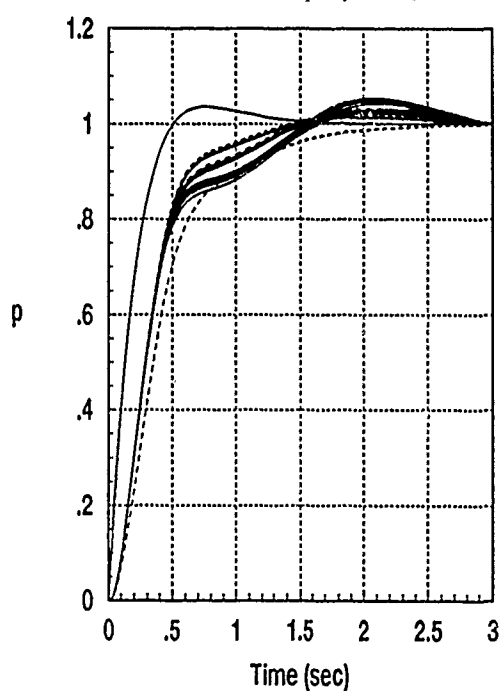
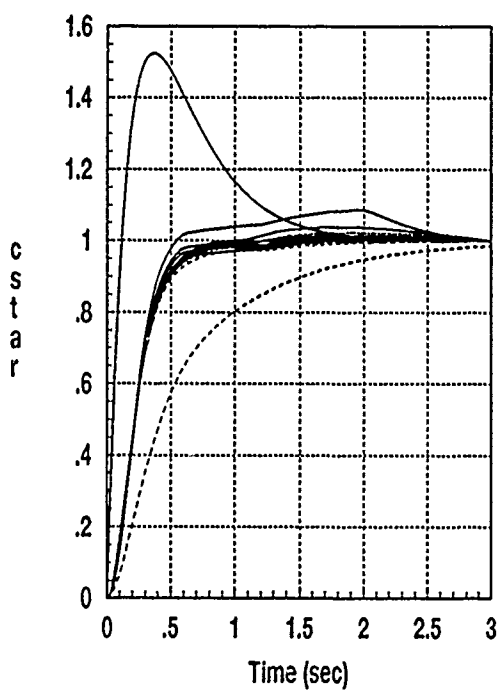
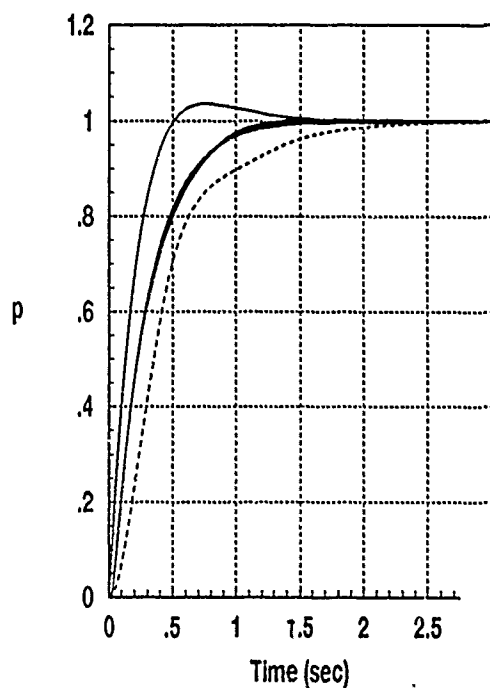
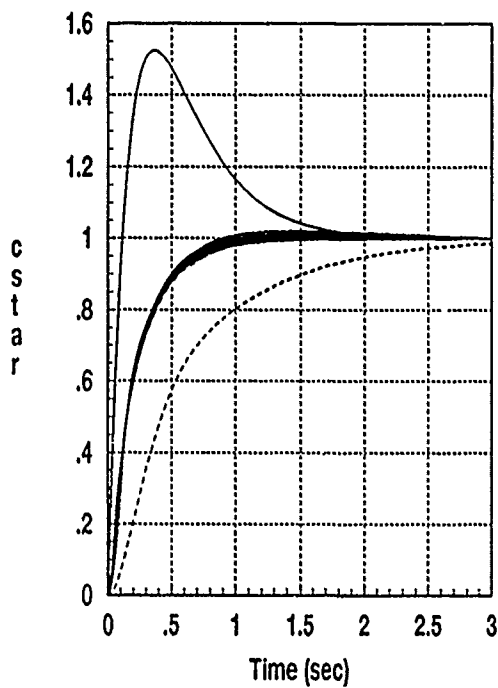


Figure 5.4. Nonlinear MIMO Simulations Over an Extended Input Range

Also note that there are essentially three distinct traces within the roll response. Note that the worst case is associated with the 3 g C^* command at the second flight condition, which again is outside the design range. As mentioned earlier, in the nonlinear design problem, it is important to base the design on the full range of desired outputs. Since the maximum command at this flight condition was 2.2 g/s and 18°/sec, the fact that these violations occur is not that surprising. The true test of the design can only involve the responses on which the design is based. The first flight condition performs well over a more extended range than the second which is good, but again, only performance over the range on which the design is based has any real implications on the technique. The roll rate responses show troublesome oscillations very similar to those seen in the linear simulation, but they are somewhat more pronounced. Again, the only problem responses are at the second flight condition, 0.6M, 30K, and the oscillations get progressively worse as the commanded magnitude grows from the original design range. The frequency of oscillation is approximated to be between 2 and 5 rad/s. This value is consistent with the peaking of the Bode plots of q_{22} at 2.5 rad/s discussed previously. One attempt to eliminate this oscillation is to include an exact cancellation of the troublesome pair of complex poles and zeros of the nominal plant (q_{22}). This additional compensation eliminates the upper violations in the response, but oscillations are still present and significant 'dips' are present before the response reaches its final value. The most obvious solution to the problem is to increase the loop transmission in this frequency range. A second look at the loop shape of the completed roll loop shows that increased loop transmission can be obtained in this critical frequency range without violating the 30 rad/s crossover requirement by the implementation of the modified compensator given by Equation (4.4). Simulations of the roll system with this modified compensator at 0.6M, 30K are shown in Figure 5.5. The plot on the left covers only the original design range, and the plot on the right covers the entire extended simulation range.

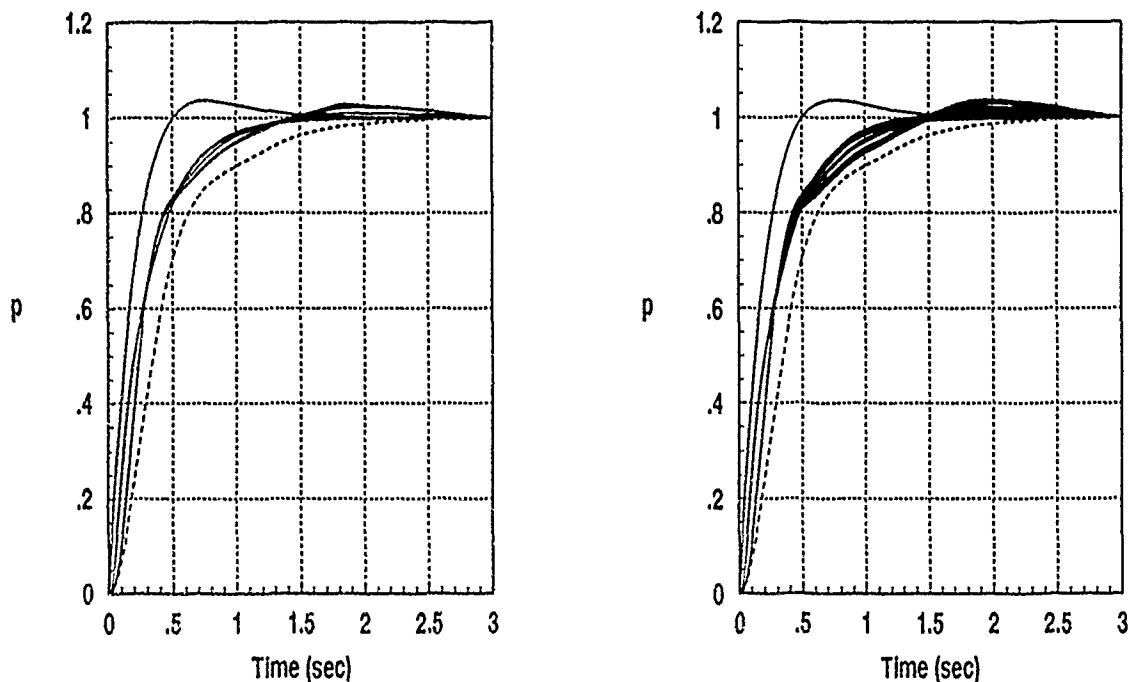


Figure 5.5. Nonlinear MIMO Simulation with the Modified Roll Compensator

The C^* responses are virtually unchanged from those of Figure 5.4, and therefore are not repeated in Figure 5.5. The resultant responses are located predominantly within the bounds, but could stand improvement.

In designing a fixed compensator, it must be expected that there be a trade off in quality of performance at the various parameter values. By examining the templates for both loops, it is apparent that superior performance will be obtained at the first flight condition. In both cases, the responses at the first flight condition are predominantly located at the top of the templates, implying a higher loop transmission for that condition. The general appearance of the template for p at 30 rad/s is shown by Figure 5.6, where points marked by 'o's are for 0.9M, 20K, and 'x's represent responses at 0.6M, 30K. In order to design a fixed compensator, the specified criteria must be met for all cases. Therefore, the loop transmission for the plants represented by the bottom of the template will always be less by

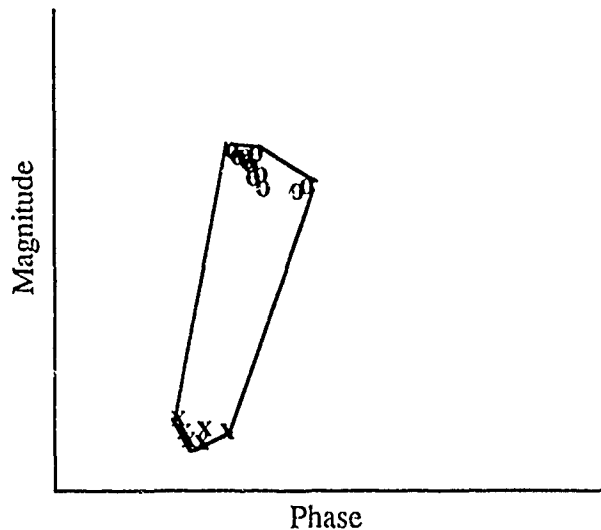


Figure 5.6. Template of q_{22} at 30 rad/s

the height of the template at any given frequency. Hence, there is a trade off between the use of a fixed compensator and optimal performance for all parameter values. The constraining criteria in this design is the 30 rad/s open loop crossover requirement, resulting in lower loop transmission in that vicinity of approximately 13 dB for roll rate, and 12 dB for C^* . Note that in a case such as this where the two flight conditions represent the extreme ends of the templates, scheduling of the compensator gain could be used to provide comparable loop transmission for all cases. An additional 7 dB of gain in the roll channel, and 3 dB in the C^* channel, for the second flight condition results in the responses of Figure 5.7 for the extended simulation range. With the gain scheduling mentioned above, the gain values used for Figure 5.7 could be achieved without violating any of the design specifications. Additional simulations would be required for this scheduling to determine whether the dominant factor causing this separation is velocity, altitude, or a combination of the two.

Additional Simulations. Several additional nonlinear simulations are given in Appendix C. Included are the full aircraft outputs and surface deflections for:

1. Simultaneous pitch and roll commands for a few of the cases of Figure 5.5,

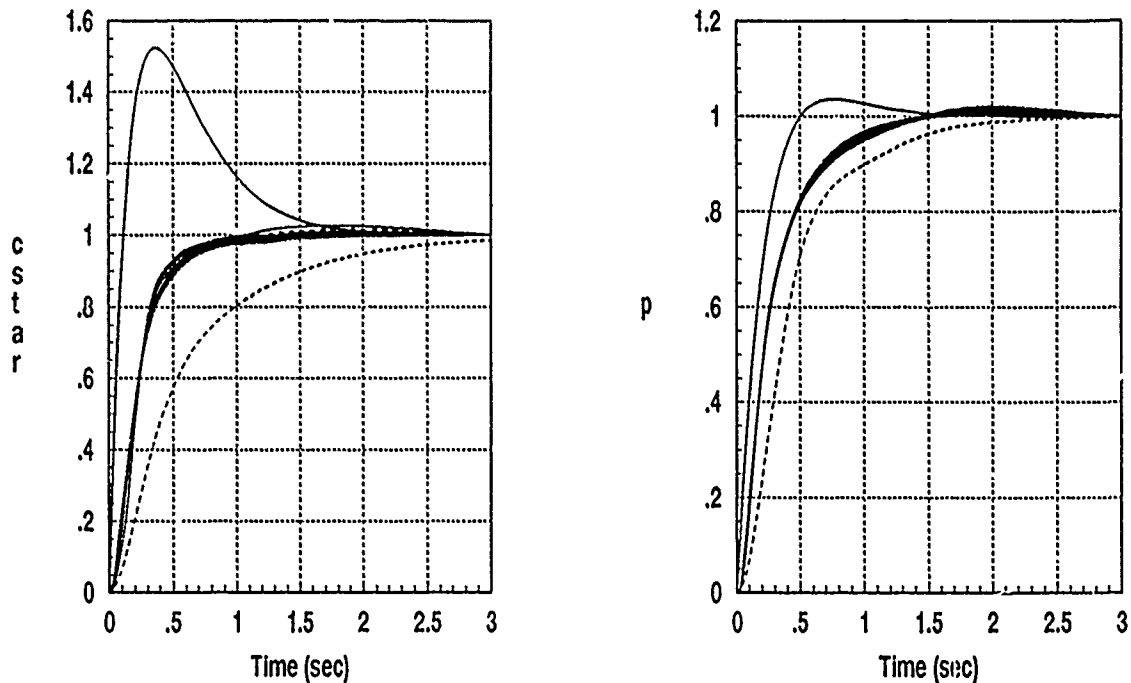


Figure 5.7. Nonlinear MIMO Simulations at 0.6M, 30K with Increased Gain

2. Roll out of a coordinated turn, and
3. A $120^\circ/\text{s}$ roll command from straight and level flight.

Summary

This chapter presents both linear and nonlinear simulations of the compensated inner loop. There are strong correlations between the two simulations, indicating that the equivalent LTI plants are at least reasonable. There are some coupling effects between the two outputs that can not be overcome with fixed compensation, but a gain scheduling option is suggested which can result in satisfactory responses over the entire design range and beyond without violations in any of the system requirements. Finally, several additional simulations are performed, and the results are provided in Appendix C.

VI. Pilot Compensation

Introduction

This chapter describes the development of the Pilot Compensation filters, f_{pc} and f_{pp} shown in Figure 6.1 to augment or replace the prefilters of Chapter 4. The purpose of this pilot compensation is to reduce the pilot's workload while ensuring acceptable responses. Essentially, the technique is to model the pilot with parameters known to give good pilot ratings and design the pilot compensation such that it shapes the responses to their desired forms. Note that the darker lines in Figure 6.1 represent feedback paths which are not physically connected.

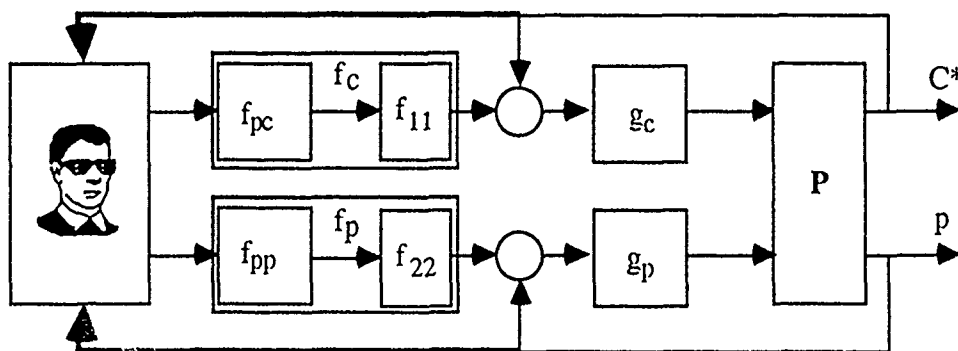


Figure 6.1. Closed Loop Control System Including Man-in-the-Loop

Kobylarz designed pilot compensation based on a single equivalent plant of the designed inner loop. This thesis, considers an equivalent plant set as in the inner loop design to shape the loop to ensure satisfactory response over a range of flight conditions, but the pilot compensation is designed as two independent SISO systems. That is, when equivalent plants for the C^* inner loop are generated, the roll command is zero and vice versa. The decision to synthesize the pilot compensation in this manner is based solely on time constraints, and the method used for the MIMO design of Chapter 4 can be used for pilot

compensation with the only difference being the requirement for more plants and the conversion to the MISO equivalent loops.

Criteria for pilot in the loop pitch response is fairly well defined and can be found in the Neal-Smith report [14] as well as MIL-STD 1797A. Criteria for roll response, however is very limited. Therefore, an approach very similar to the one used by Kobylarz is used for the longitudinal compensator, and a new approach is introduced for the lateral design. Because of the differences in the two designs, they are prescribed separately.

Plant Generation for Pilot Compensation

After the inner loop designs are completed, SISOTF is used to generate a new set of equivalent LTI plants that represent the closed *inner* loop system as shown in Figure 6.2.

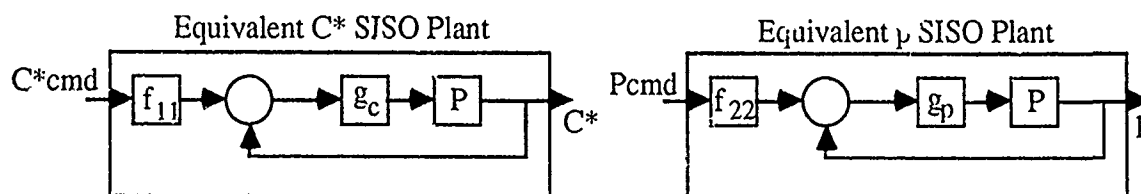


Figure 6.2. Equivalent Plants for Outer Loop Design

Plants are generated for C^* commands of 1, 3, and 5 g's at 0.9M, 20K, and 1 and 2g's at 0.6M, 30K. For the roll channel, plants are generated in $10^\circ/s$ increments from 10 to $30^\circ/s$ at both flight conditions. Templates representing the magnitude and phase uncertainty are then generated for both loops as in the inner loop design. The templates at low frequency contain very little uncertainty, and are primarily useful for moderate and high frequency regions only. A good feel for the uncertainty of the equivalent inner loop system can be obtained from the composite frequency response of Figure 6.3.

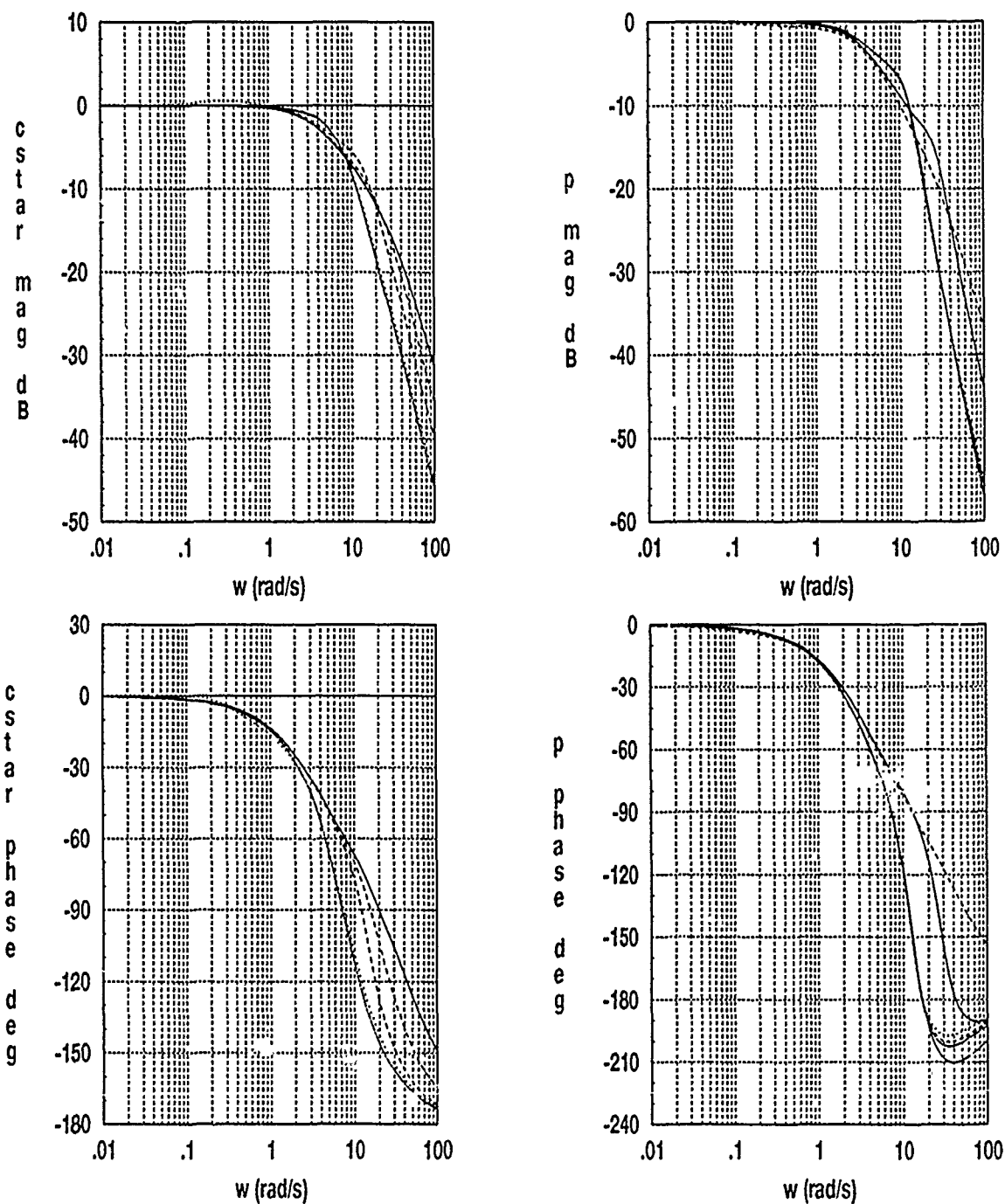


Figure 6.3. Uncertainty of the Equivalent Plants for Pilot Compensation

Pilot Model

The pilot model used for both designs is based on the Neal-Smith pilot model given by

$$\text{Pilot}(s) = K_p e^{-s\tau} \frac{\tau_{p1}s + 1}{\tau_{p2}s + 1} \quad (6.1)$$

As stated previously, Roskam asserted that the ideal pilot input is one of pure gain. Therefore, in the design of the pilot compensation, the pilot model includes only the inherent time delay and unity gain. The selection of unity gain is somewhat arbitrary, because the total gain of the inner loop is given by the product of the pilot gain and the respective compensator gain. Hence, any value of pilot gain could be achieved from the designed system by adjusting the compensator gain such that the total gain is the same as that of the original compensator. For instance, if the optimal pilot gain for a certain application is 2 instead of 1, the compensator should be implemented with half the gain determined from the design process.

Longitudinal Pilot Compensation

The Neal-Smith report [14] clearly lays out frequency domain characteristics for closed loop C^* response that result in satisfactory pilot ratings. Specifically, the report calls for a closed loop bandwidth of 3.5 rad/s and a maximum of 3 dB of droop for $\omega < \omega_{BW}$. The report defines the closed loop bandwidth as the frequency at which the closed loop response has a phase lag of 90° . The final specification is for maximum closed loop resonance of 3 dB. These criteria are readily displayed on the Nichols chart of Figure 6.4. Kobylarz pointed out that the pilots of the Neal-Smith study generally preferred responses with overshoot but no undershoot so that the droop for $\omega < \omega_{BW}$ should be held as close to zero as possible. The frequency criteria of Figure 6.4 can be modified by manipulating the templates around them in order to develop a new set of bounds as in the QFT technique so that by satisfying the modified bounds with the nominal loop the criteria would be met for all

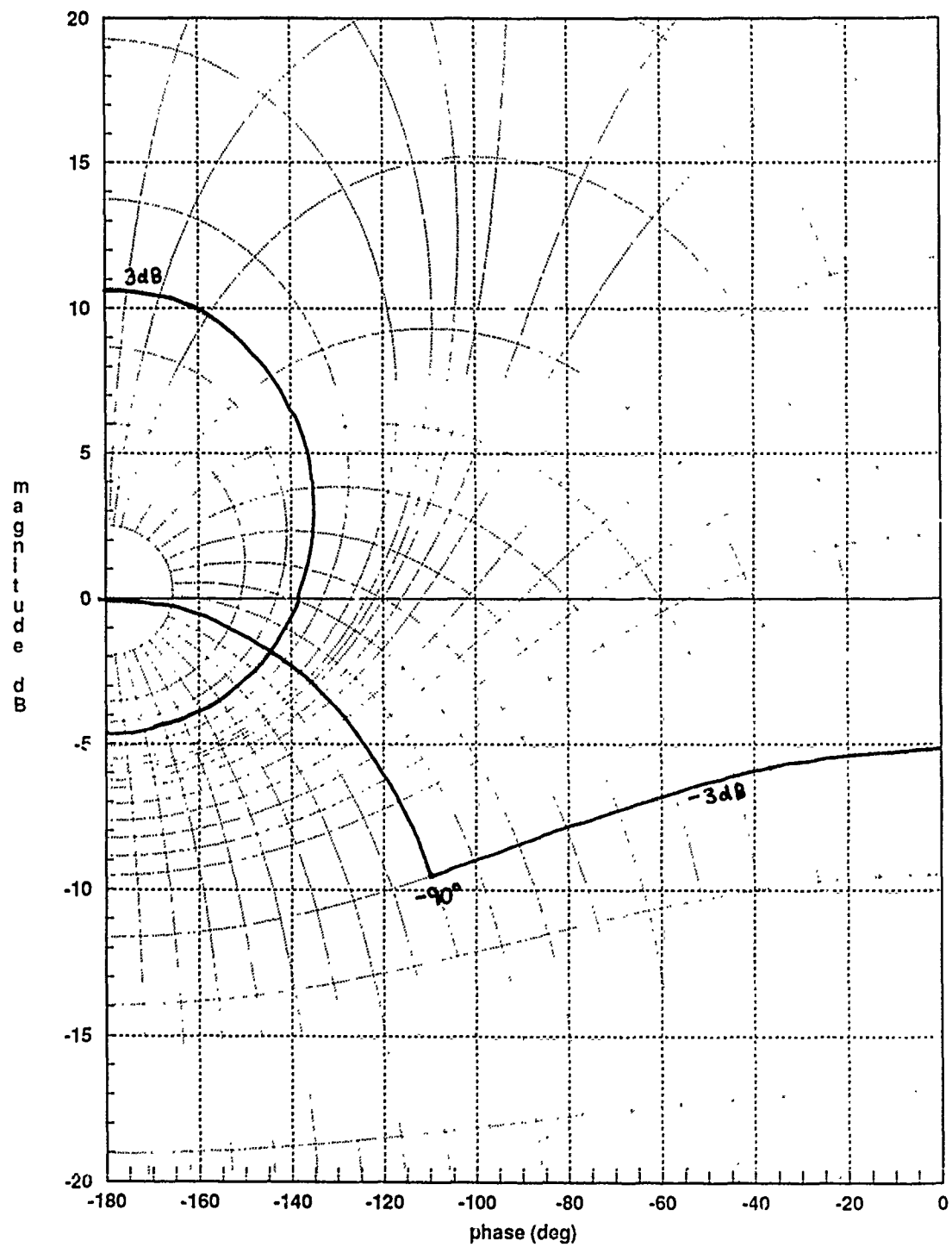


Figure 6.4. C* Pilot in the Loop Criteria

plant cases. Instead, because the templates are very small in the frequency range of primary interest, the decision is made to shape the nominal loop based on the original criteria, with the templates occasionally being placed over the nominal loop to ensure that no plant case violates the specified requirements.

The spreadsheet used for the inner loop design is again used for the synthesis of the longitudinal pilot compensator, f_{pc} , given by

$$f_{pc} = \frac{55 (s + 7)^2 (s + 300)}{s(s^2 + 100s + 10000)(s + 40)} \quad (6.2)$$

where the last pole and zero cancel a pole and zero from the original prefilter derived in Chapter 4. Therefore, the total outer loop compensation is given by

$$f_c(s) = \frac{1650 (s + 7)^2}{s(s^2 + 100s + 10000)(s + 4)} \quad (6.3)$$

Note that in shaping this loop, the phase lag of the pilot model must be included. The spreadsheet allows for a time delay term which accounts for this phase lag. The compensated loop shape is shown in Figure 6.5. Note that this compensation results in a slight violation of the bandwidth specification. The reasons for allowing this violation are given in the simulation results section.

Lateral Pilot Compensation

As mentioned earlier, specifications for closed loop roll specifications are somewhat limited. Guidelines are primarily limited to rise times and damping factors. MIL-STD 1797A (sec 4.5.1.1) indicates that rise times of the roll rate response between 0.33 and 1s generally result in satisfactory pilot ratings. Barfield [1] has indicated that desirable roll

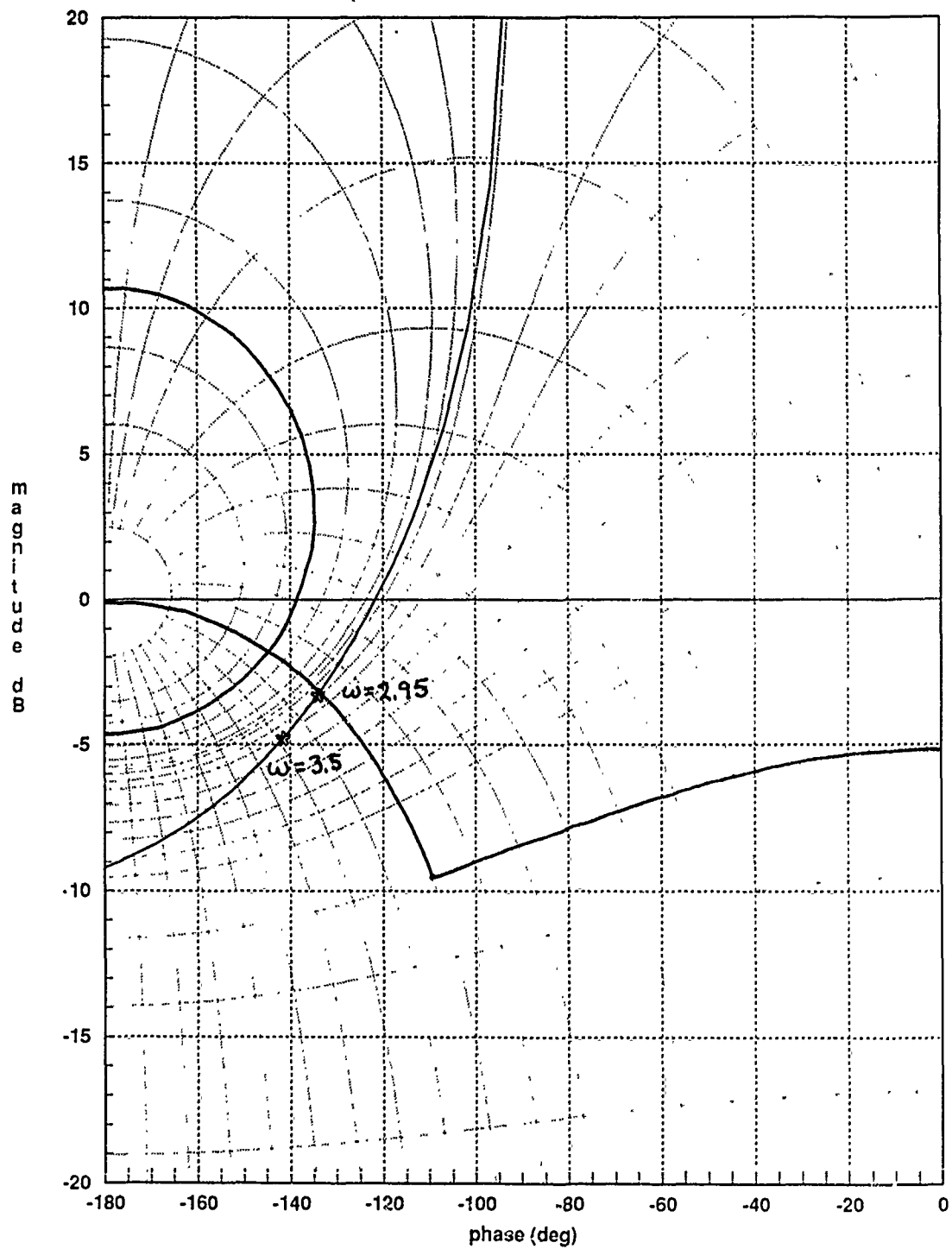


Figure 6.5. Compensated C^* Loop

rate responses have high damping factors. Since the purpose of this thesis is to introduce pilot compensation techniques, and not to meet a prespecified set of requirements, the decision is made to adopt a general criteria of

$$1) 0.33 < T_R < 1.0, \text{ and}$$

$$2) 0.8 < \zeta < 1.0$$

The first step in the synthesis technique is to develop simple-second-order transfer functions which exhibit the desired closed loop response. For this design, four transfer functions are used, representing the four extremes of damping factors and rise times, given by

$$\begin{array}{ll} \frac{5.29}{s^2 + 3.68s + 5.29} & \zeta=.8, T_R=1 \\ \frac{56.25}{s^2 + 12s + 56.25} & \zeta=.8, T_R=0.33 \\ \frac{10.24}{s^2 + 6.4s + 10.24} & \zeta=1, T_R=1 \\ \frac{100}{s^2 + 20s + 100} & \zeta=1, T_R=0.33 \end{array} \quad (6.4 \text{ a-d})$$

If these transfer functions are designated $M_T(s)$, then it can be easily derived from Figures 6.1 and 6.2 that

$$M_T(s) = \frac{L(s)}{1 + L(s)}, \quad (6.5)$$

where $L(s) = e^{-s\tau} L_1(s)$. Obviously, the pilot's delay must be considered in the closed loop response, so the design equation is given by

$$e^{-s\tau} M_T(s) = \frac{e^{-s\tau} L_1(s)}{1 + e^{-s\tau} L_1(s)} \quad (6.6)$$

Note that L_1 represents the desired transfer function of the closed inner loop plus compensation. Solving (6.6) for L_1 gives

$$L_1(s) = \frac{M_T(s)}{1 - e^{-sT} M_T(s)} \quad (6.7)$$

The next step is to plot the frequency response of $L_1(s)$ for all cases in (6.4) on a Nichols chart. Horowitz has stated that it is reasonable to expect similar time responses from any system which has a similar Nichols plot. Therefore, by using the four cases of L_1 as an approximate set of bounds, the open loop Nichols plot can be directly shaped to develop the pilot compensation which results in the desired response. Again, the templates are used to ensure that the resultant loop falls within the desirable range for all plant cases. Note that in this case, the phase lag of the pilot model has already been accounted for in L_1 , and it is not included in the loop shaping process. The four "bounds" are shown in Figure 6.6. Because of the radical behavior of the faster response models, the decision is made to emulate the slower response models. It is noted from the bounds, that larger damping factors tend to move the Nichols plot to the right, and that higher loop transmission correlates with faster responses. The compensated loop is therefore shaped to be similar in shape to the slower bounds, but to the right of the left-most bound with slightly higher loop transmission to get a response reasonably within the chosen specs. The designed lateral compensator is given by

$$f_p(s) = \frac{.314(s + 6)}{s(s + 5)} \quad (6.8)$$

In this case, the roll prefilter designed in chapter 4 is cancelled out, so (6.8) represents the complete compensator, f_p for the roll system outer loop. The completed loop shape with this compensation is shown in Figure 6.7.

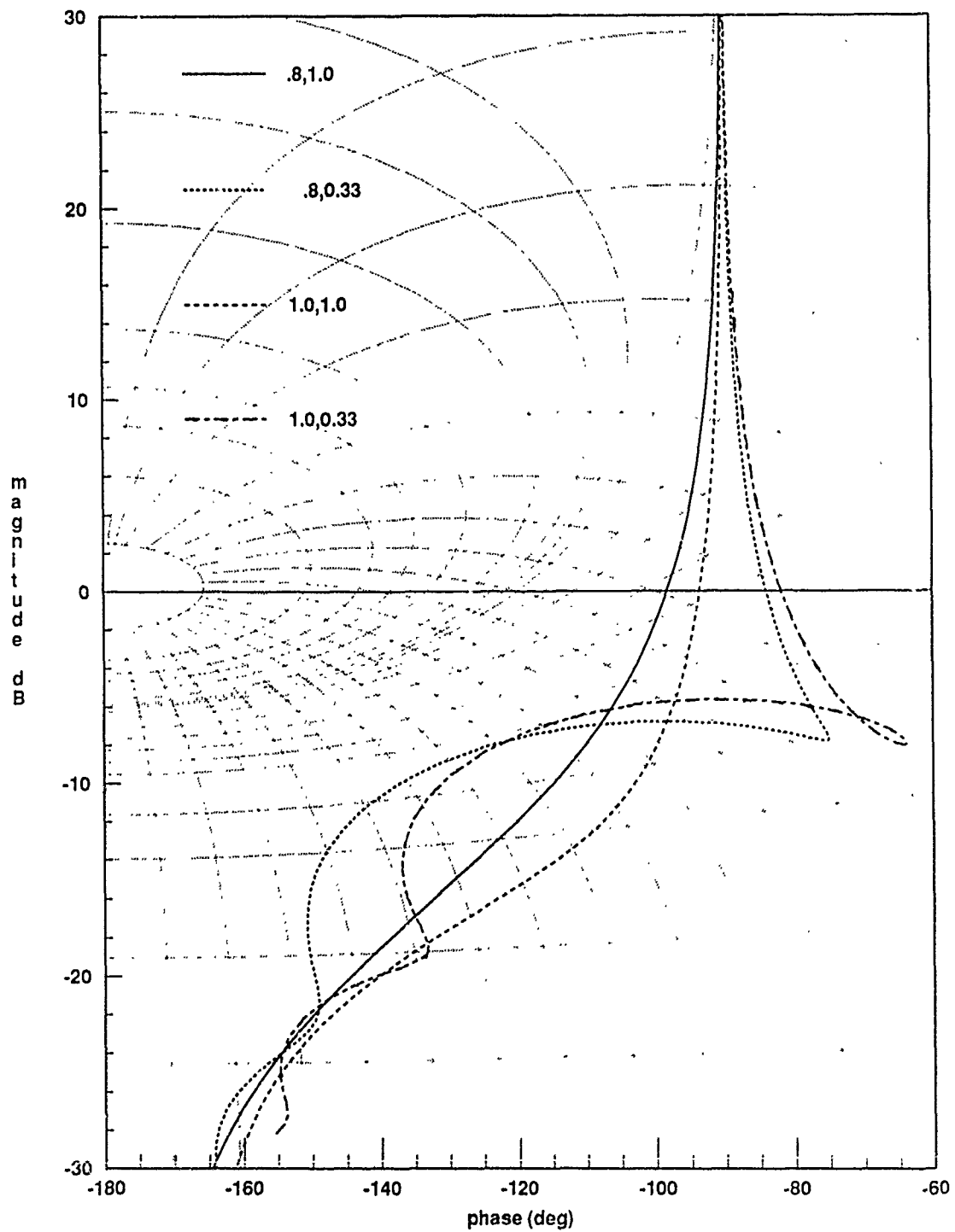


Figure 6.6. Pilot in the Loop Roll Criteria

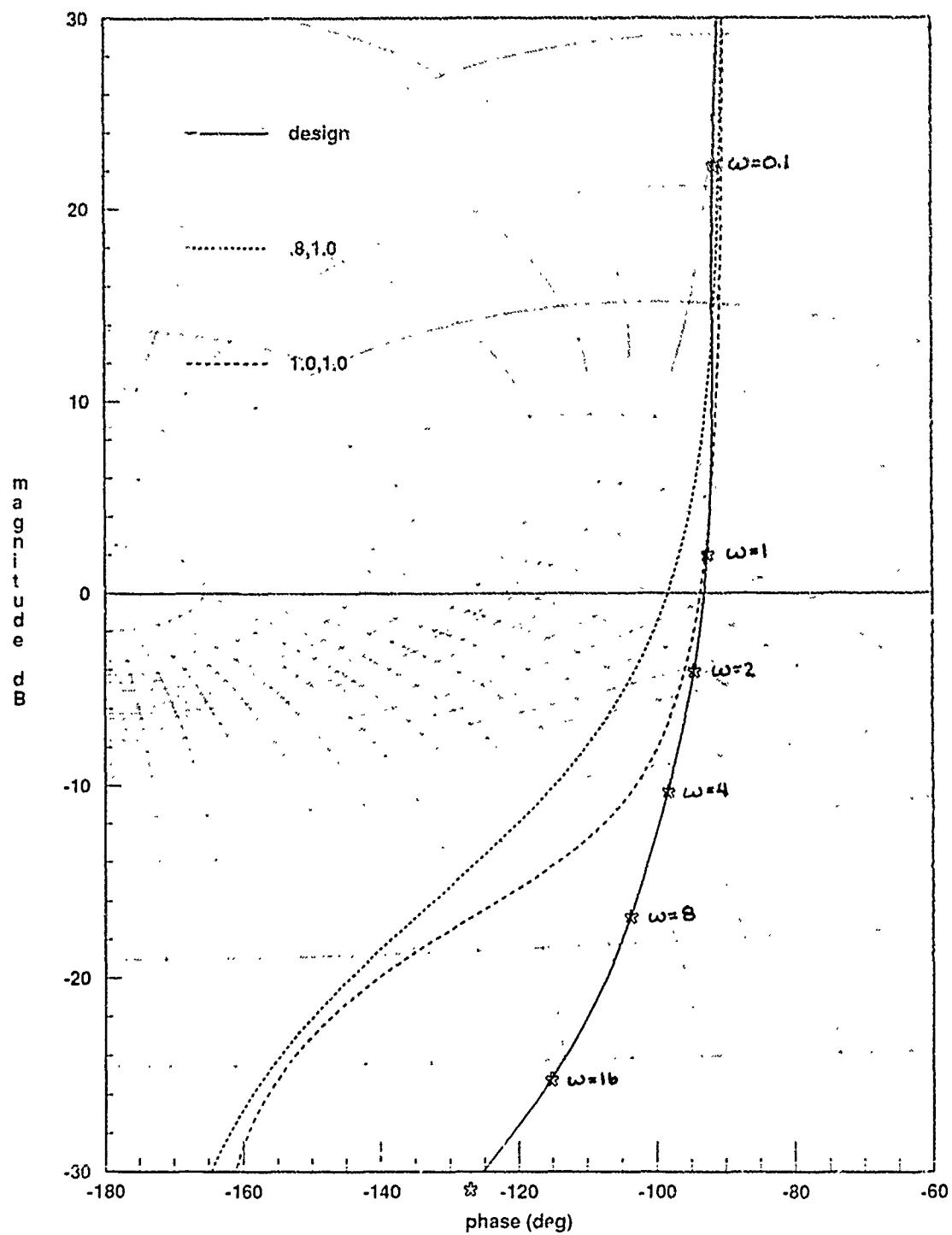


Figure 6.7. Compensated Roll Response

Simulation of the Pilot Compensation

The only simulations performed on these designs are with the actual nonlinear simulator. Originally, the fourth order Pade' approximation used by Kobylarz for the pilot model is used in the simulations. However, simulations with the designed compensator and pilot model shows periodic peaking after the response has appeared to be settled down. This peaking effect is shown in Figure 6.8. Extensions on Kobylarz's simulation of Figure 6.8 of his thesis to eight seconds showed the same problems as are experienced with this design.

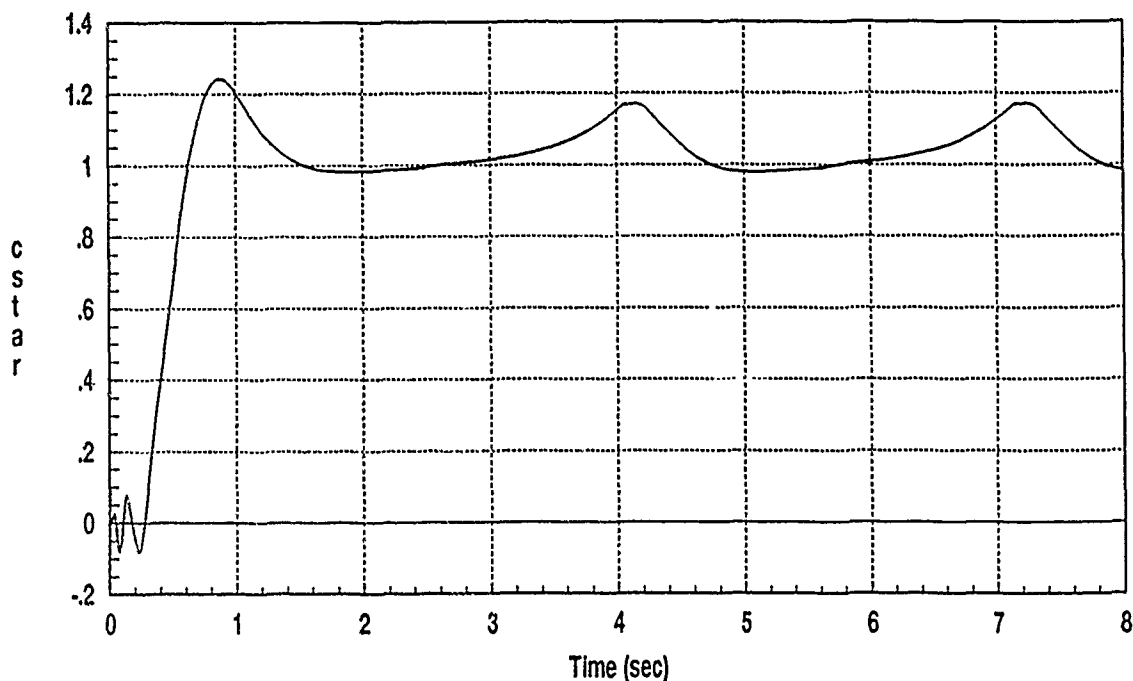


Figure 6.8. Problems Caused by the Pade' Approximation

After the Pade' approximation is replaced with a true delay, these peaks disappear. The normalized pilot in the loop simulations are given in Figure 6.9. The C* responses are enclosed in the original bounds, but since the roll synthesis is based on a new set of general requirements those responses are displayed without bounds. The C* simulations extend from 1 to 5 g's at 0.9M, 20K, and 1 to 3 g's at 0.6M, 30K, and the roll responses are

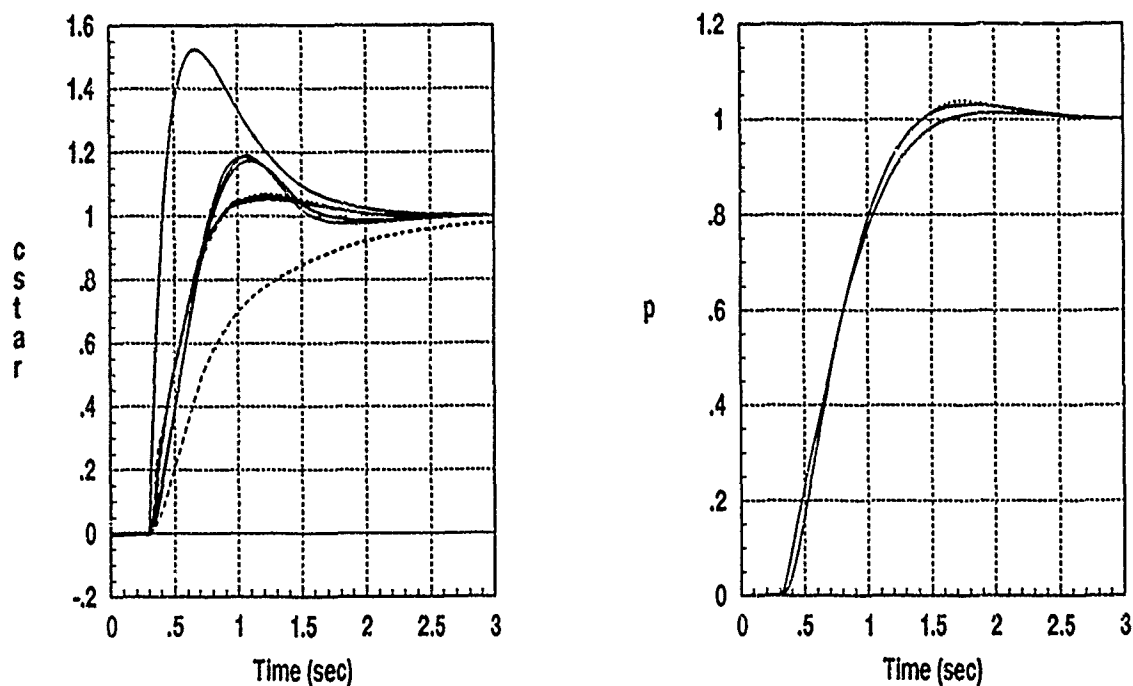


Figure 6.9. Pilot in the Loop SISO Simulations

from 10 to 30°/s at each flight condition. The C^* responses are clearly bounded by the original thumbprint, and contain overshoot without significant undershoot as desired [13]. It is difficult to obtain these desirable responses over both flight conditions while satisfying the bandwidth requirement of 3.5 rad/s. Attempts to satisfy the bandwidth requirement with fixed compensation result in at least one of the responses containing 10% or larger undershoot. As in the design of the inner loop, gain scheduling can be used to provide the desired responses while meeting all specs. It is interesting to note that in this case, however; the second flight condition requires less compensator gain to give the desired response, which is the opposite of the case in the inner loop design. The roll rate responses have relatively high damping factors, but are slightly less than 0.8 for the responses at 0.6M, 30K. An equivalent second order plant fit with SISOTF indicates that the worst case corresponds to $\zeta \approx 0.78$. The settling times for roll rate are within the specified criteria, given by $T_R \approx 0.81s$ at 0.9M, 20K, and $T_R \approx 0.73s$ for 0.6M, 30K. In both

loops, there is essentially one response form at 0.9M, 20K and a distinctly different response at the condition 0.6M, 30K. The differences indicate that even with the decreased uncertainty after closure of the inner loop the two flight conditions are significantly different.

Additional pilot in the loop simulations are included in Appendix C, including simulations as the full MIMO system.

Summary

This chapter presents the pilot compensation techniques used in this design. The chapter covers the entire process, from method to simulation. Additional simulations are provided in Appendix C.

VII. Conclusions and Recommendations

Discussion

This thesis applies nonlinear QFT and pilot compensation techniques to the design of a multi-axis FCS for the YF-16. The design is based on a nonlinear FORTRAN simulator that represents the full six degree of freedom equations of motion of the YF-16. The inner loop SAS design is based on 22 equivalent LTI plants generated from the simulator output data. The plant generation technique is extended to the MIMO case based on a method proposed by Golubev for the SISO nonlinear problem.

The inner loop design results in diagonal compensation that performs relatively well over the entire range of plant uncertainty. Of the two flight conditions considered, 0.9M, 20K and 0.6M, 30K, the best performance is obtained at the first flight condition. Analysis of the plant templates shows that higher loop transmission is always achieved at that condition. Moderate boundary violations in the roll rate response at the second flight condition are primarily a result of the 30 rad/s open loop crossover frequency requirement. Since the two different flight conditions are represented by the extreme ends of the plant templates, gain scheduling can be used to eliminate the roll rate violations.

After the completion of the inner loop SAS design, pilot compensation is designed to reduce the pilot's workload. Again, equivalent LTI plants are generated which represent the nonlinear plant, but these plants include the inner loop compensation. Since the ideal pilot input for small tracking tasks is one of pure gain, the pilot is modelled as part of the outer loop by a 0.3s delay and unity gain. Pilot compensation is developed which results in acceptable outputs while the system is driven by this optimal pilot model. The longitudinal design is based on preexisting criteria given in the Neal-Smith report [14]. Roll pilot in the loop criteria is somewhat limited, so a new technique is introduced for this aspect of the design. First, transfer functions are synthesized to meet desirable closed loop responses. The open loop transfer function is then analytically determined, based on the

desired closed loop response and the optimal pilot model. Compensation is then added to the equivalent inner loop to match the frequency response of the desired open loop system. In both axes, a set of LTI plants are used to represent the closed inner loop system. Frequency domain templates are then used to ensure that the specified criteria are satisfied for all plant cases.

Conclusions

The following conclusions are based on the results of this thesis:

1. MIMO nonlinear systems can be adequately represented by a set of LTI transfer functions based on input-output time histories from the nonlinear plant.
2. Nonlinear QFT can be used to develop fixed compensation for FCS problems over a wide range of uncertainty. There is, however, a trade off between the use of fixed compensation and the level of performance at the various conditions. Scheduling of the compensator gain may provide a means of improving the system's performance.
3. Linear Simulations of the synthesized compensation with the equivalent LTI design models provide a reasonable indication of the actual nonlinear performance.
4. Frequency domain design tools, especially the Nichols chart, are extremely convenient for the design of pilot compensation to force acceptable responses based on desirable pilot model characteristics. Frequency domain templates, as used in QFT can be used in the pilot compensation process to take in account the uncertainty associated with the compensated inner loop.

5. MATRIXx is an invaluable tool for control system design and analysis. Its versatile programming capabilities and the System Build feature make it especially useful for parametric problems such as QFT design.

Recommendations

This section provides recommendations for future work in these areas, as well as some practical advice for future researchers.

Fully investigate equivalent plant generation techniques. The success of this design indicates that the equivalent plants generated are at least reasonable representations of the actual plant. However, there is room for improvement in this aspect of the design technique. There is no question that SISOTF is capable of generating valid LTI plants to represent a nonlinear SISO system, but as mentioned in Chapter 3, the problem of ensuring that the individual components of the MIMO responses are accurately modelled has not been rigorously resolved. The equivalent plants of Appendix A indicate that in some cases there exists an unstable relationship between roll rate and elevator deflection (p_{21}). These right-half plane poles also exist in p_{22} (roll rate due to aileron), but are essentially cancelled by nearby zeros. Attempts should be made to rigorously resolve this problem. The program FRESPID has recently been provided by Dr. Mark Tischler of the U.S. Army Research and Technology Activity at Ames Research Center. This program presents a different approach to equivalent plant generation for the SISO problem. Although SISOTF does an excellent job of generating equivalent plants for the SISO problem, FRESPID should be investigated and considered for possible extension to the MIMO case.

Future designs should focus heavily on equivalent plant generation. The generation of equivalent LTI plants represents the major part of the nonlinear design problem. Care should be taken to ensure that the obtained plants are valid, since they are the foundation for the entire design. This design focused on tightly filling the response envelopes with simulator responses for plant generation, using only two flight conditions and a limited

number of magnitudes. Responses of similar magnitudes and flight conditions generally result in little plant variation, even if the responses fall in significantly different regions of the envelope (e.g. a fast response verses a slow response). In retrospect, plant generation efforts would have been better spent obtaining plants that had more magnitude and flight condition differences. Instead of using only two flight conditions, it would be beneficial to use fewer responses at each flight condition, and include additional flight conditions between the two extremes. Additionally, the generation of equivalent plants is very time consuming and tedious. Automation of the process can alleviate a large part of the workload involved. For instance, a MATRIXx program could be used to automatically generate plants for several different numerator and denominator orders and select the best fit based on some error criteria.

Apply the pilot compensation techniques to a digital design. The pilot compensation techniques used in this thesis can be equally applied to a digital FCS design. An advantage is that digital compensation can be readily implemented on AFIT's SIMSTAR hybrid computer, in conjunction with its nonlinear F-16 simulator. Pilots can then rate the design both with and without the proposed pilot compensation for validation purposes.

Apply the design techniques to a larger class of problems. The techniques used in this thesis should be applied to other MIMO problems. The techniques can be readily applied to 3x3 or larger MIMO problems. The workload of plant generation increases rapidly with system order, and automation as mentioned above should be used for systems larger than 3x3. Additionally, the techniques can be applied to any FCS problem under consideration for a linear design, as long as plant input-output time histories are available or obtainable. Possibilities include digital designs and the design of robust controllers for the cases of surface failures or saturation.

Include structural modes in the design process. The 30 rad/s crossover frequency requirement was the dominant constraint in this design. If these modes are accurately modelled, it may be possible to relax this specification. Without this constraint, fixed com-

compensation can be designed to give satisfactory performance over a larger range of uncertainty.

Expand the pilot compensation techniques. The simulations of Appendix C indicate that the neglect of cross-coupling in the outer loop design results in significant roll rate output distortions at 0.6M, 30K. Compensation should be applied to the outer loop using the equivalent MISO systems of QFT so that the cross-coupling effects can be accounted for in the design process. Additionally, nonlinearities and uncertainty of the complex pilot dynamics can be considered by using standard QFT techniques in the outer loop design. As current knowledge in the area of pilot modelling grows, QFT based pilot compensation techniques should be used to develop pilot compensation over a broad range of tasks. Finally, in some flight modes it may be possible to prefilter the data input to the pilot. Incorporation of this prefiltering would provide two degrees of freedom in the outer loop design, and provide more flexibility in the design of pilot compensation.

Compile and generalize existing MATRIXx design aids. MATRIXx is a very useful tool for QFT design, and many MATRIXx programs have been developed by various QFT thesis students. The compilation and generalization of these routines would provide a powerful tool base for future QFT designers, and would constitute an invaluable effort.

Appendix A. Thumbprints and Equivalent LTI Plants

This appendix provides all pertinent transfer functions used in the design. First, the thumbprint transfer functions are given, followed by the 22 equivalent LTI plants generated with MIMOTF for the inner loop design. Next, the equivalent MISO plants (q_{ii}) are given for all 22 cases. Finally, the 11 plants generated by SISOTF to represent the equivalent inner loop for the outer loop design are provided.

Thumbprint Transfer Functions

The original C* thumbprint was the one used by Kobylarz in the SISO design. However, after the simulator was driven to a sufficient set of outputs, the thumbprints were tightened around the obtained responses to provide a more stringent test on the design. The roll thumbprint was based on general rise time and overshoot specifications provided by the sponsor. In both cases, SISOTF was used to obtain the final thumbprint equations. First, the desired response was drawn on graph paper. Next, the values of the response for every 0.1s were used to form the output data file. Specifying a unit step input with this output file enabled SISOTF to generate the desired thumbprint transfer functions. The equations are given below, in terms of the upper response, T_{RU} , and the lower response, T_{RL} .

C* thumbprint:

$$T_{RU} = \frac{13.05 (s + 1.161)}{(s + 2.952)(s + 5.132)}$$

$$T_{RL} = \frac{18.01 (s + 3.127)}{(s + 1.359)(s + 4.881 \pm j4.198)}$$

p thumbprint:

$$T_{RU} = \frac{4.99 (s + 3.313)}{(s + 3.260 \pm j1.851)}$$

$$T_{RL} = \frac{16.44 (s + 5.901)}{(s + 2.103)(s + 3.713 \pm j5.688)}$$

Equivalent LTI Plants for Inner Loop Design

The transfer functions for all 22 equivalent LTI plants generated for this thesis, in the form

$$\mathbf{P} = \begin{bmatrix} P_{11} & P_{12} \\ P_{21} & P_{22} \end{bmatrix}$$

are provided below. Plants 1 through 16 are from simulator runs at 0.9M,20K, and plants 17 through 22 are for 0.6M,30K.

Plant 1:

$$P_{11} = \frac{-0.3140(s + .27 \pm j.35)(s + 277.24)}{(s + .3869 \pm j.3167)(s - 1.5865)(s + 24.9256)}$$

$$P_{12} = \frac{0.0063(s - 2.23 \pm j3.42)(s + 147.54)}{(s + .3869 \pm j.3167)(s - 1.5865)(s + 24.9256)}$$

$$P_{21} = \frac{-0.0739(s - 3.1494 \pm j4.3668)(s - 4.1887)}{(s - .4308 \pm j1.2246)(s + 2.8959)(s + 25.1243)}$$

$$P_{22} = \frac{12.5 (s - .44 \pm j1.22)(s - 196.62)}{(s - .4308 \pm j1.2246)(s + 2.8959)(s + 25.1243)}$$

Plant 2:

$$P_{11} = \frac{-.3459 (s + .26 \pm j.37)(s + 245.66)}{(s - .1399)(s - 1.5099)(s + .9172)(s + 24.2961)}$$

$$P_{12} = \frac{-.0293 (s - 11.5765 \pm j8.028)(s + .3193)}{(s - .1399)(s - 1.5099)(s + .9172)(s + 24.2961)}$$

$$P_{21} = \frac{-.0109 (s - 4.1462 \pm j4.9209)(s - 4.7743)}{(s - .2719 \pm j1.1755)(s + 2.8309)(s + 25.5858)}$$

$$P_{22} = \frac{13.0 (s - .28 \pm j1.17)(s - 189.0)}{(s - .2719 \pm j1.1755)(s + 2.8309)(s + 25.5858)}$$

Plant 3:

$$P_{11} = \frac{-.3583 (s + .31 \pm j.32)(s + 236.03)}{(s - .0638)(s - 1.5315)(s + .9261)(s + 23.9755)}$$

$$P_{12} = \frac{-.0539 (s - 5.7258 \pm j8.9278)(s - .4588)}{(s - .0638)(s - 1.5315)(s + .9261)(s + 23.9755)}$$

$$P_{21} = \frac{-.0472 (s - 3.1411 \pm j4.4044)(s - 4.1669)}{(s - .4403 \pm j1.2486)(s + 2.8962)(s + 25.3727)}$$

$$P_{22} = \frac{13.2 (s - .44 \pm j1.24)(s - 187.97)}{(s - .4403 \pm j1.2486)(s + 2.8962)(s + 25.3727)}$$

Plant 4:

$$P_{11} = \frac{-.3190 (s + .27 \pm j.32)(s + 2.7137)}{(s - 1.5606)(s + .1817)(s + .6130)(s + 24.9303)}$$

$$P_{12} = \frac{.0612 (s - 1.3922 \pm j2.6745)(s + 17.4543)}{(s - 1.5606)(s + .1817)(s + .6130)(s + 24.9303)}$$

$$P_{21} = \frac{-.0069 (s - 5.4556 \pm j5.326)(s - 5.411)}{(s - .2771 \pm j1.1707)(s + 2.8305)(s + 25.4856)}$$

$$P_{22} = \frac{12.8 (s - .29 \pm j1.17)(s - 192.4)}{(s - .2771 \pm j1.1707)(s + 2.8305)(s + 25.4856)}$$

Plant 5:

$$P_{11} = \frac{-.3446 (s + .22 \pm j.38)(s + 246.61)}{(s - 1.507)(s - .1941)(s + .9044)(s + 24.4117)}$$

$$P_{12} = \frac{.0663 (s + 1.0098)(s + 12.0836)(s - 5.7362)}{(s - 1.507)(s - .1941)(s + .9044)(s + 24.4117)}$$

$$P_{21} = \frac{.0048 (s - 4.1935 \pm j2.2094)(s + 5.5326)}{(s - .15 \pm j1.1123)(s + 2.7608)(s + 25.9204)}$$

$$P_{22} = \frac{13.1 (s - .16 \pm j1.11)(s - 187.52)}{(s - .15 \pm j1.1123)(s + 2.7608)(s + 25.9204)}$$

Plant 6:

$$P_{11} = \frac{-.2956 (s + .24 \pm j.39)(s + 298.04)}{(s + .3526 \pm j.5132)(s - 1.6102)(s + 25.3285)}$$

$$P_{12} = \frac{.0291 (s - 2.0131 \pm j4.1436)(s + 33.9288)}{(s + .3526 \pm j.5132)(s - 1.6102)(s + 25.3285)}$$

$$P_{21} = \frac{-.1154 (s - 3.2438 \pm j4.3645)(s - 4.2674)}{(s - .4233 \pm j1.2018)(s + 2.8977)(s + 24.8401)}$$

$$P_{22} = \frac{11.7 (s - .43 \pm j1.2)(s - 207.89)}{(s - .4233 \pm j1.2018)(s + 2.8977)(s + 24.8401)}$$

Plant 7:

$$P_{11} = \frac{-.3124 (s + .019)(s + .586)(s + 278.8587)}{(s - 1.5968)(s + .1708)(s + .6791)(s + 24.9519)}$$

$$P_{12} = \frac{.0261 (s + 1.6464 \pm j4.5908)(s + 28.3099)}{(s - 1.5968)(s + .1708)(s + .6791)(s + 24.9519)}$$

$$P_{21} = \frac{-.0844 (s - 3.8015 \pm j4.6889)(s - 4.7182)}{(s - .2095 \pm j1.4376)(s + 2.8862)(s + 24.6045)}$$

$$P_{22} = \frac{10.1 (s - .21 \pm j1.43)(s - 234.31)}{(s - .2095 \pm j1.4376)(s + 2.8862)(s + 24.6045)}$$

Plant 8:

$$P_{11} = \frac{-.2851 (s + .0645)(s + .4775)(s + 310.4726)}{(s + .4017 \pm j.2715)(s - 1.6087)(s + 25.6875)}$$

$$P_{12} = \frac{.0866 (s - .3067 \pm j5.0381)(s + 10.2866)}{(s + .4017 \pm j.2715)(s - 1.6087)(s + 25.6875)}$$

$$P_{21} = \frac{-.0094 (s - 6.9775 \pm j3.5682)(s - 7.956)}{(s - .1735 \pm j1.287)(s + 2.7335)(s + 26.1771)}$$

$$P_{22} = \frac{11.6 (s - .18 \pm j1.28)(s - 208.52)}{(s - .1735 \pm j1.287)(s + 2.7335)(s + 26.1771)}$$

Plant 9:

$$P_{11} = \frac{-.2989 (s - 1.3753)(s + 1.3976)(s + 283.4249)}{(s - 1.2281)(s - 1.5037)(s + 1.6486)(s + 28.2901)}$$

$$P_{12} = \frac{.3979 (s + 1.0128 \pm j7.0858)(s - .3954)}{(s - 1.2281)(s - 1.5037)(s + 1.6486)(s + 28.2901)}$$

$$P_{21} = \frac{-.0445 (s - 4.0378 \pm j4.4269)(s - 4.8199)}{(s + .8987)(s + 2.2301)(s + 5.0714)(s + 22.221)}$$

$$P_{22} = \frac{4.0 (s + .7283)(s + 4.4099)(s - 491.448)}{(s + .8987)(s + 2.2301)(s + 5.0714)(s + 22.221)}$$

Plant 10:

$$P_{11} = \frac{-.3252 (s + .0806)(s + .4960)(s + 270.3689)}{(s - 1.5679)(s + .07)(s + .7508)(s + 25.6362)}$$

$$P_{12} = \frac{.0586 (s - .2148 \pm j2.9383)(s + 24.3299)}{(s - 1.5679)(s + .07)(s + .7508)(s + 25.6362)}$$

$$P_{21} = \frac{-.0487 (s - 3.4395 \pm j5.1491)(s - 4.4587)}{(s - .1926 \pm j1.2422)(s + 2.8391)(s + 24.2866)}$$

$$P_{22} = \frac{8.5 (s - .2 \pm j1.23)(s - 274.46)}{(s - .1926 \pm j1.2422)(s + 2.8391)(s + 24.2866)}$$

Plant 11:

$$P_{11} = \frac{-.2166 (s + .25 \pm j.41)(s + 434.56)}{(s + .3615 \pm j.6873)(s - 1.6295)(s + 27.7991)}$$

$$P_{12} = \frac{.0626 (s - .1836 \pm j4.8853)(s + 21.4134)}{(s + .3615 \pm j.6873)(s - 1.6295)(s + 27.7991)}$$

$$P_{21} = \frac{.1777 (s - 2.925 \pm j4.6398)(s - 4.0236)}{(s - .2896 \pm j1.1479)(s + 2.7237)(s + 28.5771)}$$

$$P_{22} = \frac{18.8 (s - .3 \pm j1.15)(s - 141.17)}{(s - .2896 \pm j1.1479)(s + 2.7237)(s + 28.5771)}$$

Plant 12:

$$P_{11} = \frac{-0.3292 (s + .0107)(s + .4651)(s + 255.6391)}{(s - .1295)(s - 1.3674)(s + .8398)(s + 28.2645)}$$

$$P_{12} = \frac{.0794 (s + .136 \pm j1.4785)(s + 17.5566)}{(s - .1295)(s - 1.3674)(s + .8398)(s + 28.2645)}$$

$$P_{21} = \frac{.0091 (s - 2.6075 \pm j2.8847)(s - 2.5251)}{(s - .0717 \pm j1.4514)(s + 2.8098)(s + 25.8774)}$$

$$P_{22} = \frac{13.1 (s - .07 \pm j1.44)(s - 186.58)}{(s - .0717 \pm j1.4514)(s + 2.8098)(s + 25.8774)}$$

Plant 13:

$$P_{11} = \frac{-.4996 (s + .0540)(s + 2.207)(s + 3.9871)(s + 157.7545)}{(s + 3.3047 \pm j.3978)(s - 1.4545)(s - .1246)(s + 21.8672)}$$

$$P_{12} = \frac{-.0255 (s + 1.8038 \pm j9.9503)(s - 1.4856)(s + 13.2653)}{(s + 3.3047 \pm j.3978)(s - 1.4545)(s - .1246)(s + 21.8672)}$$

$$P_{21} = \frac{3.0 (s + 2.8506 \pm j1.7687)(s - 8.3761 \pm j14.9647)}{(s + 1.5873 \pm j3.3906)(s - 1.5518)(s + 2.818)(s + 25.2054)}$$

$$P_{22} = \frac{14.0 (s + 1.65 \pm j3.34)(s - 1.55)(s - 183.96)}{(s + 1.5873 \pm j3.3906)(s - 1.5518)(s + 2.818)(s + 25.2054)}$$

Plant 14:

$$P_{11} = \frac{-.3 (s - .1903)(s + 2.8209)(s + 11.0232) + 252.2958}{(s - .2471)(s - 1.4847)(s + 3.4722)(s + 9.8258) + (s + 26.0541)}$$

$$P_{12} = \frac{-.0503 (s + 2.4767 \pm j8.1244)(s - 1.037)(s + 23.5822)}{(s - .2471)(s - 1.4847)(s + 3.4722)(s + 9.8258)(s + 26.0541)}$$

$$P_{21} = \frac{2.0 (s + 2.5558 \pm j1.6644)(s - 8.3421 \pm j15.37776)}{(s + 1.5486 \pm j3.2413)(s - 3.0397)(s + 3.1797)(s + 23.8742)}$$

$$P_{22} = \frac{12.0 (s + 1.69 \pm j3.27)(s - 3.04)(s - 205.4)}{(s + 1.5486 \pm j3.2413)(s - 3.0397)(s + 3.1797)(s + 23.8742)}$$

Plant 15:

$$P_{11} = \frac{-0.521 (s + .17)(s + 1.79)(s - 2.52)(s + 152.27)}{(s - .5674 \pm j.3551)(s - 2.9824)(s + 2.4421)(s + 22.0326)}$$

$$P_{12} = \frac{.0008 (s + 2.67 \pm j4.68)(s - 3.25)(s - 394.71)}{(s - .5674 \pm j.3551)(s - 2.9824)(s + 2.4421)(s + 22.0326)}$$

$$P_{21} = \frac{3.4 (s + 2.3523 \pm j2.4551)(s - 10.9636 \pm j12.6972)}{(s + 1.4546 \pm j3.5011)(s - 1.2929)(s + 1.9519)(s + 37.0281)}$$

$$P_{22} = \frac{12.0 (s + 1.49 \pm j3.51)(s - 1.29)(s - 210.1)}{(s + 1.4546 \pm j3.5011)(s - 1.2929)(s + 1.9519)(s + 37.0281)}$$

Plant 16:

$$P_{11} = \frac{-.3 (s - .3115)(s + 3.1996)(s + 10.5889)(s + 335.1456)}{(s - .3311)(s - 1.5017)(s + 3.94)(s + 9.2736)(s + 26.796)}$$

$$P_{12} = \frac{.0007 (s + 6.2 \pm j7.4)(s - .6)(s - 1062.4)}{(s - .3311)(s - 1.5017)(s + 3.94)(s + 9.2736)(s + 26.796)}$$

$$P_{21} = \frac{-(s + 16.8919 \pm j5.92)(s + 1.2536)(s - 3.07)}{(s + 1.4437 \pm j1.3882)(s + 2.5794 \pm j3.1846)(s + 41.0257)}$$

$$P_{22} = \frac{15 (s + 2.1 \pm j3.02)(s + 2.33)(s - 178.81)}{(s + 1.4437 \pm j1.3882)(s + 2.5794 \pm j3.1846)(s + 41.0257)}$$

Plant 17:

$$P_{11} = \frac{-.1629 (s + .93 \pm j4.4)(s + 1.06)(s + 134.86)}{(s + 1.0032 \pm j4.3811)(s - .7798)(s + 1.8683)(s + 18.0345)}$$

$$P_{12} = \frac{.1633 (s + .7866 \pm j4.1148)(s + 9.8944)(s + 15.6052)}{(s + 1.0032 \pm j4.3811)(s - .7798)(s + 1.8683)(s + 18.0345)}$$

$$P_{21} = \frac{-.0217 (s - 5.8174 \pm j2.1211)(s - 4.199 \pm j6.6882)}{(s + .8632 \pm j2.903)(s - .7169)(s + 1.427)(s + 28.2258)}$$

$$P_{22} = \frac{4.3 (s + .69 \pm j2.36)(s - .73)(s - 136.92)}{(s + .8632 \pm j2.903)(s - .7169)(s + 1.427)(s + 28.2258)}$$

Plant 18:

$$P_{11} = \frac{-0.0065 (s + .2 \pm j1.1)(s - 1.9)(s + 4735.2)}{(s + .3895 \pm j1.319)(s - .8989)(s - 1.8049)(s + 28.6698)}$$

$$P_{12} = \frac{.0468 (s + .1544 \pm j2.5222)(s - 3.6814)(s + 40.2836)}{(s + .3895 \pm j1.319)(s - .8989)(s - 1.8049)(s + 28.6698)}$$

$$P_{21} = \frac{-.0074 (s - 7.7526 \pm j2.151)(s - 6.249 \pm j6.5219)}{(s + .9769 \pm j2.904)(s + 1.3558 \pm j.3167)(s + 28.3468)}$$

$$P_{22} = \frac{4.0 (s - .73 \pm j2.34)(s + 1.44)(s - 142.82)}{(s + .9769 \pm j2.904)(s + 1.3558 \pm j.3167)(s + 28.3468)}$$

Plant 19:

$$P_{11} = \frac{-.168 (s + 3.12 \pm j3.08)(s + .78)(s + 123.55)}{(s + 3.7997 \pm j2.638)(s - .6507)(s + 1.1433)(s + 15.7975)}$$

$$P_{12} = \frac{.0799 (s + .8917 \pm j1.7096)(s + 7.1705 \pm j8.703)}{(s + 3.7997 \pm j2.638)(s - .6507)(s + 1.1433)(s + 15.7975)}$$

$$P_{21} = \frac{-.0204 (s - 5.7687 \pm j2.1496)(s - 4.1616 \pm j6.8226)}{(s + .9496 \pm j2.8375)(s - .2859)(s + 1.2766)(s + 28.6797)}$$

$$P_{22} = \frac{4.3 (s + .74 \pm j2.29)(s - .3)(s - 135.8)}{(s + .9496 \pm j2.8375)(s - .2859)(s + 1.2766)(s + 28.6797)}$$

Plant 20:

$$P_{11} = \frac{-.3058 (s + 1.4717 \pm j2.7703)(s + 57.111)}{(s + 1.7342 \pm j3.1302)(s - .7304)(s + 14.6544)}$$

$$P_{12} = \frac{.0666 (s - 3.4067 \pm j13.411)(s + 1.923)}{(s + 1.7342 \pm j3.1302)(s - .7304)(s + 14.6544)}$$

$$P_{21} = \frac{-.2984 (s - 3.441 \pm j4.125)(s - 4.4862)}{(s + .9379 \pm j2.9016)(s + 1.3186)(s + 29.1944)}$$

$$P_{22} = \frac{3.2 (s + .84 \pm j2.29)(s - 192.74)}{(s + .9379 \pm j2.9016)(s + 1.3186)(s + 29.1944)}$$

Plant 21:

$$p_{11} = \frac{-.1097 (s + .58 \pm j.29)(s + 3.94)(s + 226.72)}{(s - .5534 \pm j.5361)(s + 2.8149 \pm j1.5486)(s + 22.5077)}$$

$$p_{12} = \frac{-.0103 (s + 5.0228 \pm j1.0488)(s - 3.3155 \pm j17.4382)}{(s - .5534 \pm j.5361)(s + 2.8149 \pm j1.5486)(s + 22.5077)}$$

$$p_{21} = \frac{-.0183 (s - 5.8002 \pm j2.1733)(s - 4.1918 \pm j6.9027)}{(s + 1.1052 \pm j2.7195)(s - .3679)(s + 1.3553)(s + 26.261)}$$

$$p_{22} = \frac{4.3 (s + .92 \pm j2.32)(s - .33)(s - 140.53)}{(s + 1.1052 \pm j2.7195)(s - .3679)(s + 1.3553)(s + 26.261)}$$

Plant 22:

$$p_{11} = \frac{-.11 (s + .27 \pm j.72)(s + 1.7 \pm j7.01)(s + 233.46)}{(s - .3771 \pm j.3374)(s + 1.6449 \pm j7.0144)(s + 1.1581)(s + 21.8478)}$$

$$p_{12} = \frac{-.0099 (s + 3.8997 \pm j5.1272)(s - 1.9269 \pm j18.6132)(s + 3.0669)}{(s - .3771 \pm j.3374)(s + 1.6449 \pm j7.0144)(s + 1.1581)(s + 21.8478)}$$

$$p_{21} = \frac{.0174 (s - 6.7816 \pm j4.374)(s - 4.9128 \pm j9.3707)(s - 7.412)}{(s + 1.0801 \pm j2.8068)(s - .3868)(s + 1.2168)(s + 1.8125)(s + 27.1018)}$$

$$p_{22} = \frac{3.9 (s + .96 \pm j2.4)(s - .31)(s + 1.47)(s - 148.86)}{(s + 1.0801 \pm j2.8068)(s - .3868)(s + 1.2168)(s + 1.8125)(s + 27.1018)}$$

Equivalent MISO Plants for Inner Loop Design

The equivalent MISO plants (design models) are listed below for all 22 plant cases.

Appropriate pole-zero cancellations have been accomplished when warranted.

Plant 1:

$$q_{11} = \frac{-.3140 (s + .2684 \pm j.3483)(s + 277.25)}{(s + .3869 \pm j.3167)(s - 1.5865)(s + 24.926)}$$

$$q_{22} = \frac{12.47 (s - 196.6)}{(s + 2.8959)(s + 25.124)}$$

Plant 2 (C* nominal):

$$q_{11} = \frac{-.346 (s + .25838 \pm j.3736)(s + 245.65)}{(s - .13989)(s + .91724)(s - 1.5099)(s + 24.296)}$$

$$q_{22} = \frac{13.03 (s - 189)}{(s + 2.8309)(s + 25.586)}$$

Plant 3:

$$q_{11} = \frac{-.359 (s + .30764 \pm j.31508)(s + 235.95)}{(s - .0638)(s + .92608)(s - 1.5315)(s + 23.975)}$$

$$q_{22} = \frac{13.17 (s - 187.93)}{(s + 2.8962)(s + 25.373)}$$

Plant 4:

$$q_{11} = \frac{-.319 (s + .26569 \pm j.3213)(s + 271.39)}{(s + .18169)(s + .61297)(s - 1.5606)(s + 24.93)}$$

$$q_{22} = \frac{12.75 (s - 192.41)}{(s + 2.8305)(s + 25.486)}$$

Plant 5:

$$q_{11} = \frac{-.345 (s + .21854 \pm j.3758)(s + 246.6)}{(s - .19413)(s + .90437)(s - 1.507)(s + 24.412)}$$

$$q_{22} = \frac{13.12 (s - 187.51)}{(s + 2.7608)(s + 25.92)}$$

Plant 6:

$$q_{11} = \frac{-.295 (s + .23583 \pm j.38663)(s + 298.2)}{(s + .3526 \pm j.51321)(s - 1.6102)(s + 25.328)}$$

$$q_{22} = \frac{11.67 (s - 207.98)}{(s + 2.8977)(s + 24.84)}$$

Plant 7:

$$q_{11} = \frac{-.312 (s + .01791)(s + .58714)(s + 278.96)}{(s + .17082)(s + .67914)(s - 1.5968)(s + 24.952)}$$

$$q_{22} = \frac{10.14 (s - 234.39)}{(s + 2.8862)(s + 24.605)}$$

Plant 8:

$$q_{11} = \frac{-.285 (s + .06376)(s + .47812)(s + 310.52)}{(s + .40173 \pm j.27152)(s - 1.6087)(s + 25.688)}$$

$$q_{22} = \frac{11.61 (s - 208.54)}{(s + 2.7335)(s + 26.117)}$$

Plant 9:

$$q_{11} = \frac{-.295 (s + 1.398)(s + 284.92)}{(s - 1.5037)(s + 1.6486)(s + 28.29)}$$

$$q_{22} = \frac{4.35 (s + .72802)(s + 4.4095)(s - 495.55)}{(s + .8987)(s + 2.2301)(s + 5.0714)(s + 22.221)}$$

Plant 10:

$$q_{11} = \frac{-.325 (s + .07983)(s + .49673)(s + 270.5)}{(s + .07001)(s + .75077)(s - 1.5679)(s + 25.636)}$$

$$q_{22} = \frac{8.52 (s - 274.61)}{(s + 2.8391)(s + 24.287)}$$

Plant 11:

$$q_{11} = \frac{-.217 (s + .2519 \pm j.40803)(s + 433.69)}{(s + .36147 \pm j.68732)(s - 1.6295)(s + 27.799)}$$

$$q_{22} = \frac{18.86 (s - 141.07)}{(s + 2.7237)(s + 28.577)}$$

Plant 12:

$$q_{11} = \frac{-.329 (s + .01071)(s + .46506)(s + 255.62)}{(s - .12946)(s + .83982)(s - 1.3674)(s + 28.246)}$$

$$q_{22} = \frac{13.1 (s - 186.56)}{(s + 2.8098)(s + 25.877)}$$

Plant 13:

$$q_{11} = \frac{-.494 (s + .06779)(s + 2.1959)(s + 3.9923)(s + 158.59)}{(s - .1246)(s - 1.4545)(s + 3.3047 \pm j.39783)(s + 21.867)}$$

$$q_{22} = \frac{13.66 (s + .06779)(s + 1.6484 \pm j.3.3429)(s - 185.05)}{(s + .05401)(s + 2.818)(s + 1.5873 \pm j.3.3906)(s + 25.205)}$$

Plant 14:

$$q_{11} = \frac{-.335 (s + 2.8194)(s + 11.027)(s + 255.81)}{(s + 3.1797)(s + 1.5486 \pm j3.2413)(s + 23.874)}$$

$$q_{22} = \frac{11.67 (s + 1.6904 \pm j3.2728)(s - 207.77)}{(s + 3.1797)(s + 1.5486 \pm j3.2413)(s + 23.874)}$$

Plant 15:

$$q_{11} = \frac{-.521 (s + .15212)(s + 1.7987)(s + 152.16)}{(s - .56744 \pm j.35513)(s + 2.4421)(s + 22.033)}$$

$$q_{22} = \frac{12.04 (s + .15212)(s + 1.4877 \pm j3.5102)(s - 210.14)}{(s + 1.6969)(s + 1.9519)(s + 1.4546 \pm j3.5011)(s + 37.028)}$$

Plant 16:

$$q_{11} = \frac{-.267 (s + 3.2086)(s + 10.588)(s + 335.3)}{(s - 1.5017)(s + 3.94)(s + 9.2736)(s + 26.796)}$$

$$q_{22} = \frac{15.2 (s + 2.321)(s + 2.1002 \pm j3.0195)(s - 178.74)}{(s + 1.4437 \pm j1.3882)(s + 2.5794 \pm j3.1846)(s + 41.026)}$$

Plant 17:

$$q_{11} = \frac{-.162 (s + 1.0438)(s + .6915 \pm j2.3544)(s + .92911 \pm j4.402)(s + 135.19)}{(s - .77976)(s + 1.8683)(s + .6884 \pm j2.3563)(s + 1.0032 \pm j4.3811)(s + 18.035)}$$

$$q_{22} = \frac{4.28 (s + .6915 \pm j2.3544)(s + 135.19)(s - 137.27)}{(s + 1.427)(s + .8632 \pm j2.9029)(s + 28.226)(s + 134.86)}$$

Plant 18:

$$q_{11} = \frac{-.0064 (s + .2444 \pm j1.1101)(s + 4796.9)}{(s - .89895)(s + .38949 \pm j1.3187)(s + 28.67)}$$

$$q_{22} = \frac{3.96 (s + 1.4489)(s + .72889 \pm j2.3398)(s - 142.87)}{(s + 1.3558 \pm j3.1675)(s + .9769 \pm j2.9039)(s + 28.347)}$$

Plant 19:

$$q_{11} = \frac{-.168 (s + .77389)(s + 3.1254 \pm j3.0781)(s + 123.69)}{(s - .65074)(s + 1.1433)(s + 3.7997 \pm j2.638)(s + 15.798)}$$

$$q_{22} = \frac{4.33 (s + .73949 \pm j2.2855)(s - 135.95)}{(s + 1.2766)(s + .94958 \pm j2.8375)(s + 28.68)}$$

Plant 20:

$$q_{11} = \frac{-0.299 (s + 1.4611 \pm j2.7785)(s + 57.515)}{(s - .73042)(s + 1.7342 \pm j3.1302)(s + 14.654)}$$

$$q_{22} = \frac{3.11 (s + .85121 \pm j2.2855)(s - 195.53)}{(s + 1.3168)(s + .93795 \pm j2.9016)(s + 29.194)}$$

Plant 21:

$$q_{11} = \frac{-.110 (s + .58244 \pm j3.1101)(s + 3.9353)(s + 226.65)}{(s - .55341 \pm j.53613)(s + 2.8149 \pm j1.5486)(s + 22.508)}$$

$$q_{22} = \frac{4.28 (s + .58244 \pm j3.1101)(s + .91586 \pm j2.3151)(s - 140.52)}{(s + .5777 \pm j.28569)(s + 1.3553)(s + 1.1052 \pm j2.7195)(s + 26.261)}$$

Plant 22: (p nominal)

$$q_{11} = \frac{-.106 (s + .27955 \pm j.76382)(s + 1.6965 \pm j7.0098)(s + 233.53)}{(s - .37709 \pm j.33739)(s + 1.1581)(s + 1.6449 \pm j7.0144)(s + 21.848)}$$

$$q_{22} = \frac{3.92 (s + .27955 \pm j.76382)(s + 1.4947)(s + .96561 \pm j2.3987)(s - 148.88)}{(s + .27039 \pm j.71526)(s + 1.2168)(s + 1.8125)(s + 1.0801 \pm j2.8068)(s + 27.102)}$$

Equivalent LTI SISO Plants for the Compensated Inner Loop

The equivalent SISO plants which represent the compensated inner loop are given below.

C equivalent plants:*

1g at 0.9M,20K

$$\frac{C^*}{C_{and}^*} = \frac{313.8 (s + 8.0405)}{(s + 3.7433)(s + 13.5335)(s + 48)}$$

3g at 0.9M,20K

$$\frac{C^*}{C_{and}^*} = \frac{169.8 (s + .9441)(s + 11.01)}{(s + .9417)(s + 4.0196)(s + 17.025 \pm j12.6838)}$$

5g at 0.9M,20K

$$\frac{C^*}{C_{\text{and}}^*} = \frac{101.8 (s + 8.4673)}{(s + 3.756)(s + 9.6438 \pm j11.4036)}$$

1g at 0.6M,30K

$$\frac{C^*}{C_{\text{and}}^*} = \frac{56.87 (s + .1931)(s + .7086)}{(s + .2228)(s + .5912)(s + 6.5933 \pm j3.8185)}$$

2g at 0.6M,30K

$$\frac{C^*}{C_{\text{and}}^*} = \frac{51.99 (s + 1.9574)}{(s + 1.8406)(s + 5.9432 \pm j4.2389)}$$

p equivalent plants:

10°/s at 0.9M,20K

$$\frac{p}{p_{\text{and}}} = \frac{52.6 (s + 51.0205)}{(s + 3.5428)(s + 12.4287 \pm j24.5786)}$$

20°/s at 0.9M,20K

$$\frac{p}{p_{\text{and}}} = \frac{15.4 (s + .0016 \pm j2.3695)(s + 35.1249)}{(s + .0018 \pm j2.3679)(s + 3.6354)(s + 5.1947 \pm j11.0401)}$$

30°/s at 0.9M,20K

$$\frac{p}{p_{\text{and}}} = \frac{164.16 (s + .1399)}{(s + .1332)(s + 3.7392)(s + 44.2895)}$$

10°/s at 0.6M,30K

$$\frac{p}{p_{\text{and}}} = \frac{16.9 (s + .0422 \pm j1.7017)(s + 30.2609)}{(s + .0394 \pm j1.7011)(s + 3.5992)(s + 4.9324 \pm j10.8324)}$$

20°/s at 0.6M,30K

$$\frac{p}{p_{\text{and}}} = \frac{14.9 (s + .3531 \pm j2.3073)(s + 37.8398)}{(s + .3529 \pm j2.3017)(s + 3.7098)(s + 5.1837 \pm j11.2158)}$$

30°/s at 0.6M,30K

$$\frac{p}{p_{\text{and}}} = \frac{12.1226 (s + 1.2922 \pm j2.9289)(s + 55.1569)}{(s + 1.3205 \pm j2.9075)(s + 3.9282)(s + 5.851 \pm j11.6793)}$$

Appendix B. Equivalent Plant Fits

This appendix provides the equivalent plant fits and errors for all 22 equivalent LTI plants. In each case, C^* (g) is given first, followed by p (deg/s). Each plot on the left shows both the actual and equivalent responses, and the errors are shown on the right. The plots are not normalized or enclosed within the respective bounds, since the composite normalized responses with the bounds are shown in Figure 3.3.

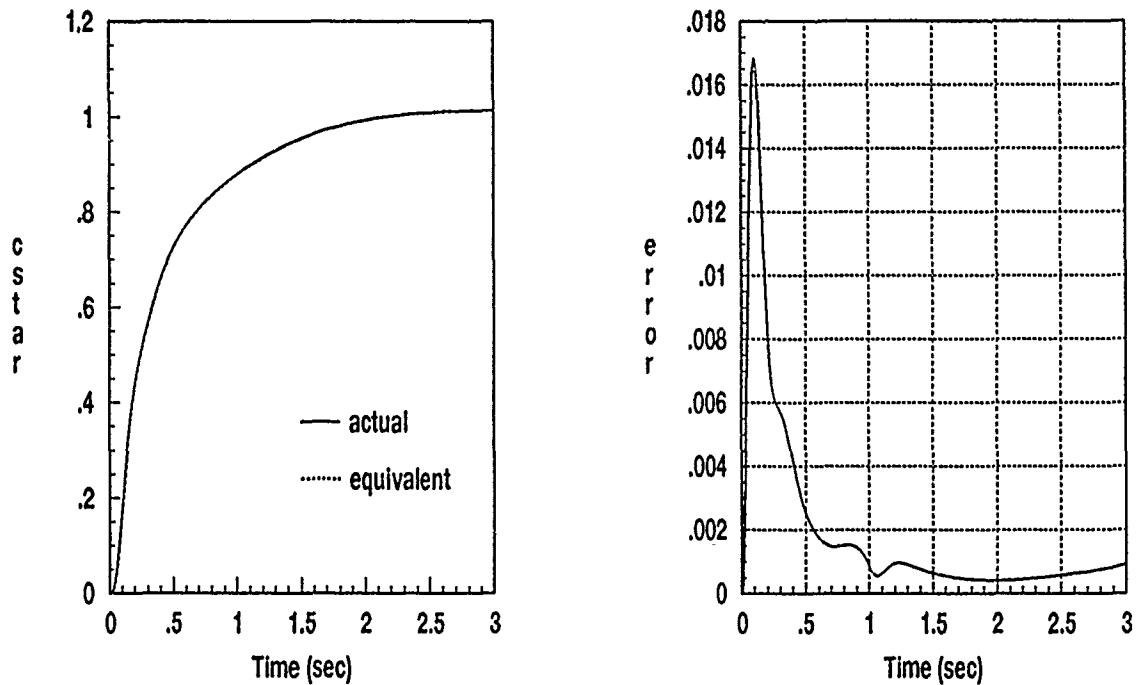


Figure B.1. Fit and Error for C^* , Plant 1

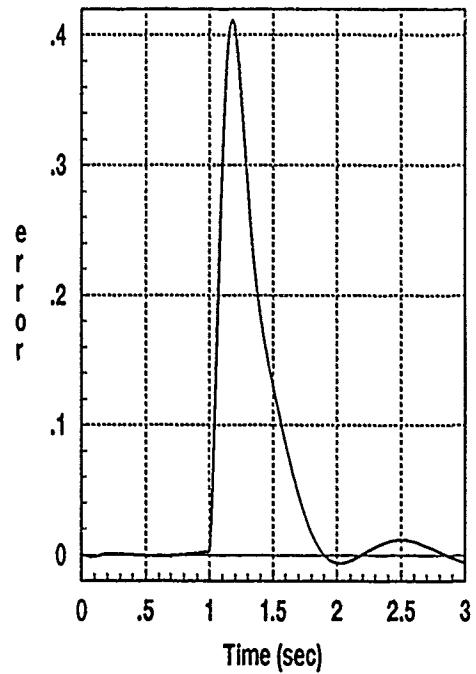
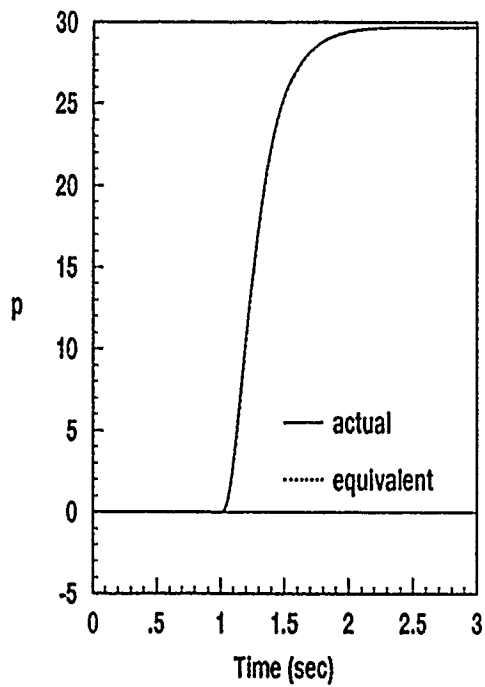


Figure B.2. Fit and Error for p , Plant 1

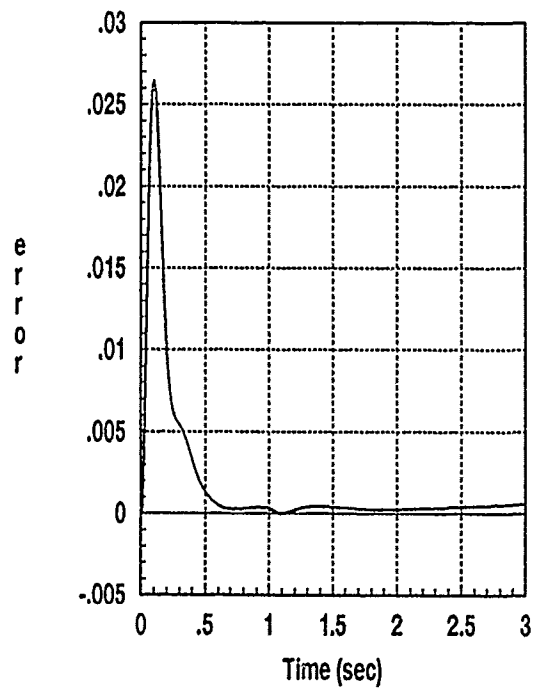
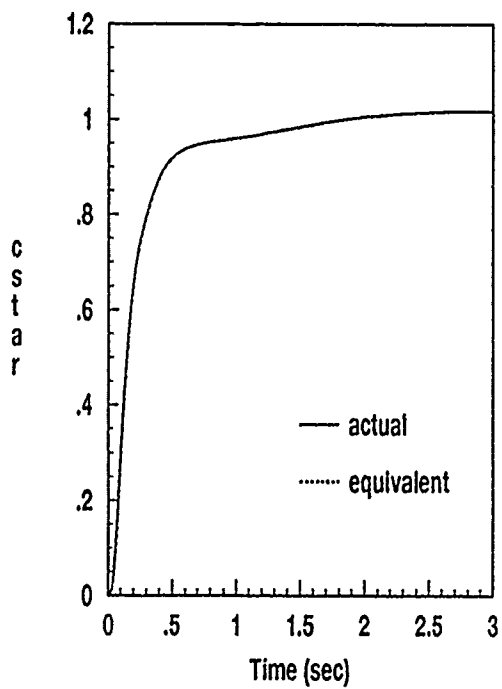


Figure B.3. Fit and Error for C^* , Plant 2

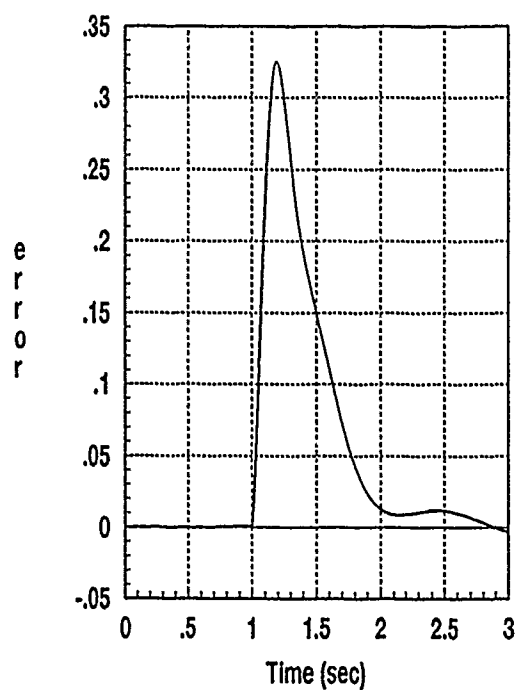
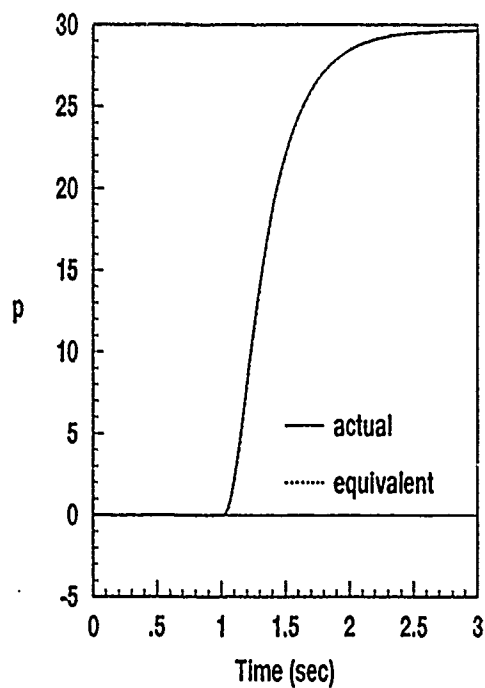


Figure B.4. Fit and Error for p , Plant 2

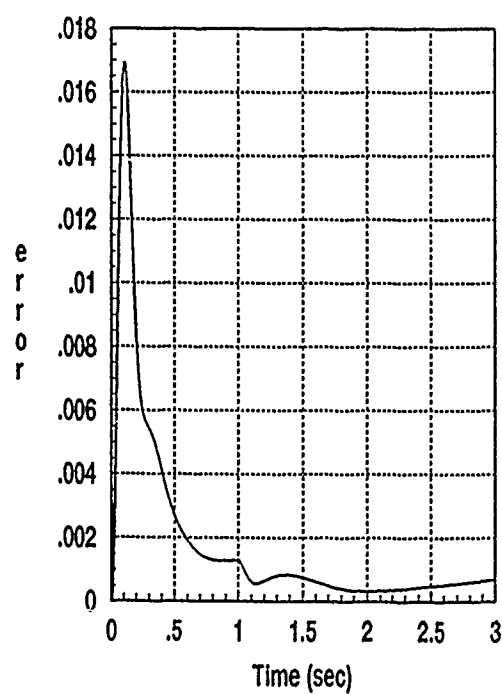
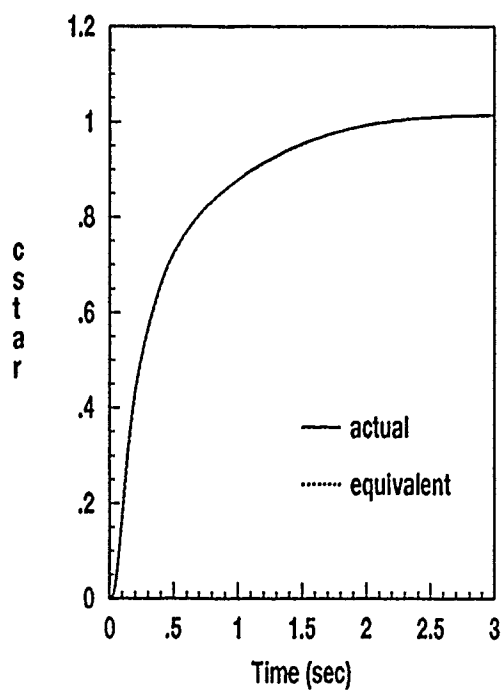


Figure B.5. Fit and Error for C^* , Plant 3

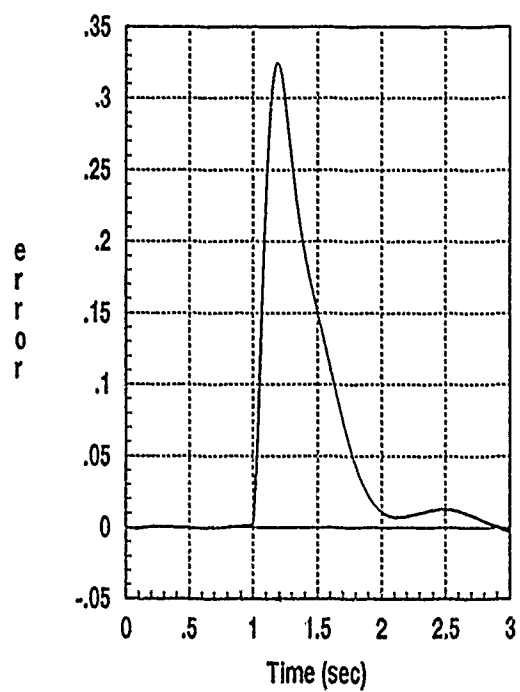
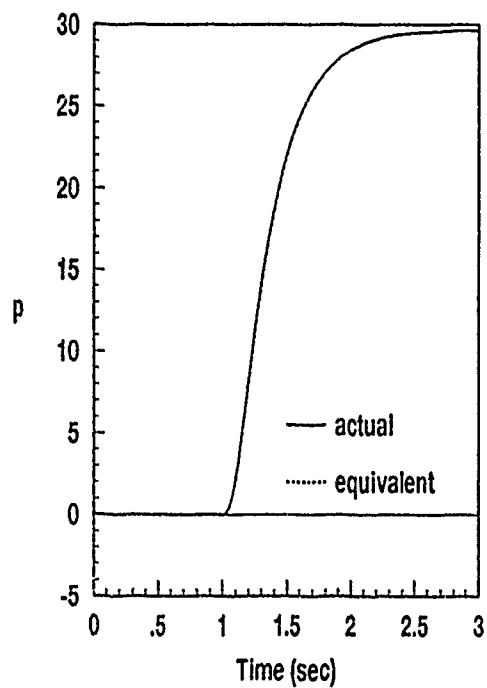


Figure B.6. Fit and Error for p , Plant 3

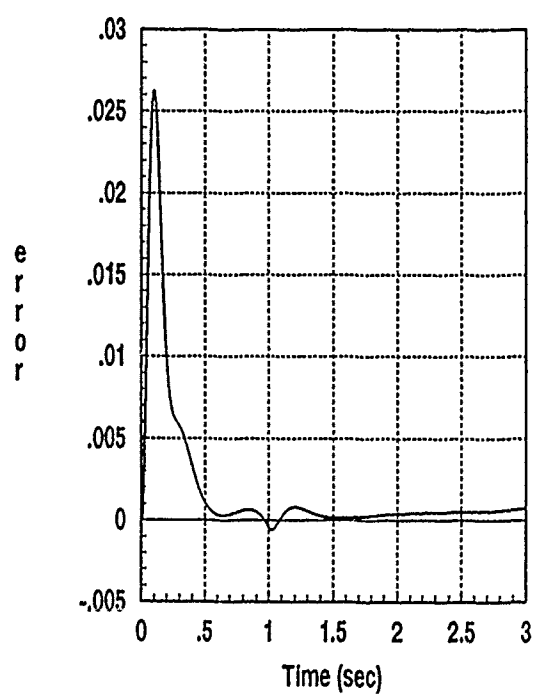
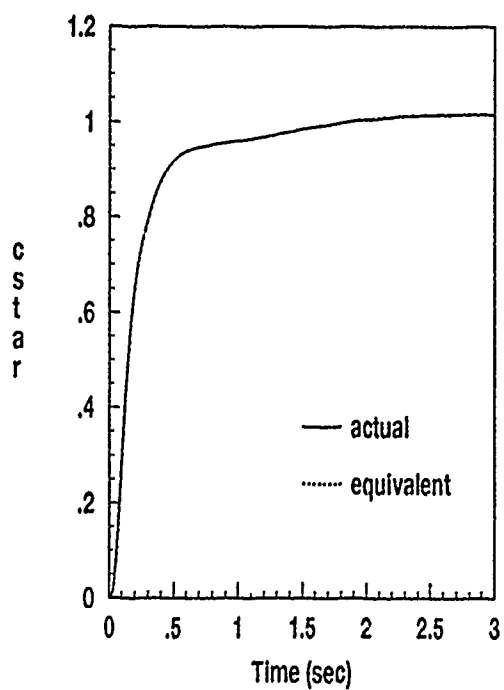


Figure B.7. Fit and Error for C^* , Plant 4

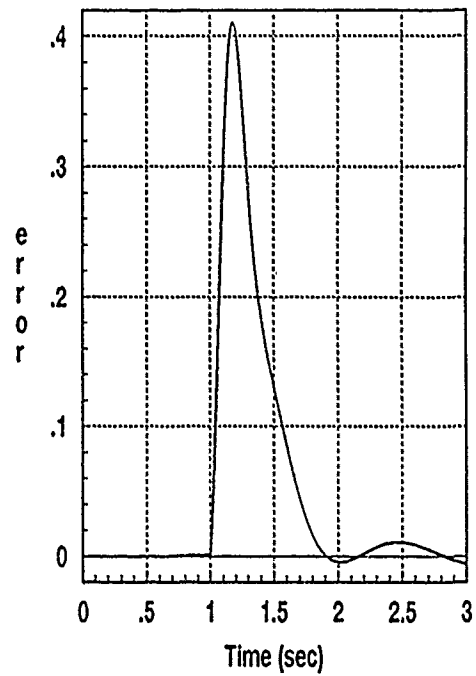
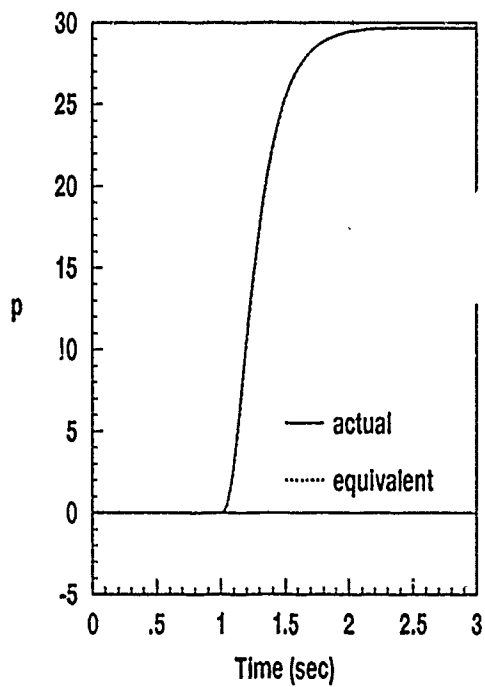


Figure B.8. Fit and Error for p , Plant 4

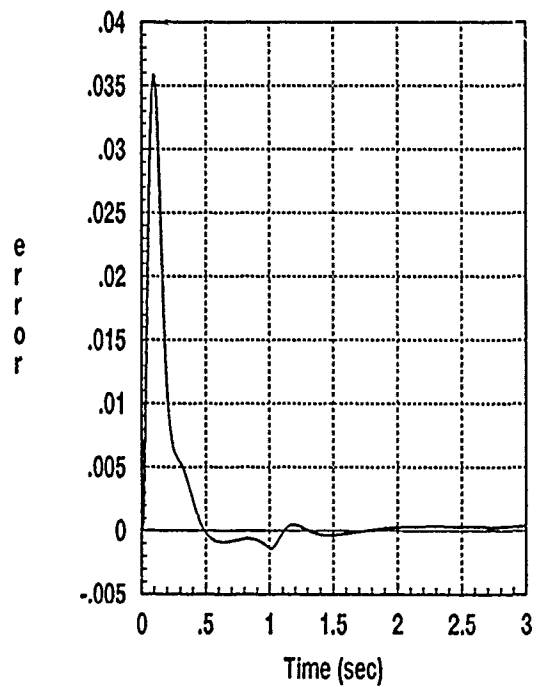
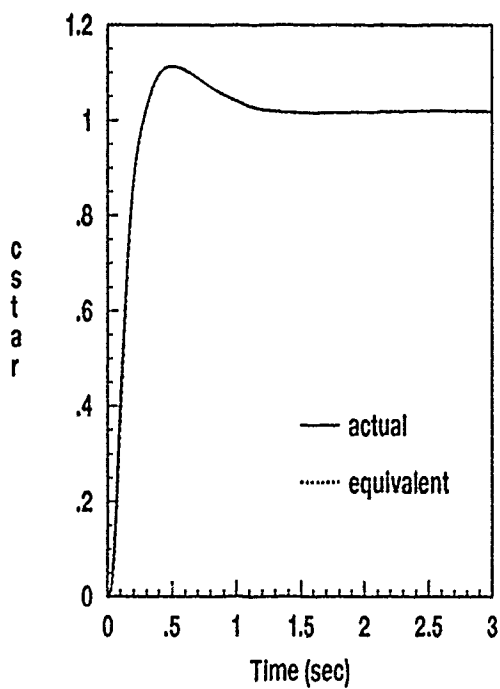


Figure B.9. Fit and Error for C^* , Plant 5

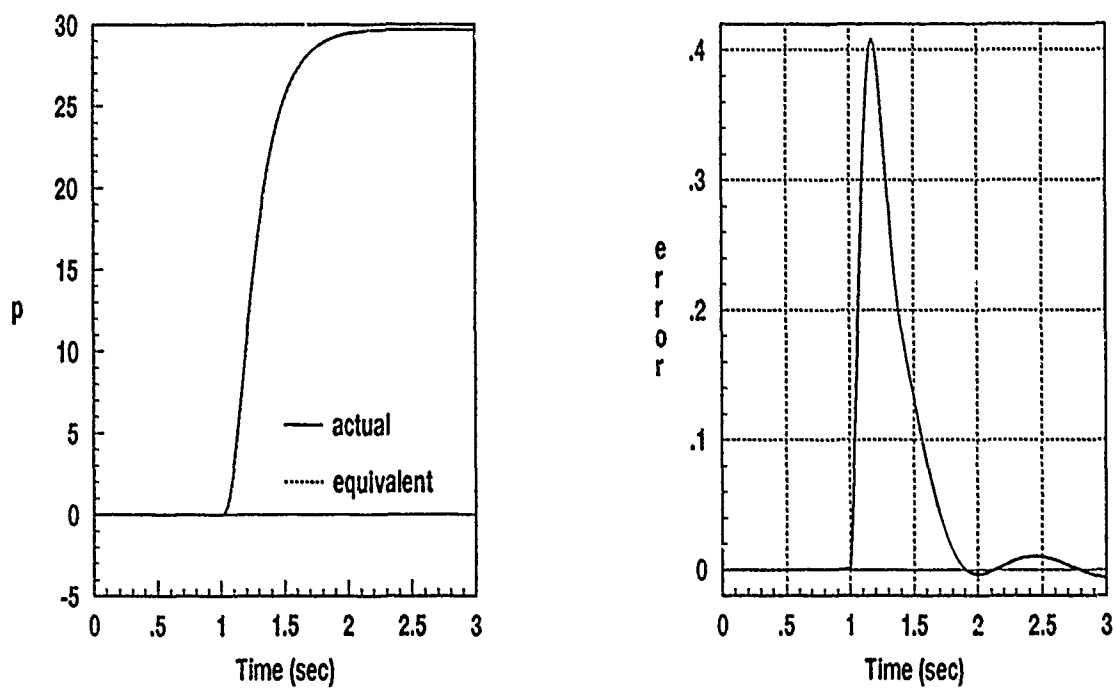


Figure B.10. Fit and Error for p , Plant 5

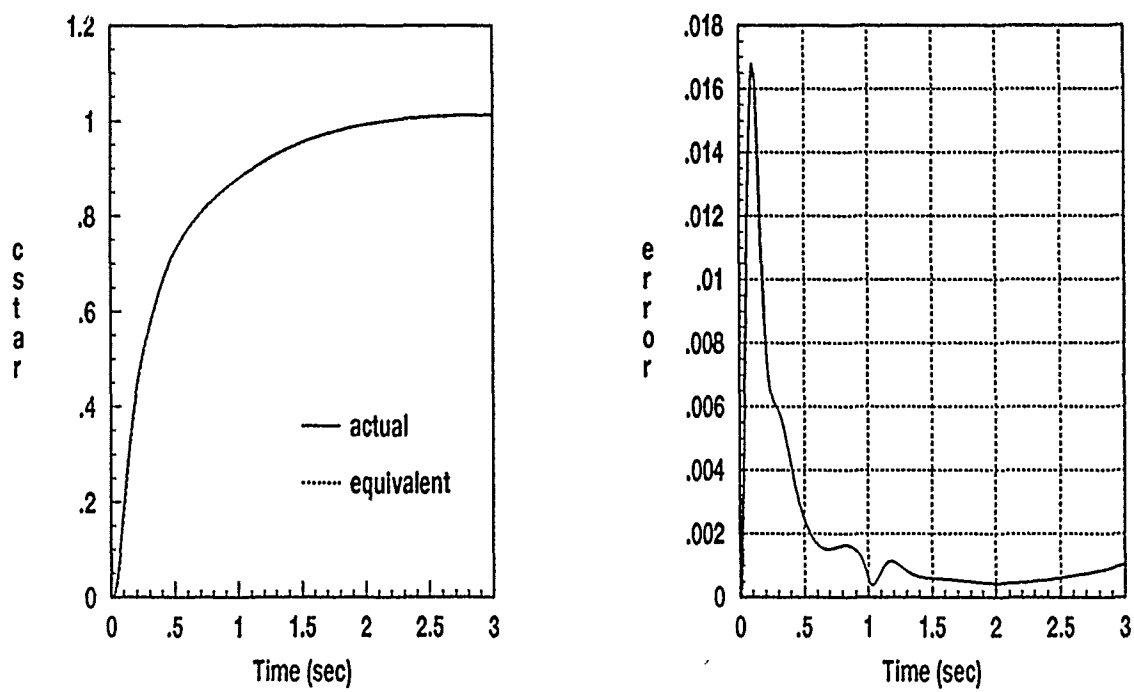


Figure B.11. Fit and Error for C^* , Plant 6

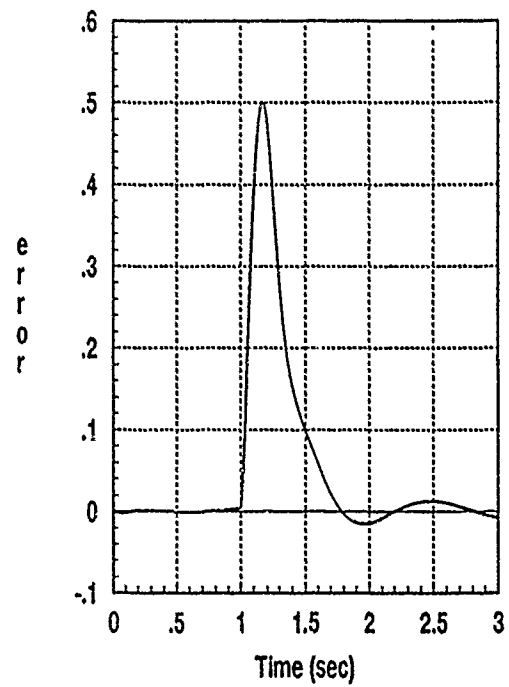
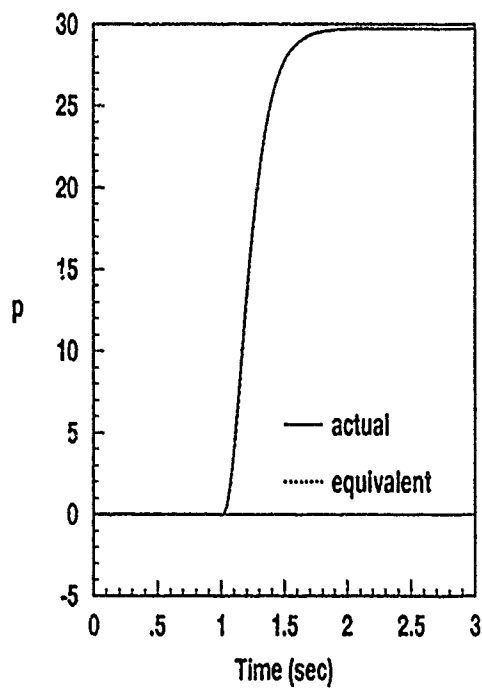


Figure B.12. Fit and Error for p , Plant 6

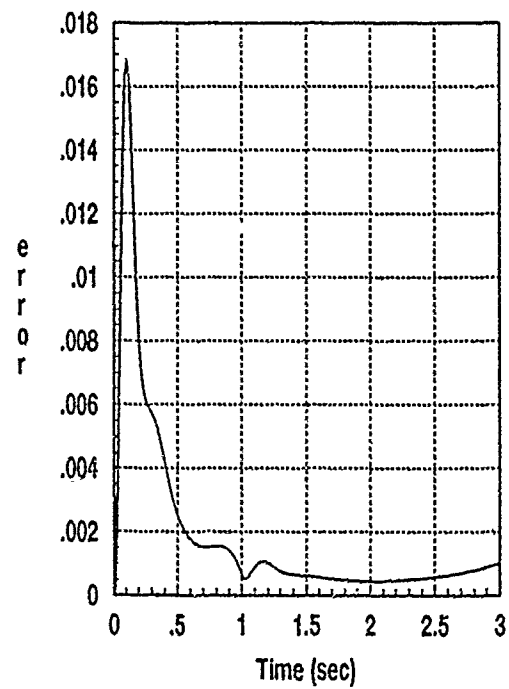
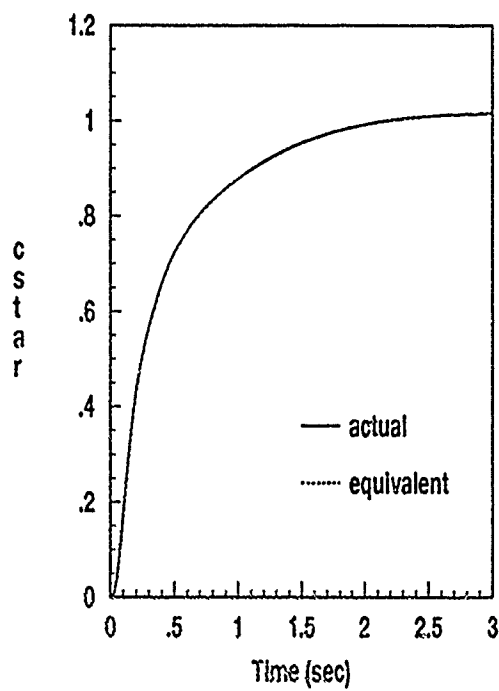


Figure B.13. Fit and Error for C^* , Plant 7

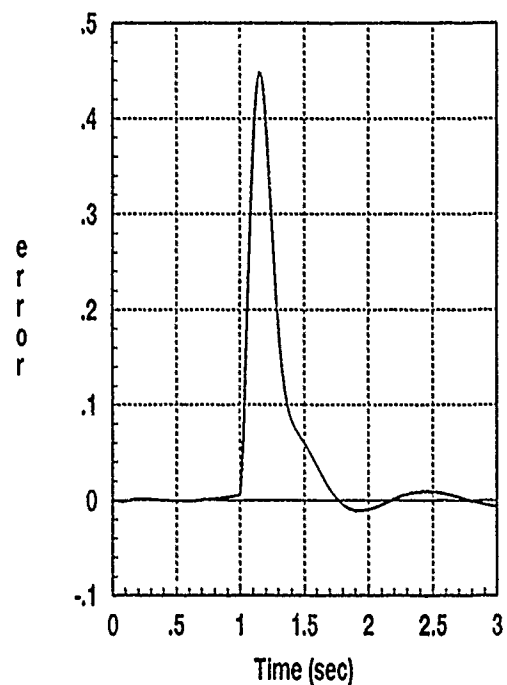
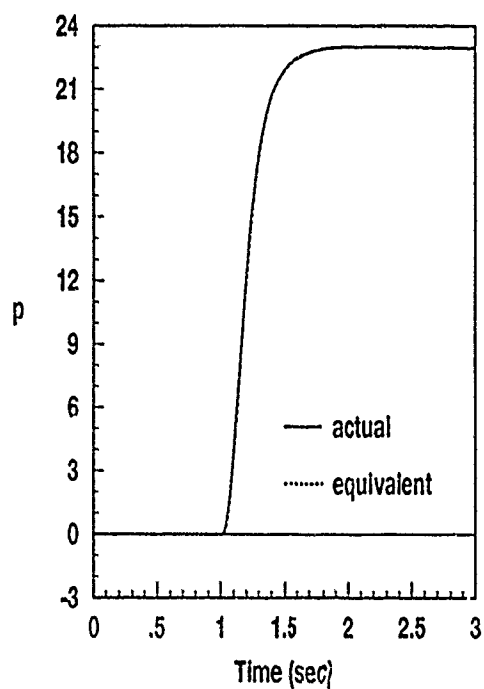


Figure B.14. Fit and Error for p , Plant 7

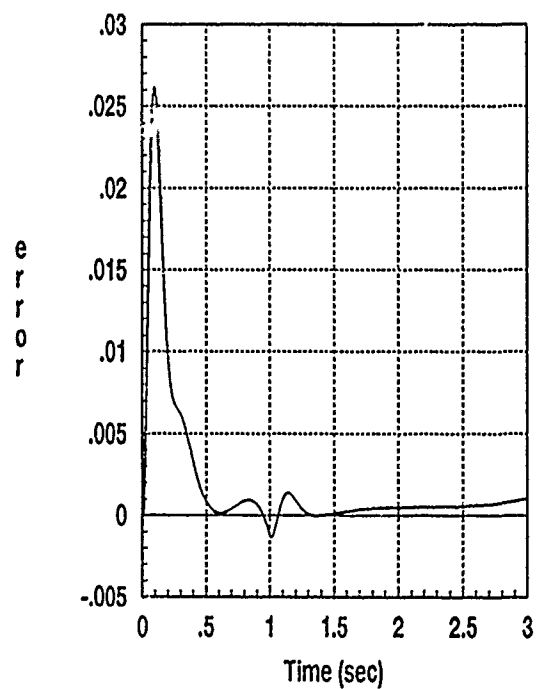
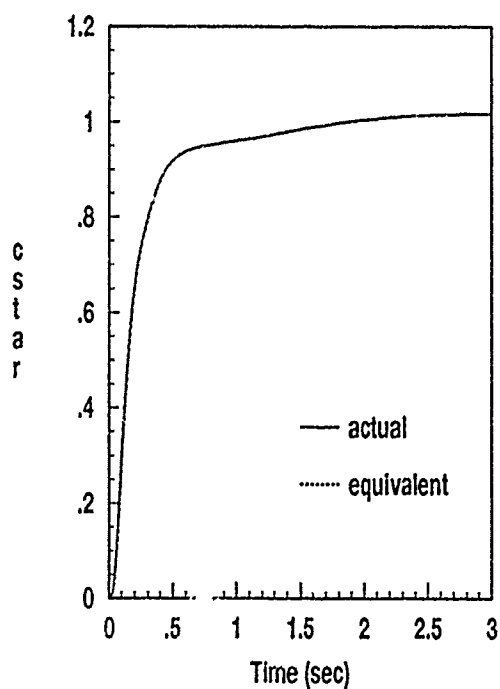


Figure B.15. Fit and Error for C^* , Plant 8

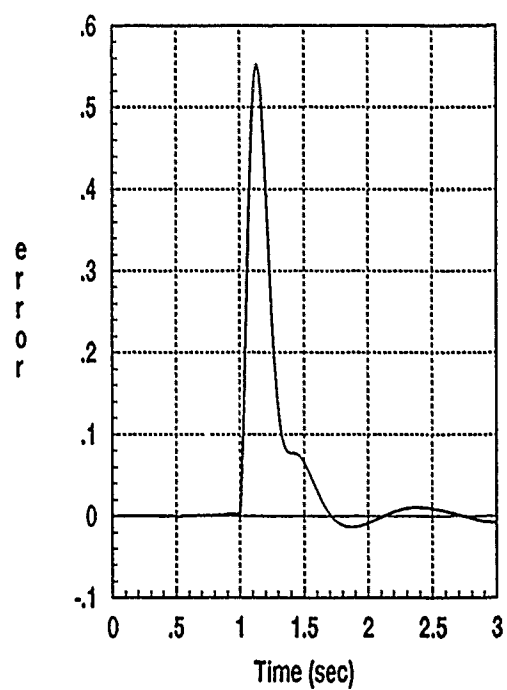
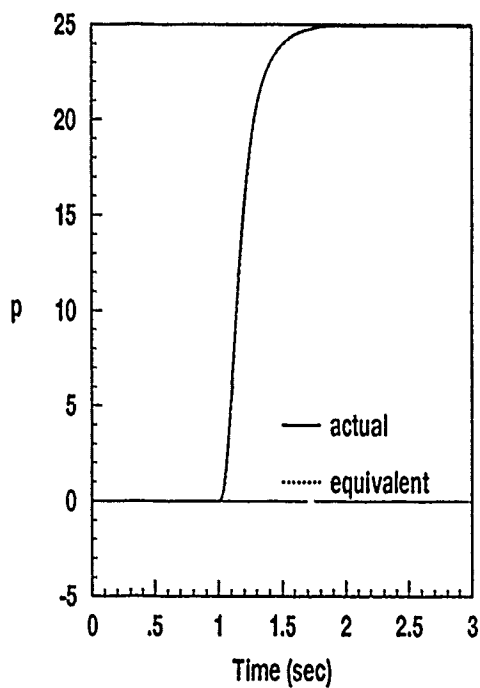


Figure B.16. Fit and Error for p , Plant 8

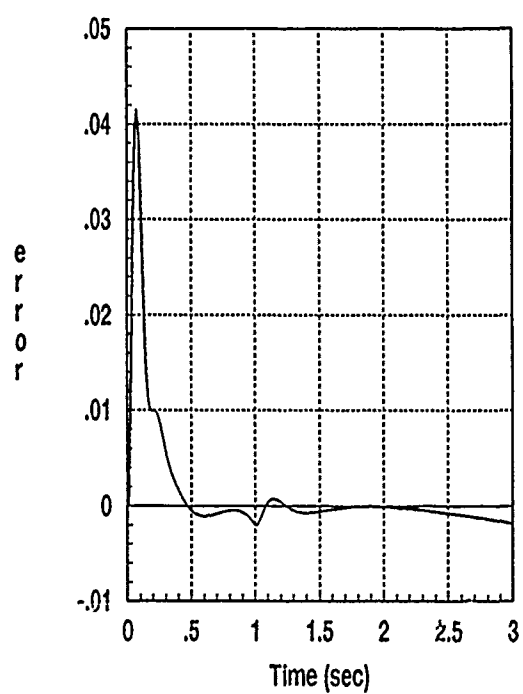
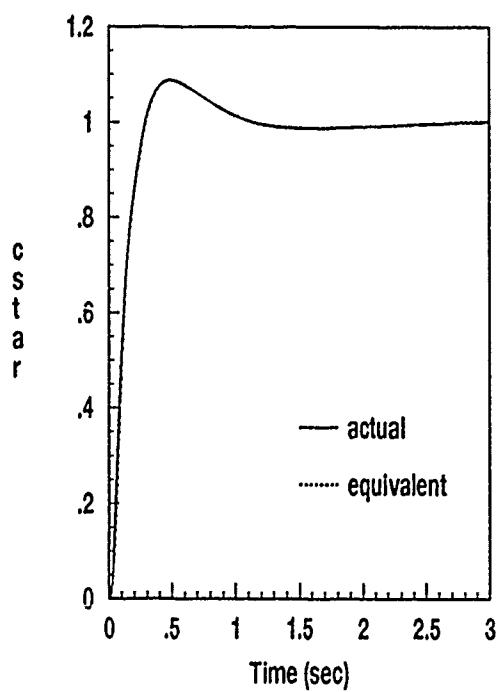


Figure B.17. Fit and Error for C^* , Plant 9

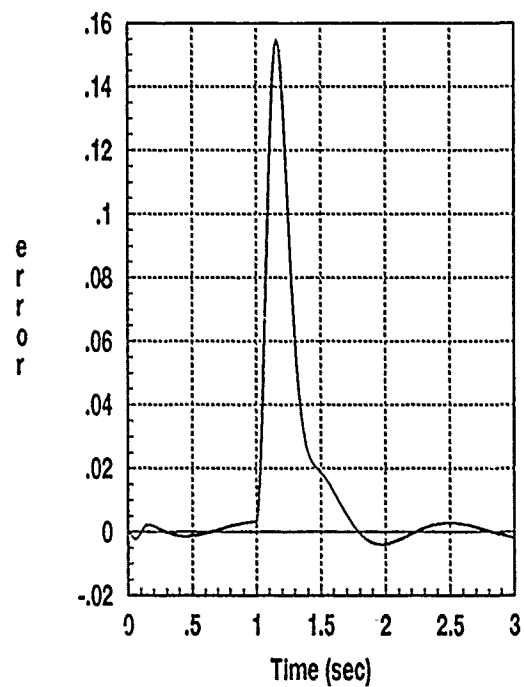
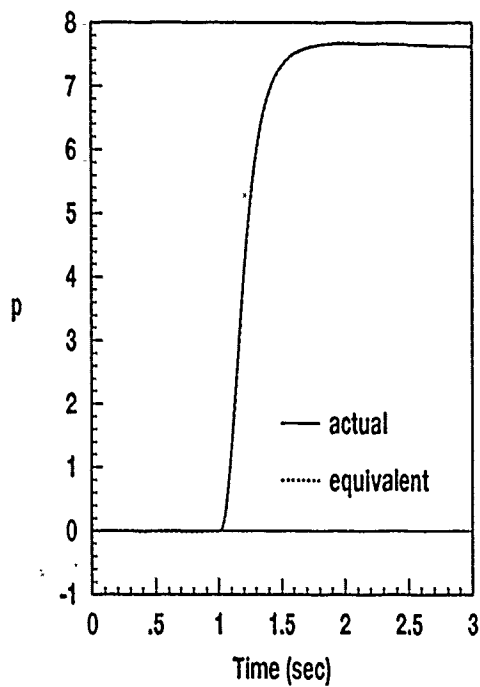


Figure B.18. Fit and Error for p , Plant 9

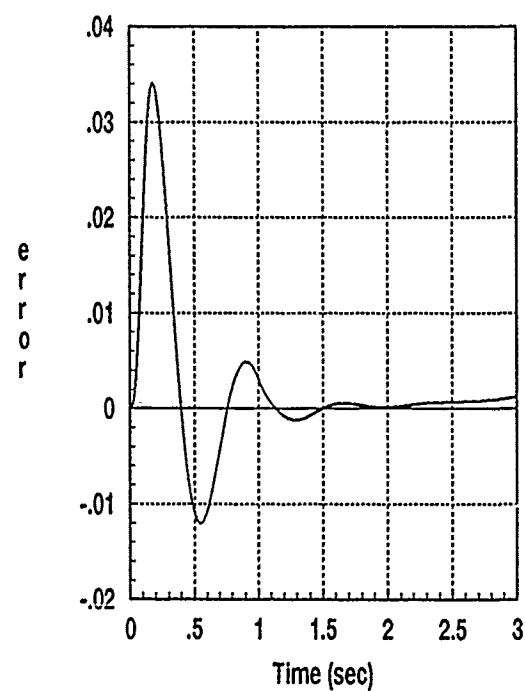
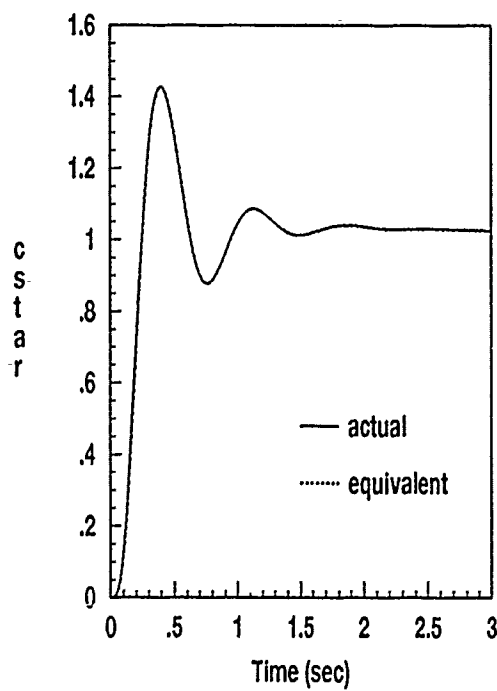


Figure B.19. Fit and Error for C^* , Plant 10

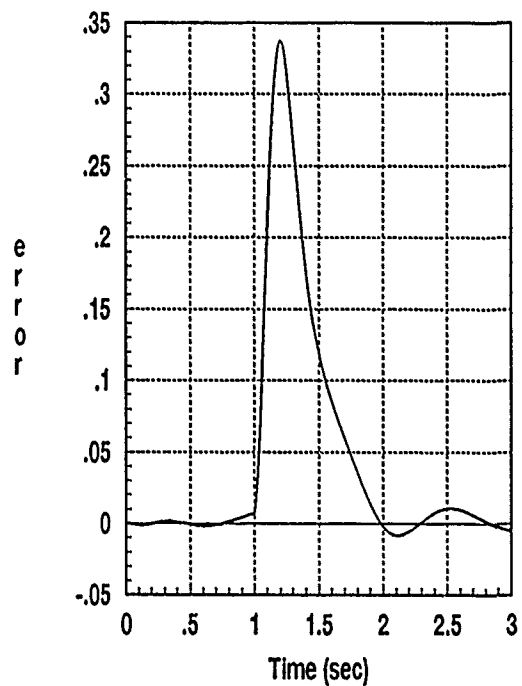
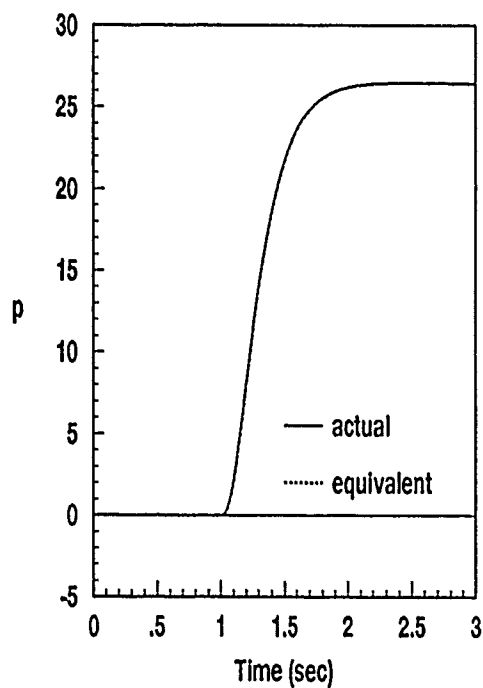


Figure B.20. Fit and Error for p , Plant 10

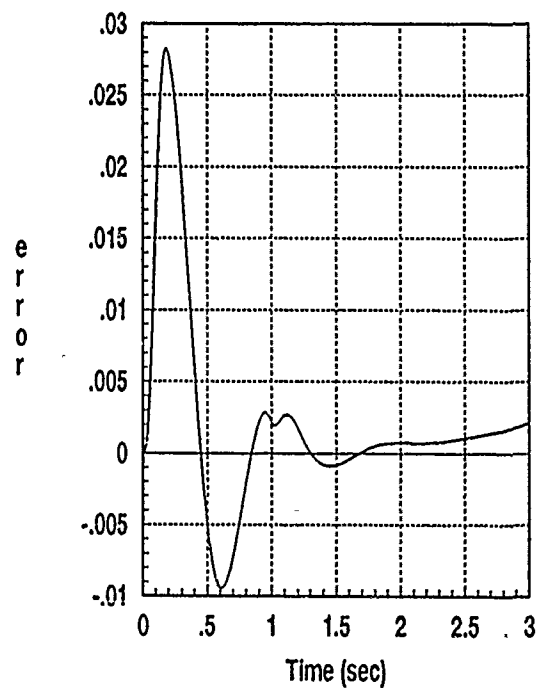
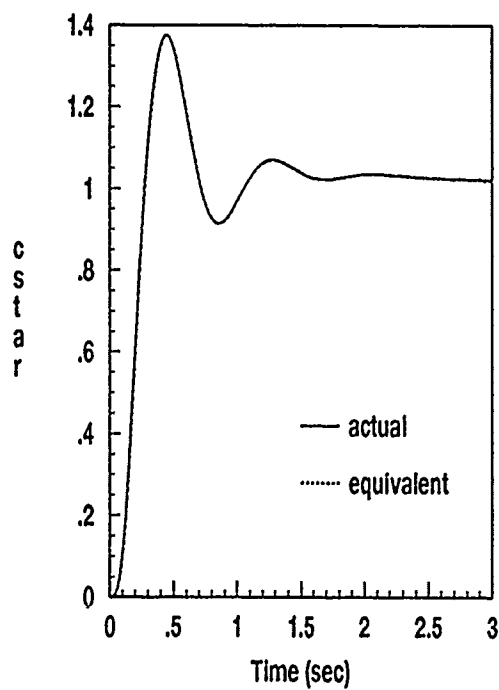


Figure B.21. Fit and Error for C^* , Plant 11

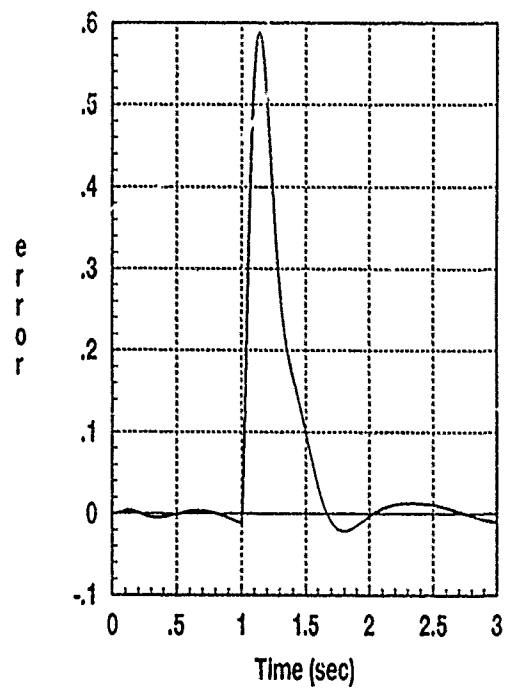
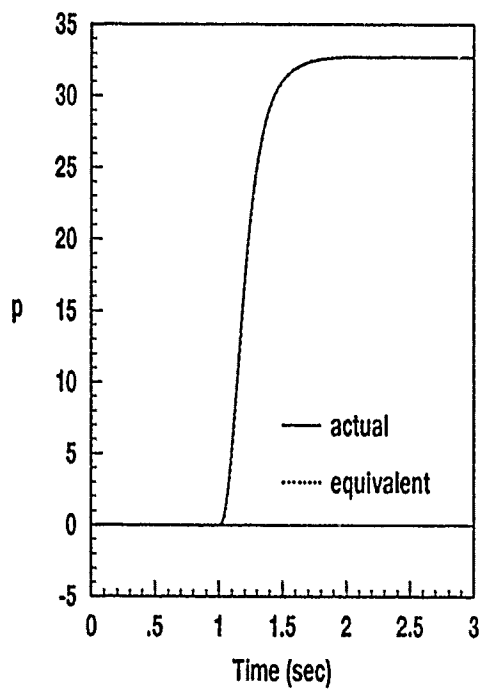


Figure B.22. Fit and Error for p , Plant 11

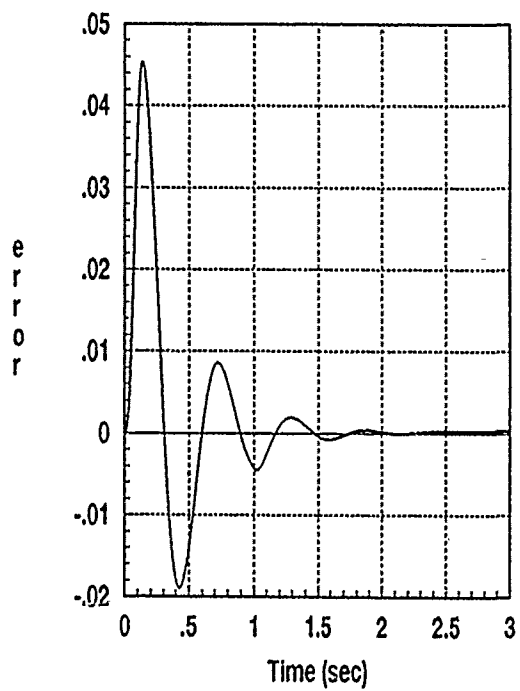
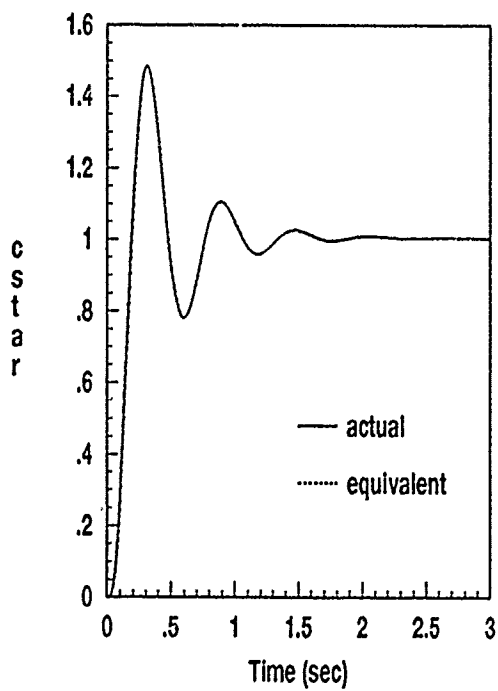


Figure B.23. Fit and Error for C^* , Plant 12

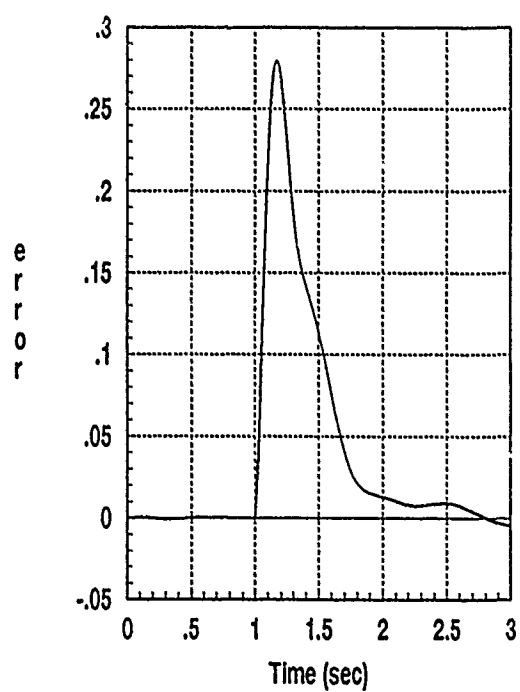
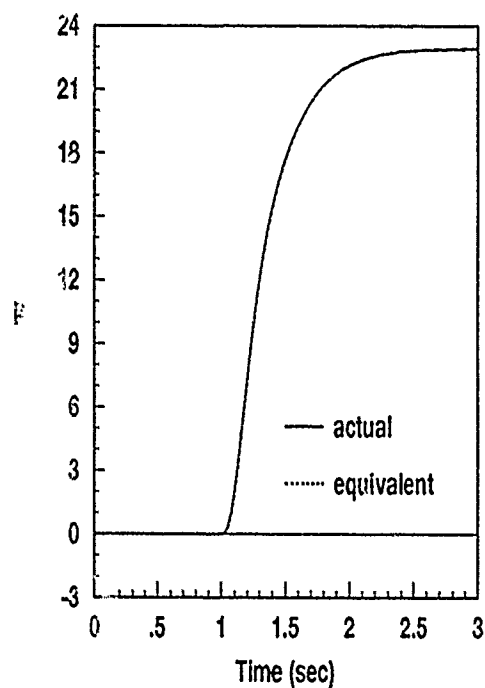


Figure B.24. Fit and Error for p , Plant 12

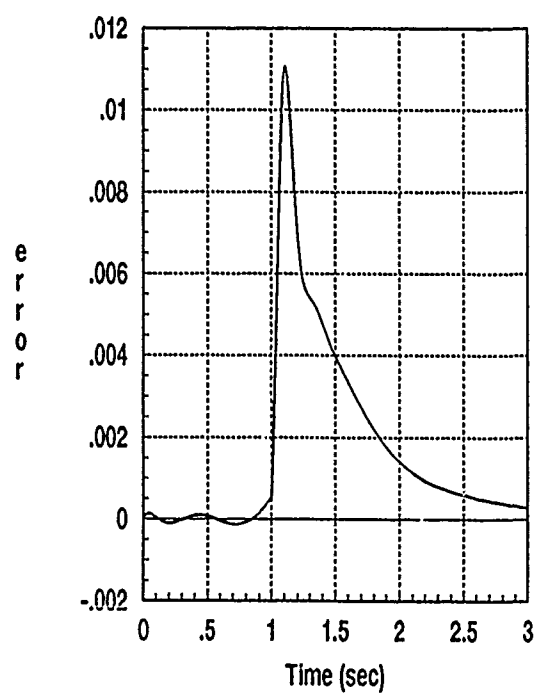
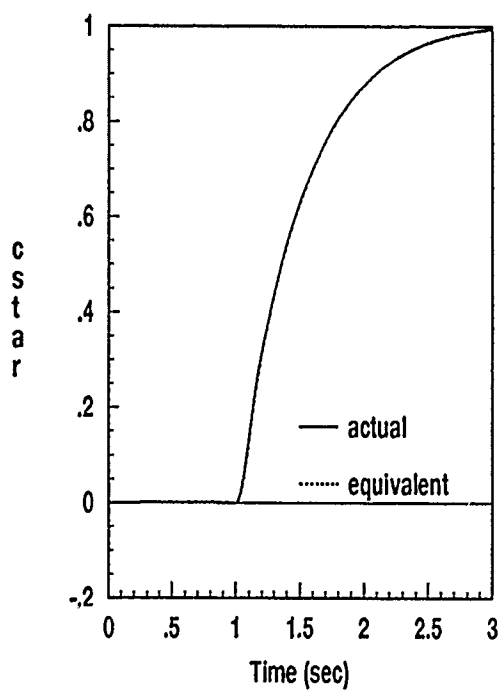


Figure B.25. Fit and Error for C^* , Plant 13

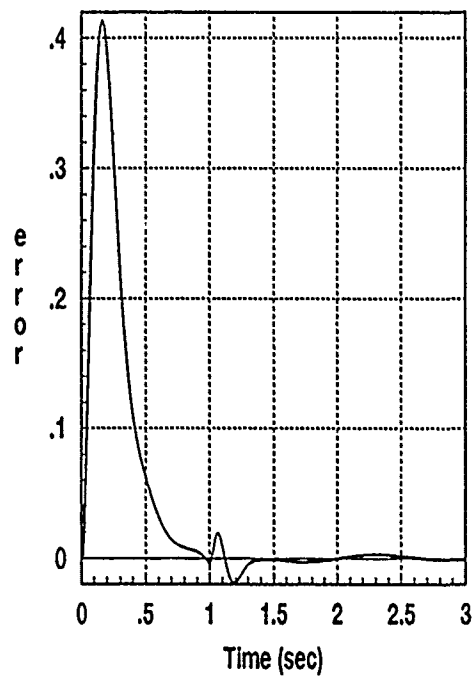
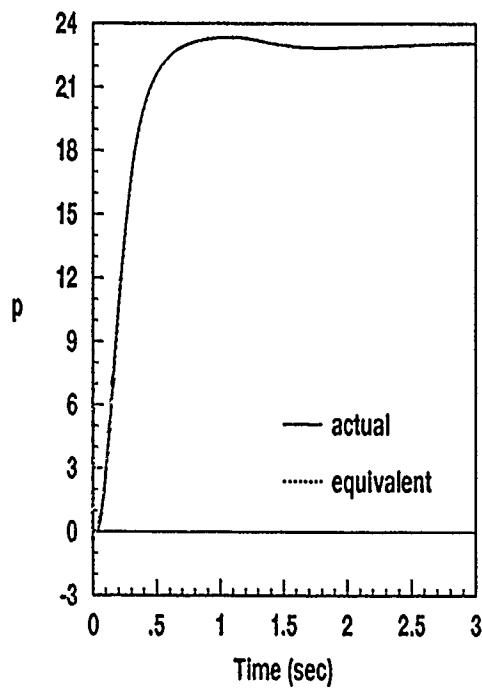


Figure B.26. Fit and Error for p , Plant 13

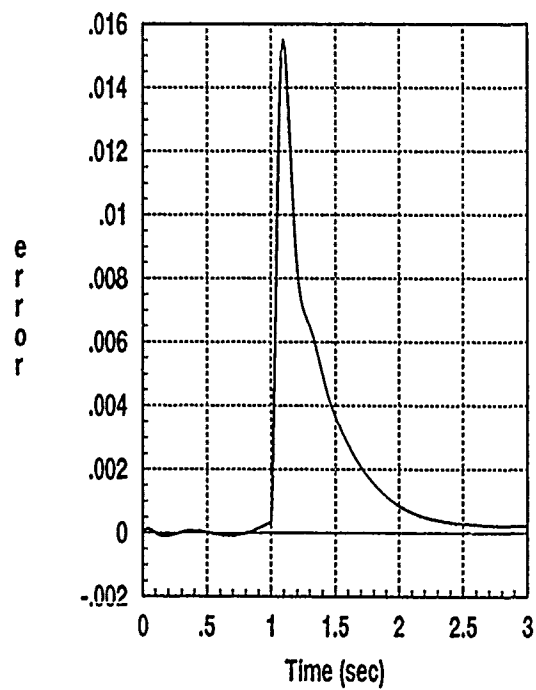
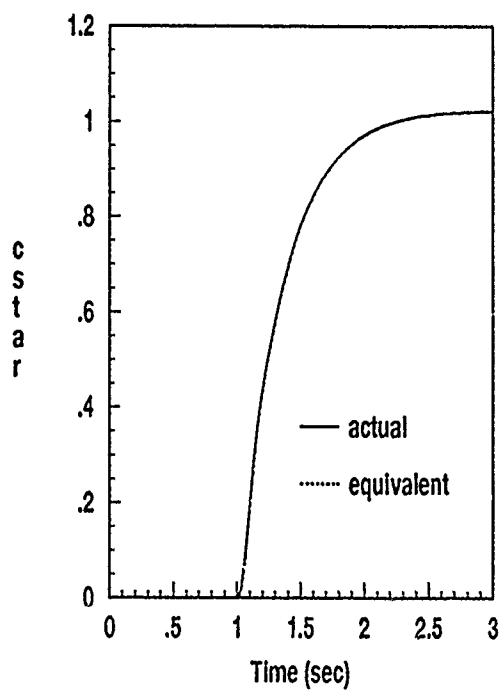


Figure B.27. Fit and Error for C^* , Plant 14

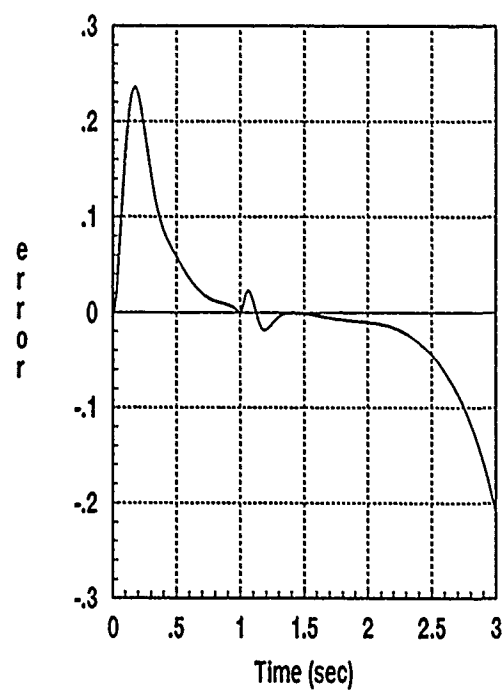
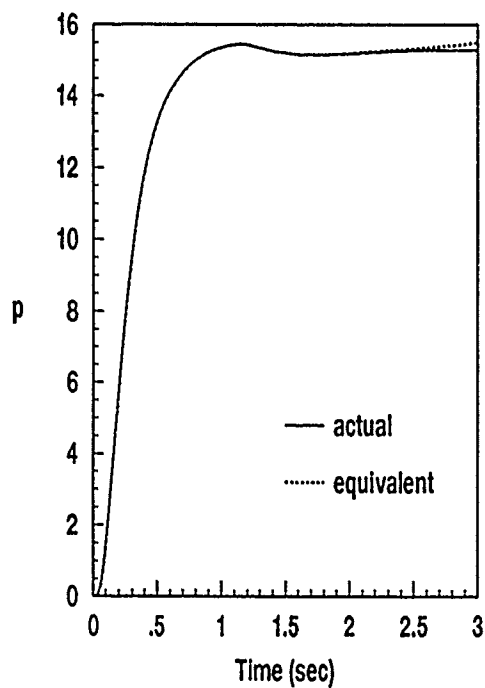


Figure B.28. Fit and Error for p , Plant 14

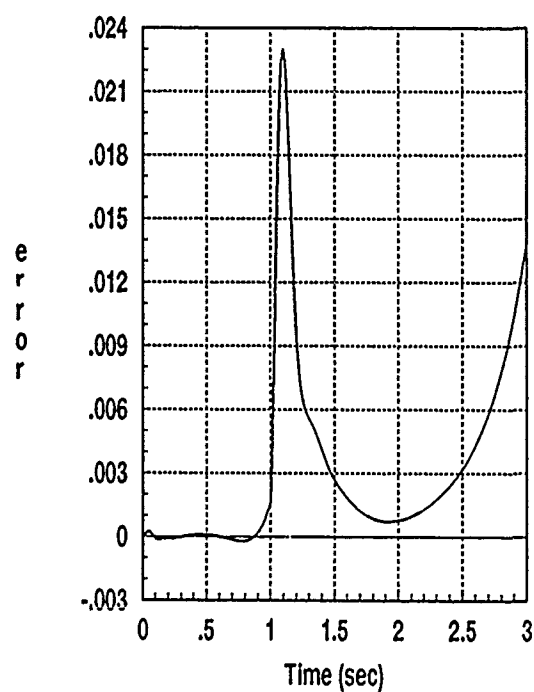
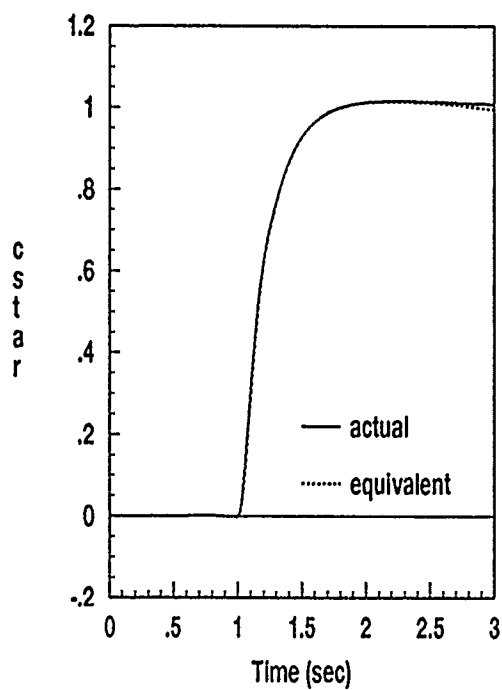


Figure B.29. Fit and Error for C^* , Plant 15

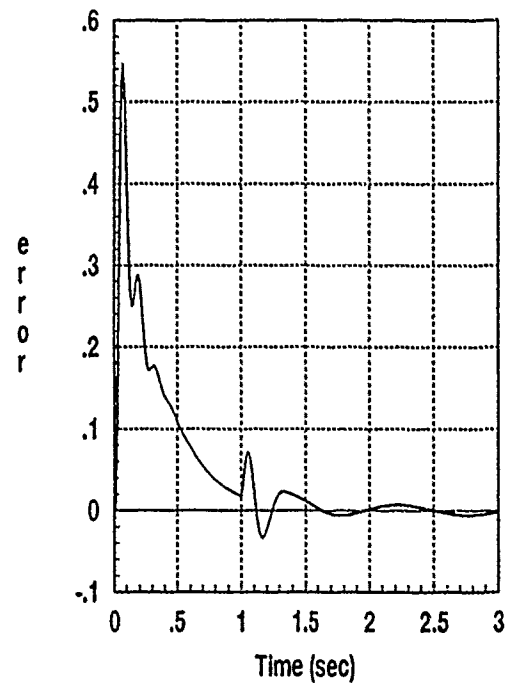
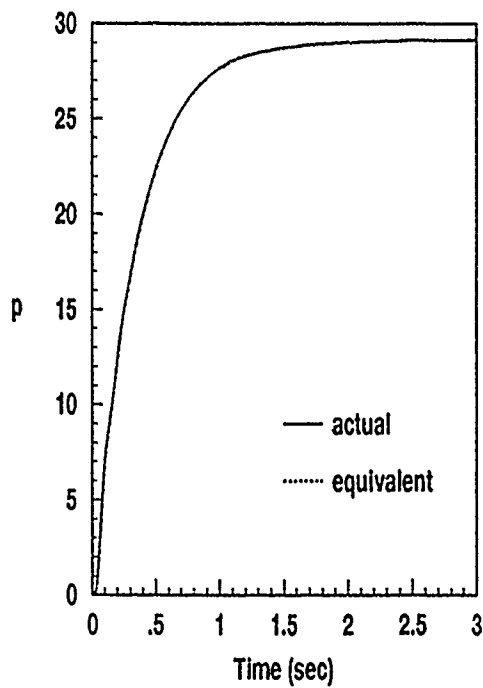


Figure B.30. Fit and Error for p , Plant 15

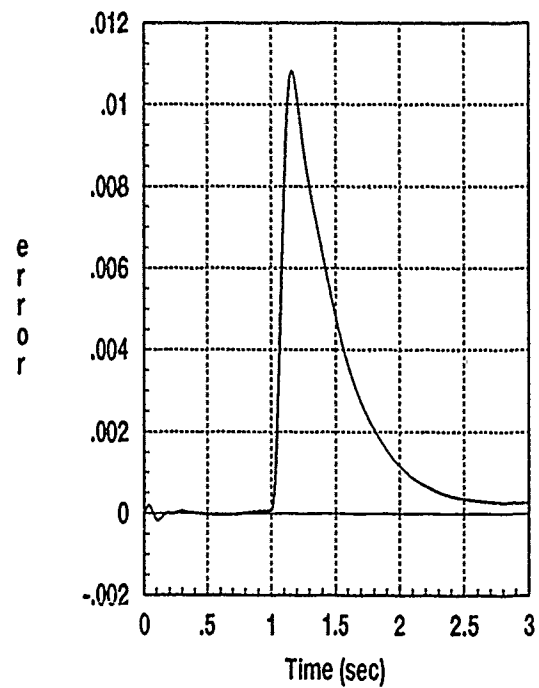
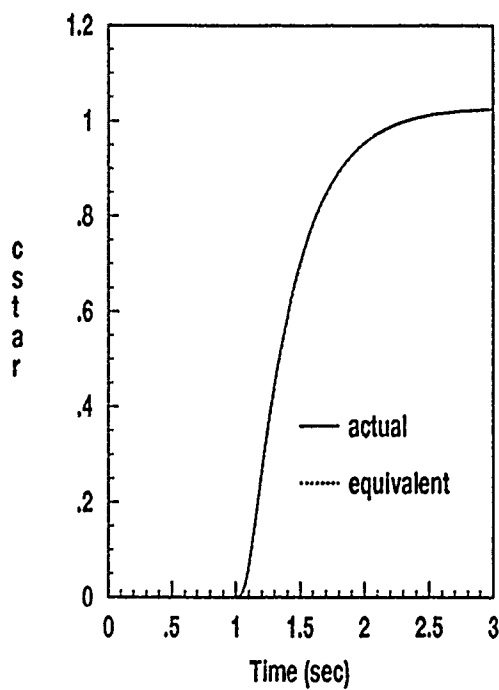


Figure B.31. Fit and Error for C^* , Plant 16

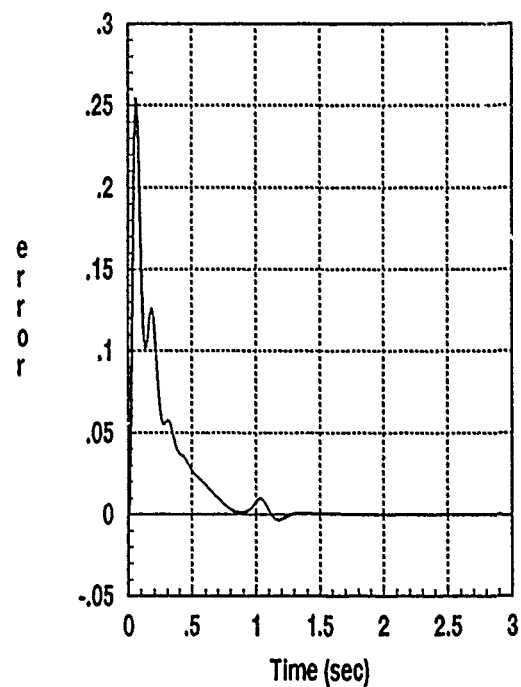
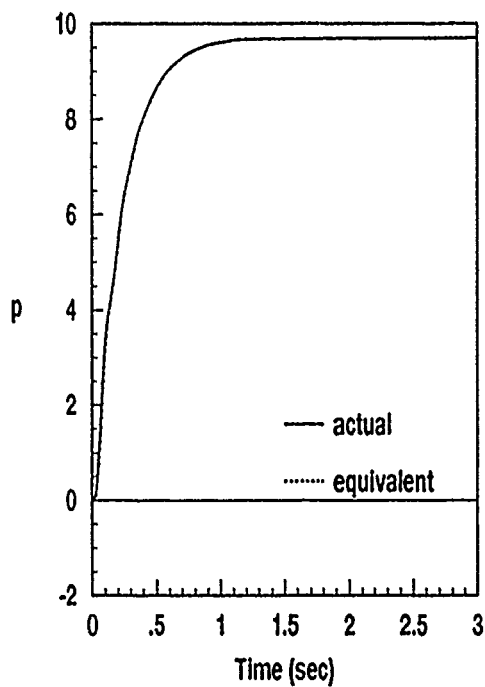


Figure B.32. Fit and Error for p , Plant 16

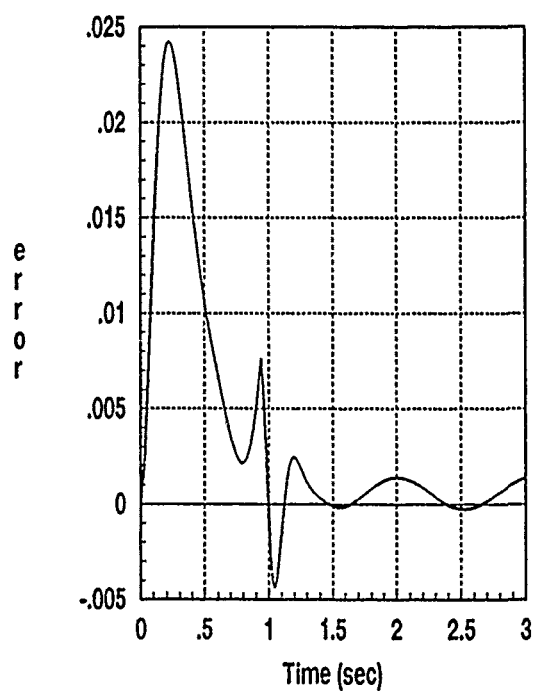
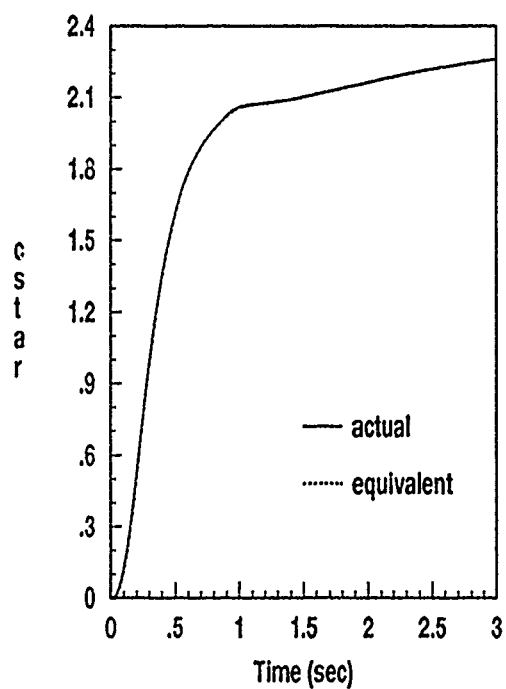


Figure B.33. Fit and Error for C^* , Plant 17

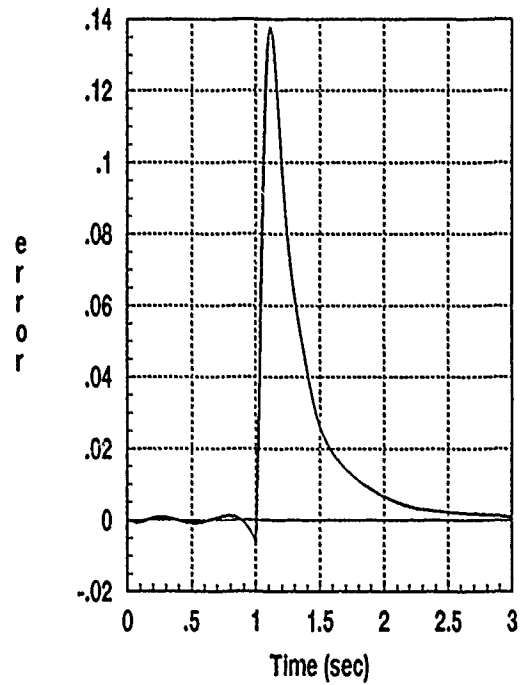
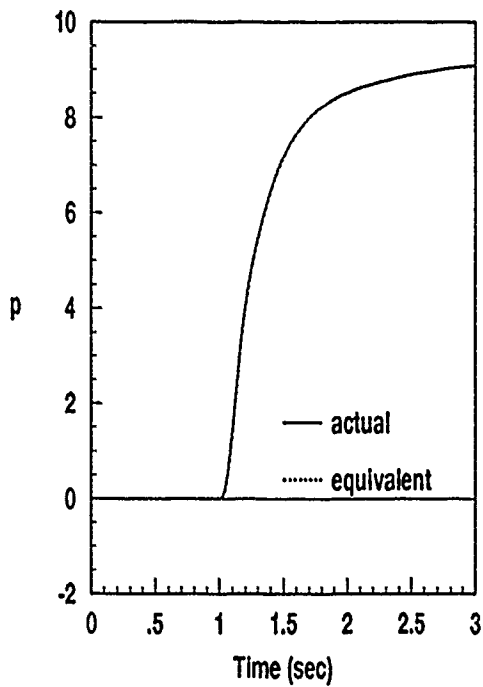


Figure B.34. Fit and Error for p , Plant 17

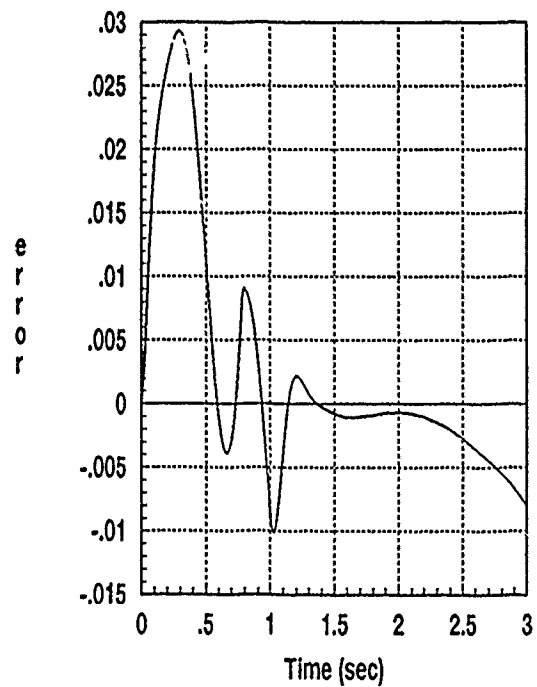
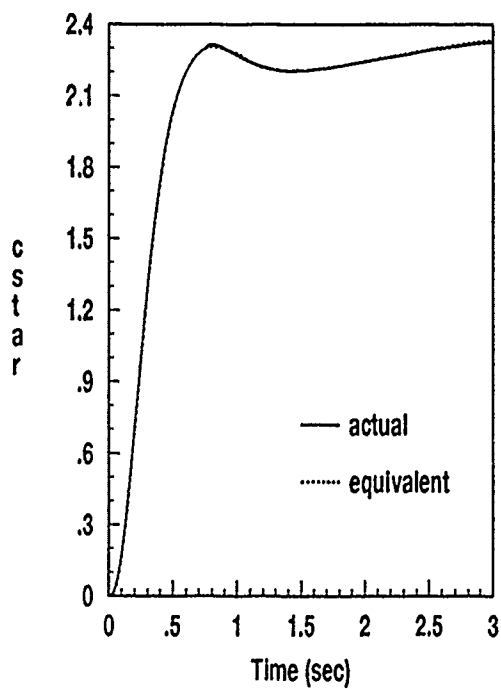


Figure B.35. Fit and Error for C^* , Plant 18

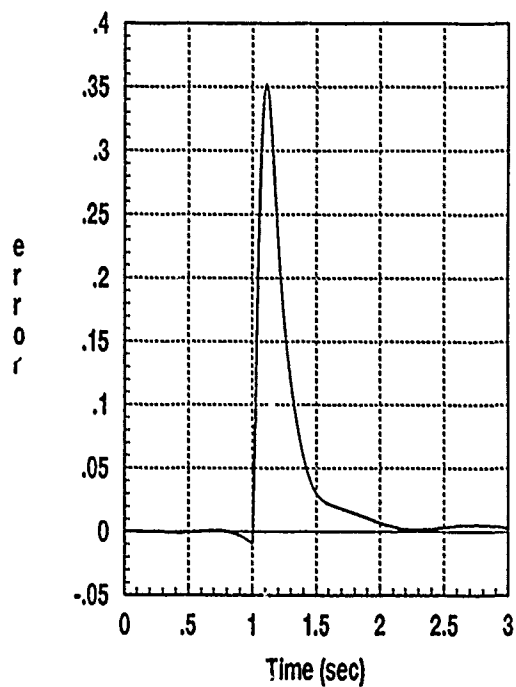
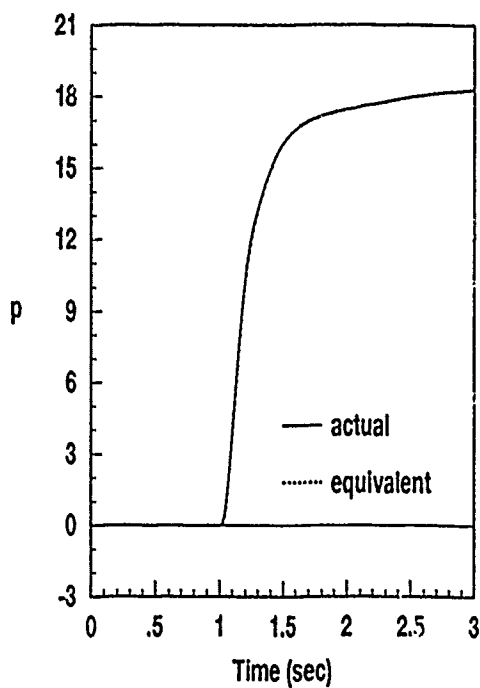


Figure B.36. Fit and Error for p , Plant 18

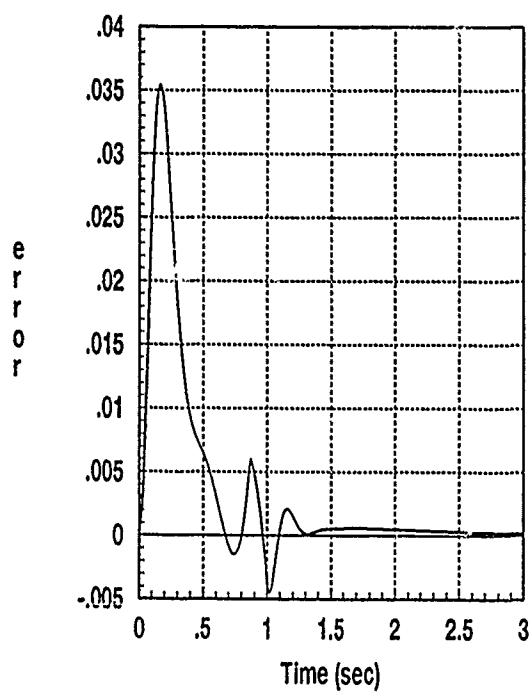
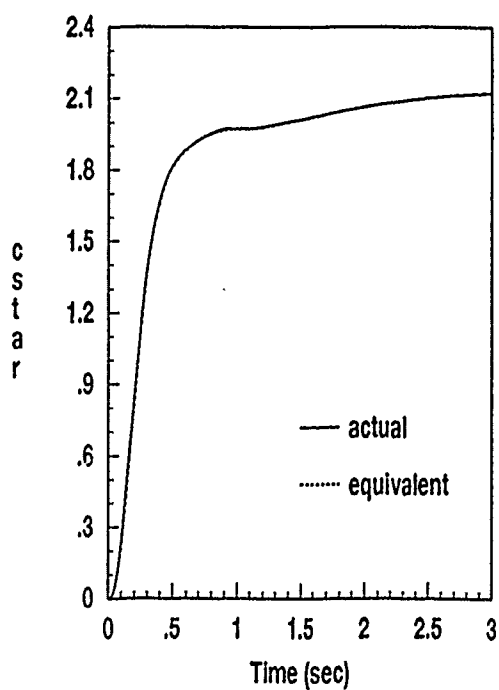


Figure B.37. Fit and Error for C^* , Plant 19

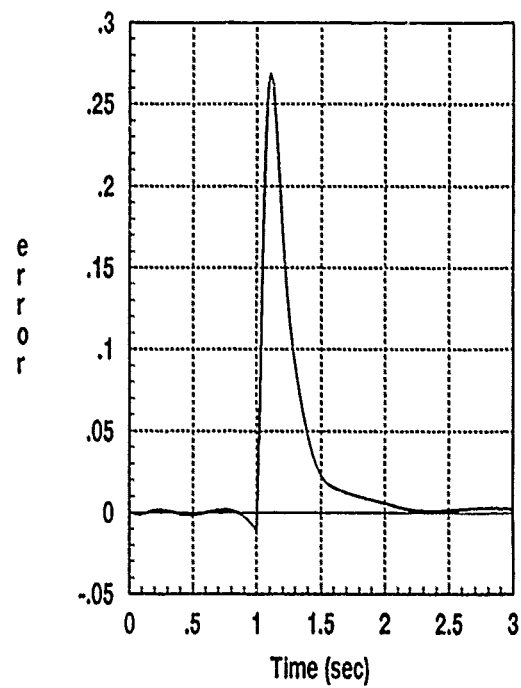
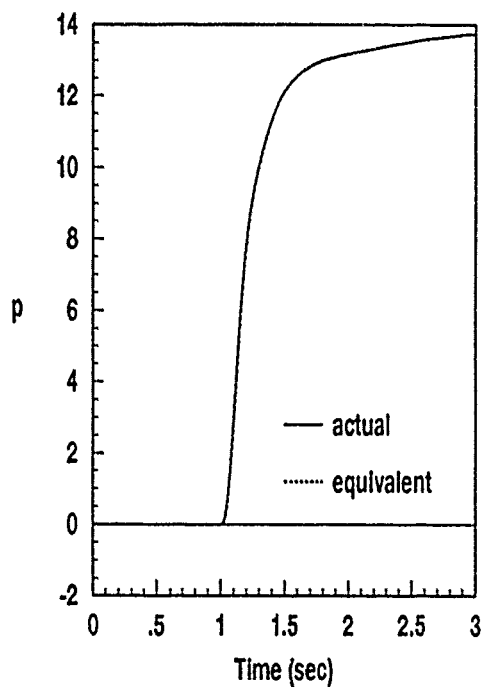


Figure B.38. Fit and Error for p , Plant 19

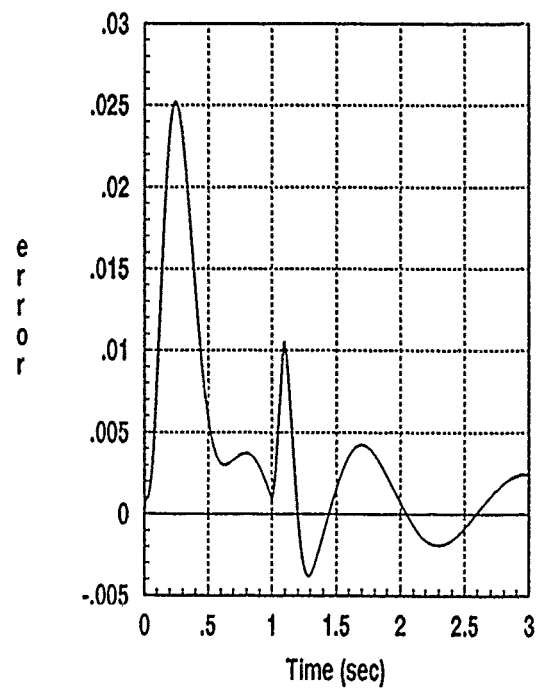
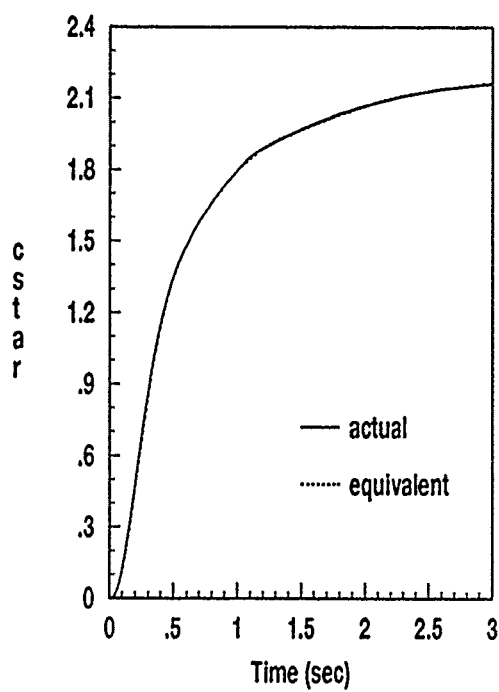


Figure B.39. Fit and Error for C^* , Plant 20

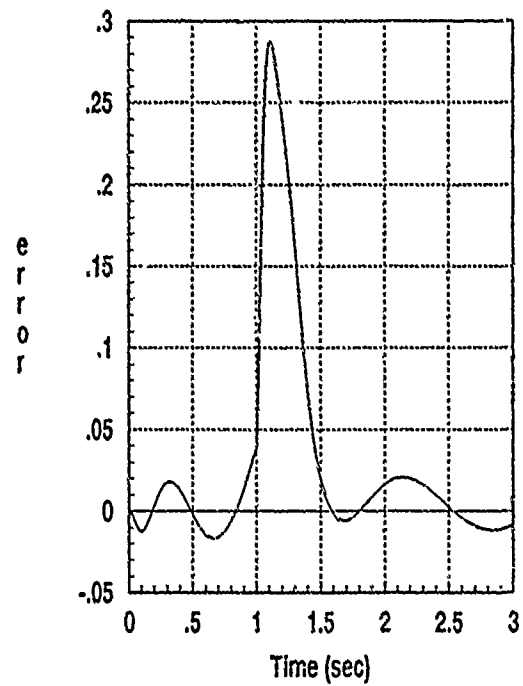
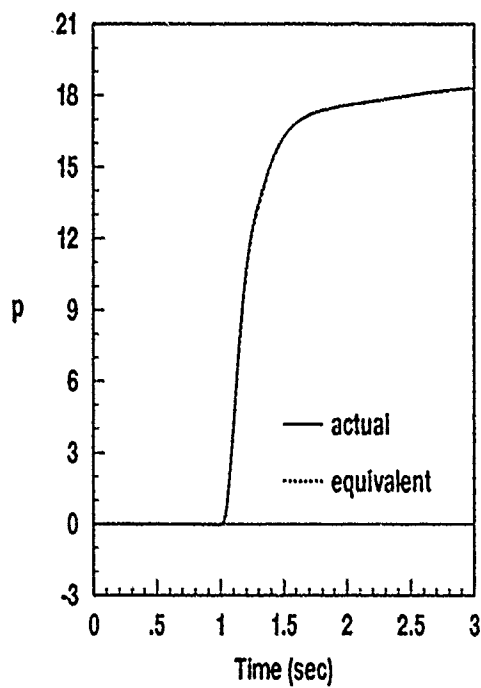


Figure B.40. Fit and Error for p , Plant 20

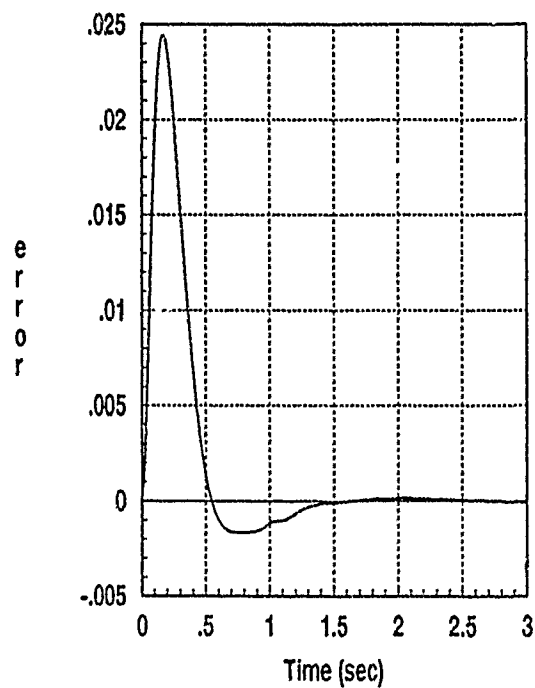
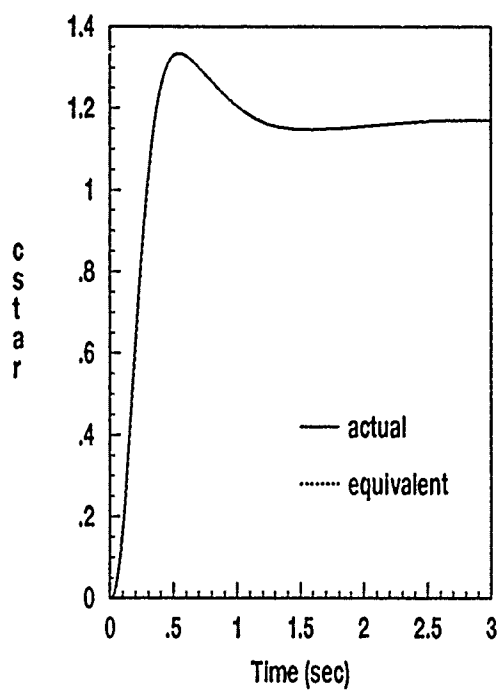


Figure B.41. Fit and Error for C^* , Plant 21

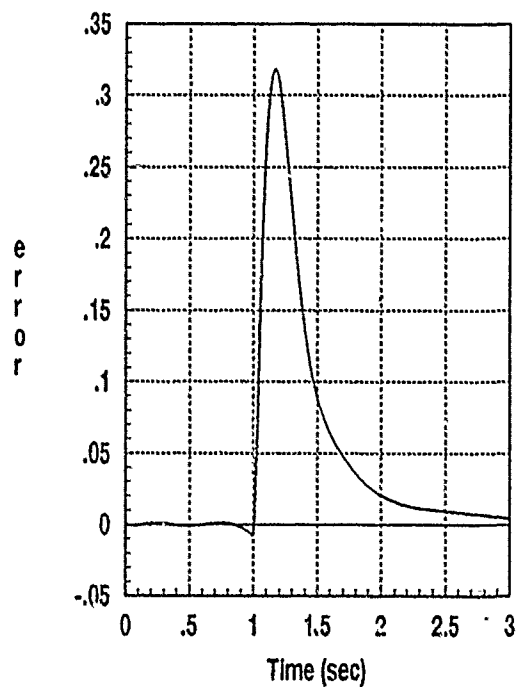
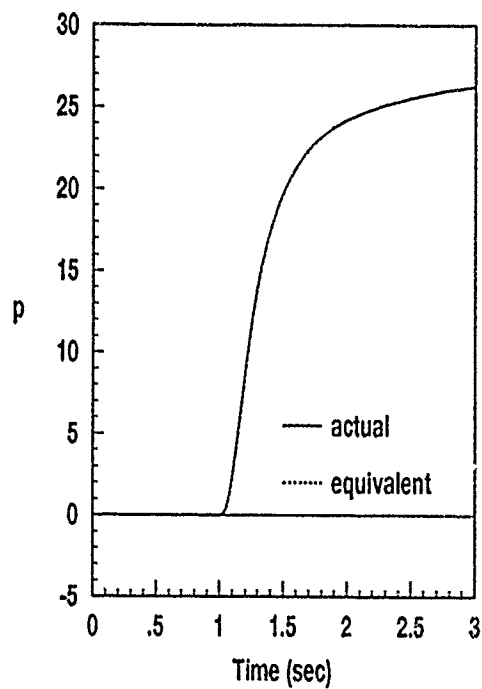


Figure B.42. Fit and Error for p , Plant 21

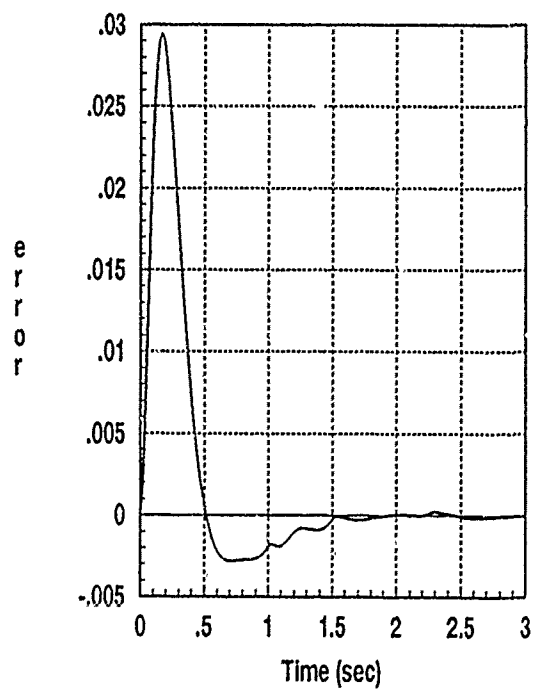
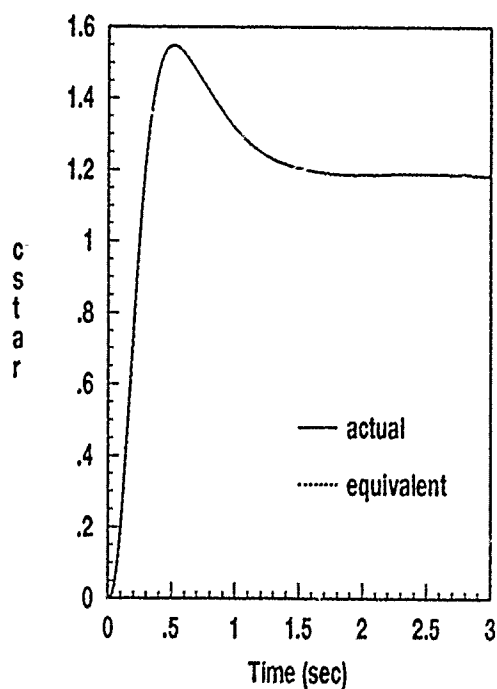


Figure B.43. Fit and Error for C^* , Plant 22

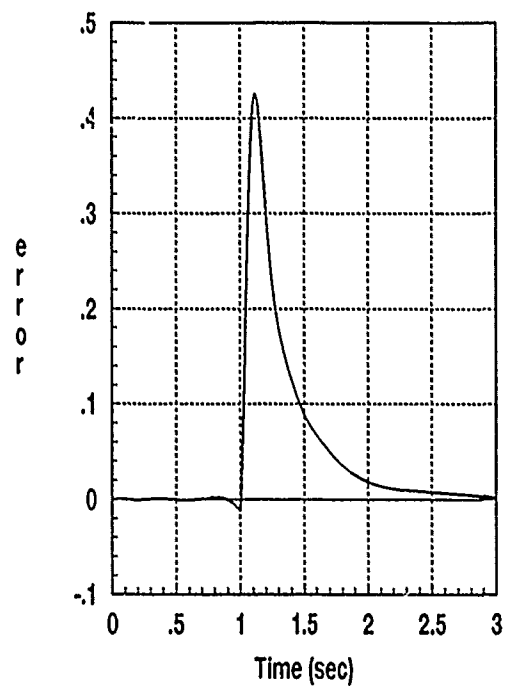
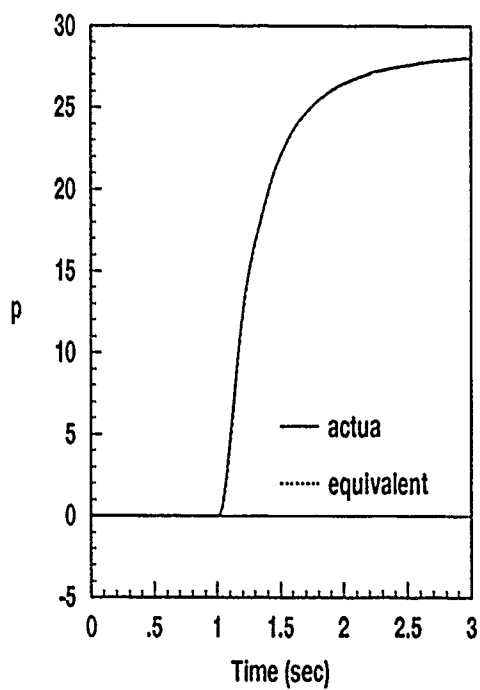


Figure B.44. Fit and Error for p , Plant 22

Appendix C. Additional Simulations

This appendix provides additional simulations of both the inner and outer loops. In some cases, additional aircraft surface deflections and responses are given. Each set of plots is briefly described below. In all cases, C^* is given in g's (except when normalized) and p is given in degrees/second (except when normalized). All angles and surface deflections are given in degrees, and all rates are given in degrees/sec.

The first set of plots, Figures C.1 (a)-(g), provide the angles, rates, and surface deflections for three of the cases given in Figure 5.5. The three cases are:

- case 1: 5g C^* and 30°/s p commands at 0.9M, 20K
- case 2: 1g C^* and 30°/s p commands at 0.9M, 20K
- case 3: 1g C^* and 20°/s p commands at 0.6M, 30K

In this set, C^* and p are normalized and displayed with their respective bounds, and the remaining responses are shown at full magnitude.

The next set of plots, Figures C.2 (a)-(c), gives some of the responses and deflections for a roll out of a 2g coordinated turn at 0.6M, 30K. Note that Figure C.2 (a), shows the *change* in C^* .

The third set of plots, C.3 (a)-(c), shows several of the responses for a 120°/s roll rate command from straight and level flight at 0.9M, 20K. p is shown normalized within its bounds, and the other responses are shown at full magnitude.

The final set of plots provides the C^* and p responses for MIMO simulations of the outer loop. C.4 (a) is for 1 to 3g C^* commands with simultaneous p commands from 10 to 30°/s for each value of C^* at the flight condition 0.9M, 20K. C.4 (b) covers C^* commands of 1 and 2g's with the same set of roll commands at 0.6M, 30K.

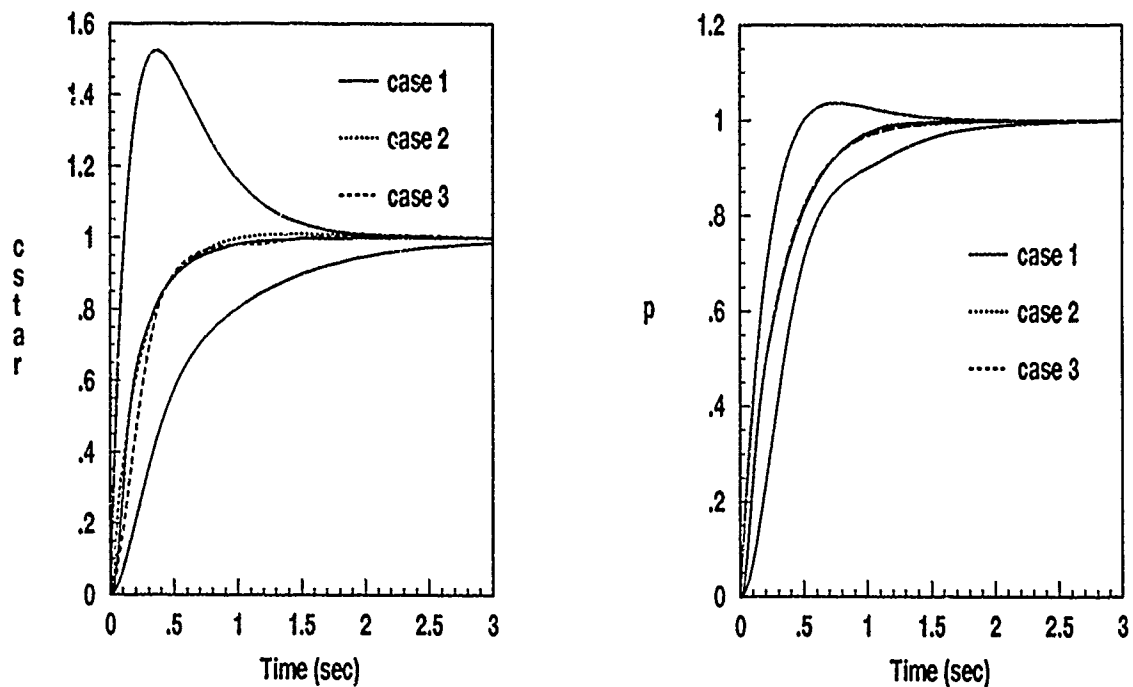


Figure C.1 (a). Commanded Outputs for 3 Cases from Ch 5

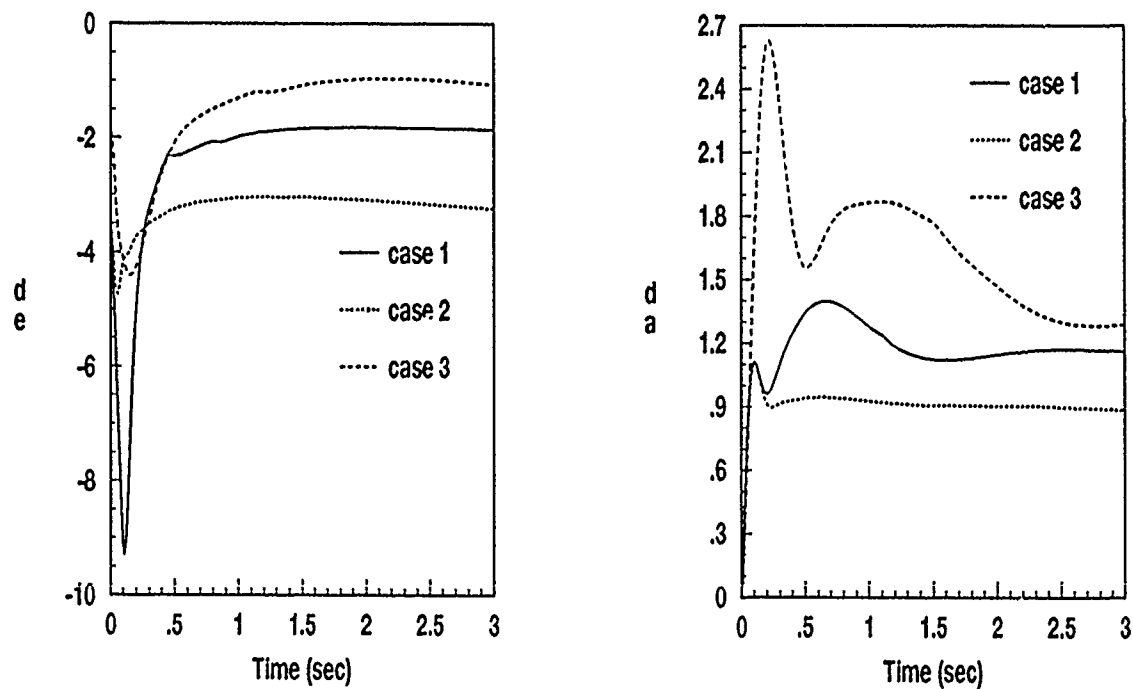


Figure C.1 (b). Elevator and Aileron Deflections for 3 Cases from Ch 5

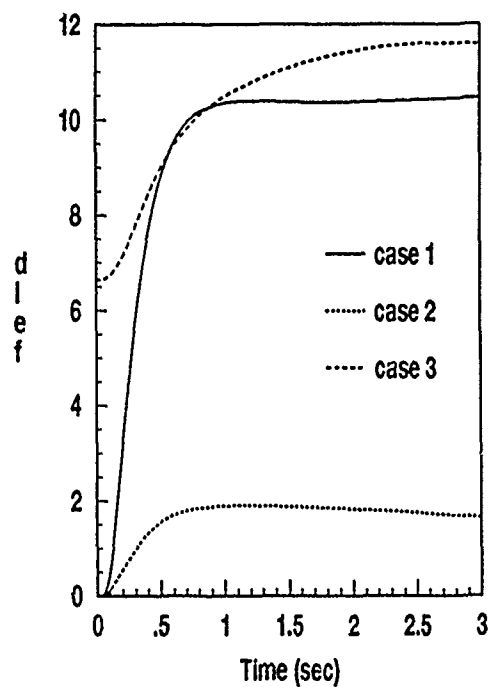
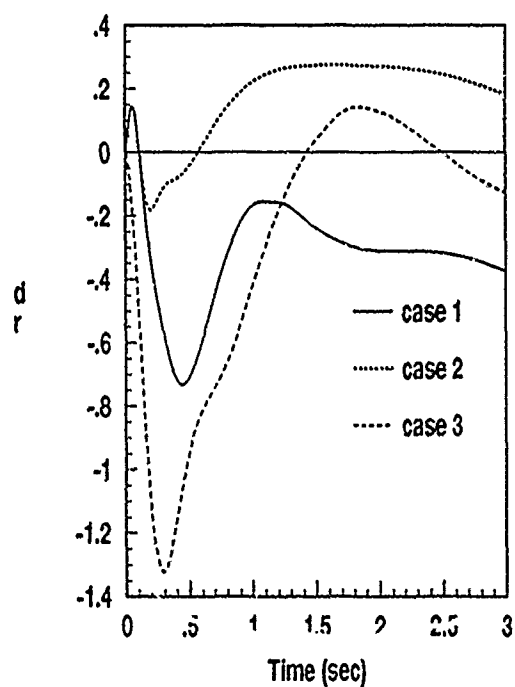


Figure C.1 (c). Rudder and Leading Edge Flap Deflections for 3 Cases from Ch 5

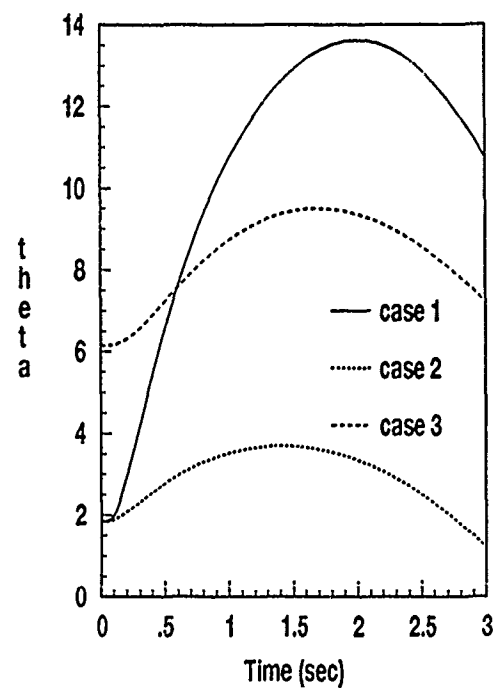
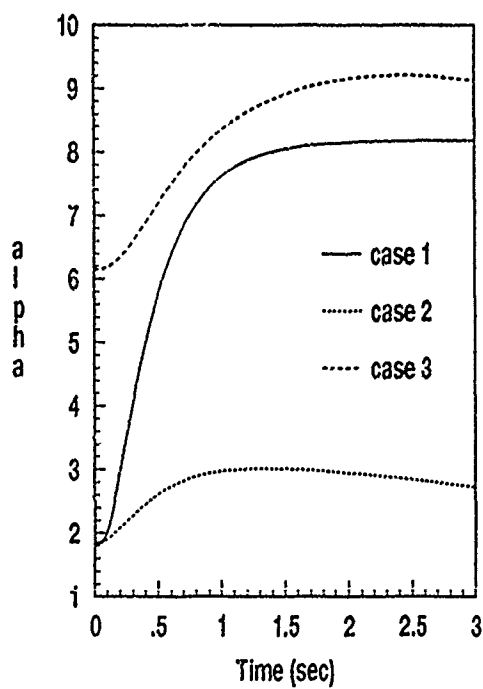


Figure C.1 (d). Angle of Attack and Pitch Attitude for 3 Cases from Ch 5

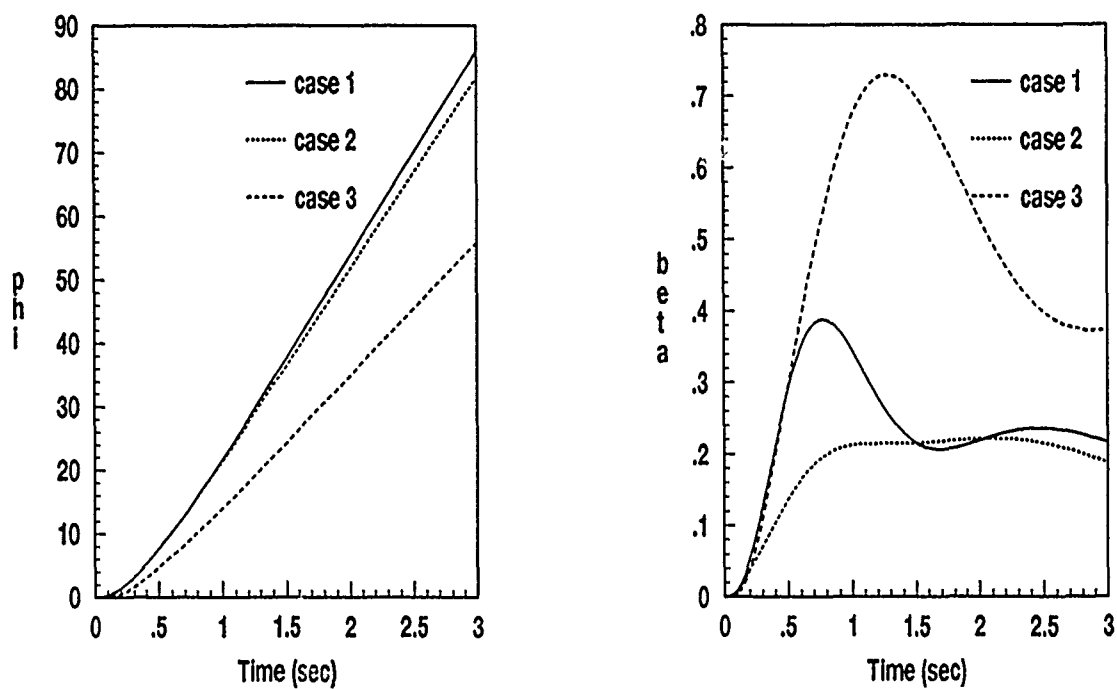


Figure C.1 (e). Roll and Sideslip Angles for 3 Cases from Ch 5

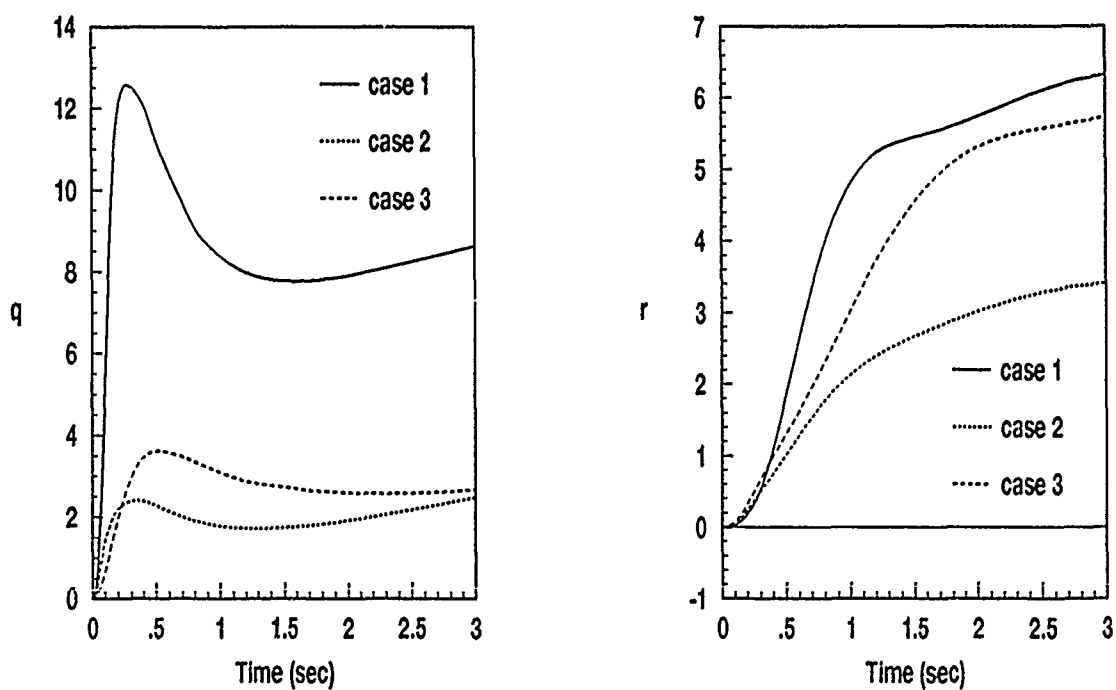


Figure C.1 (f). Pitch and Yaw Rates for 3 Cases from Ch 5

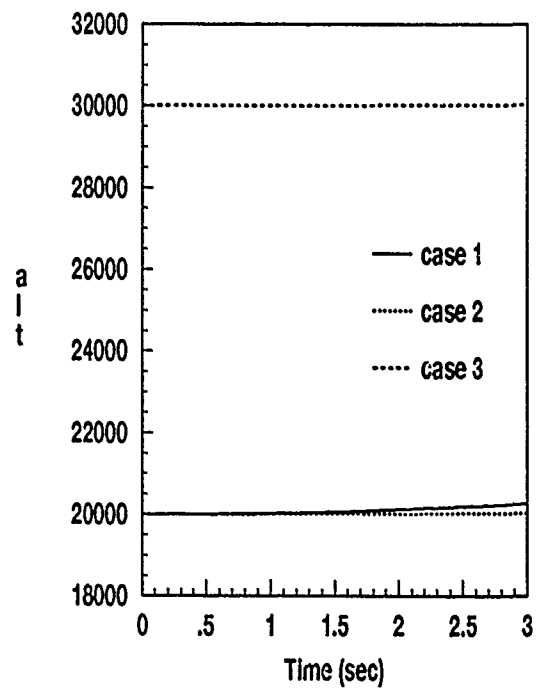
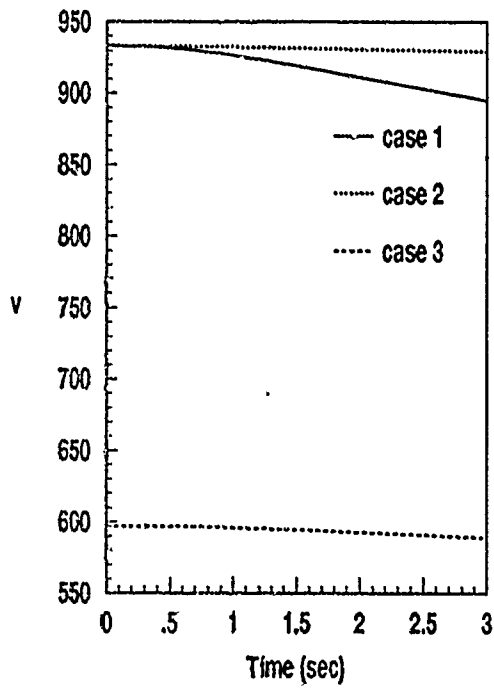


Figure C.1 (g). Velocity and Altitude for 3 Cases from Ch 5

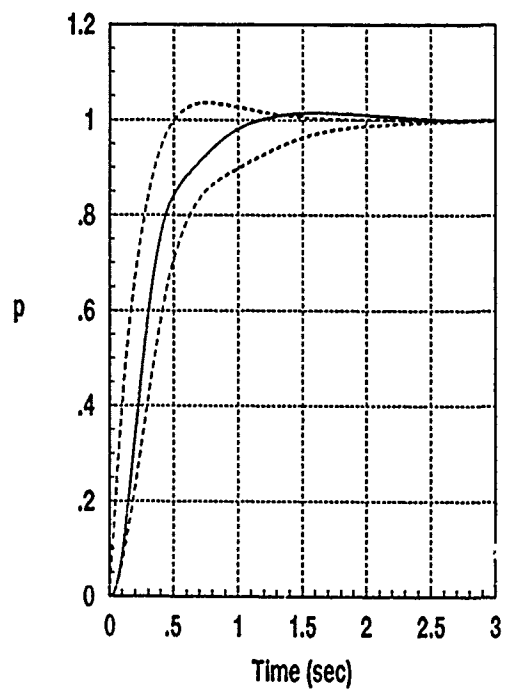
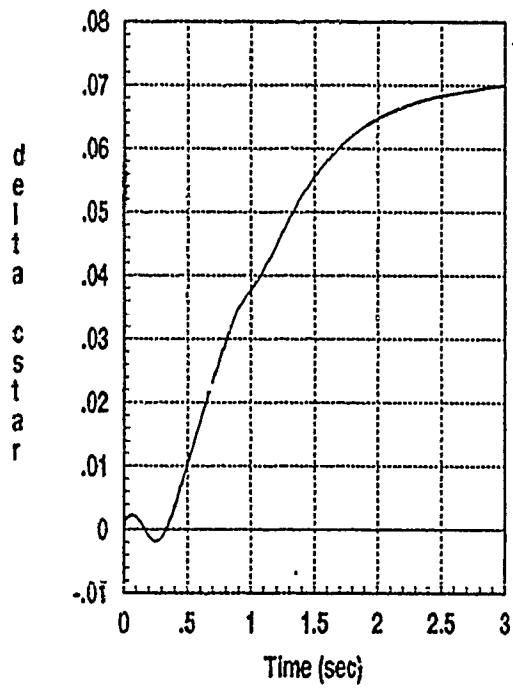


Figure C.2 (a). ΔC^* and p for a Roll Out of a 2g Turn

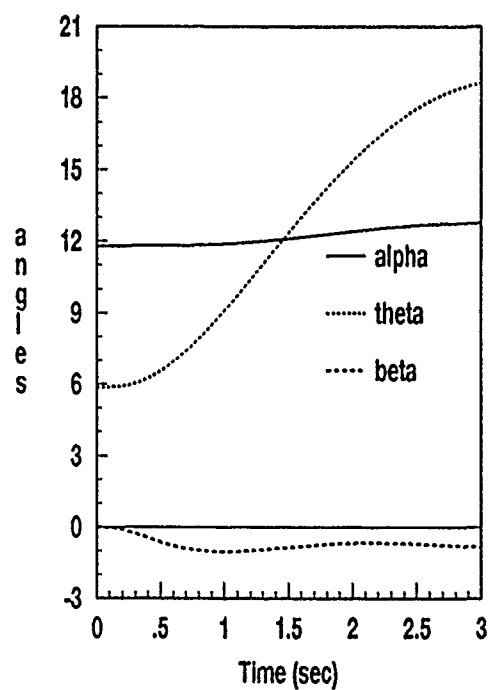
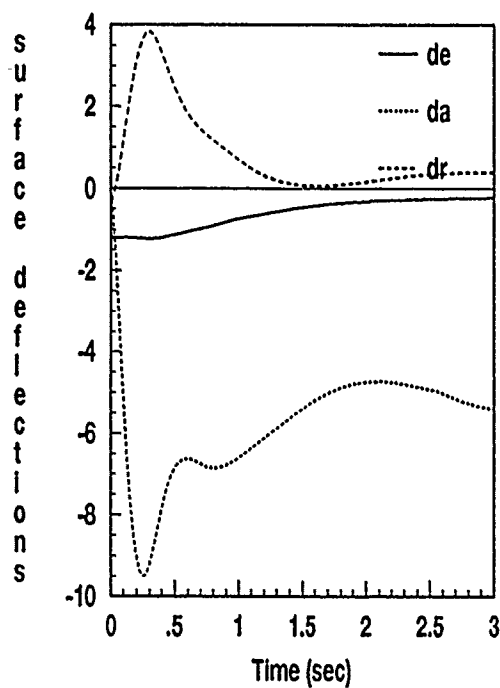


Figure C.2 (b). Surface Deflections and Angles for a Roll Out of a 2g Turn

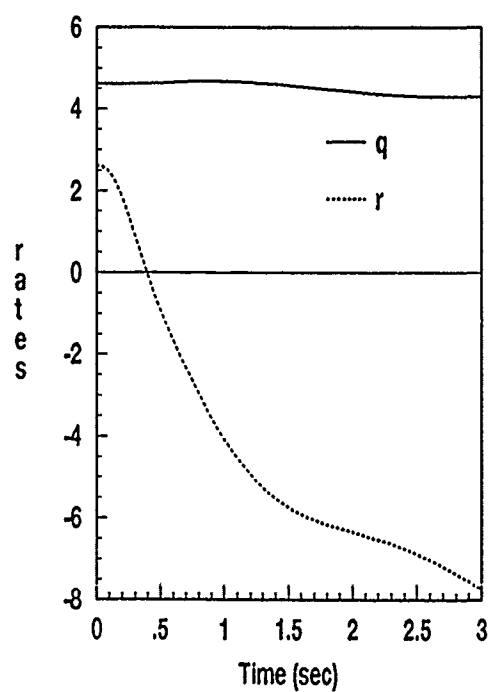
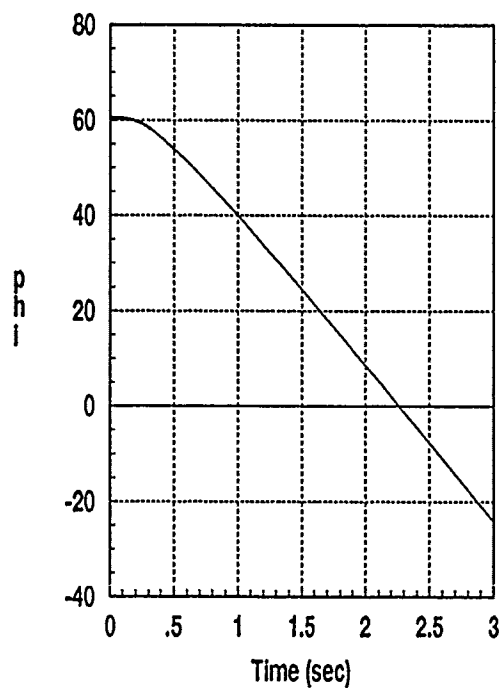


Figure C.2 (c). Roll Angle and Misc Rates for a Roll Out of a 2g Turn

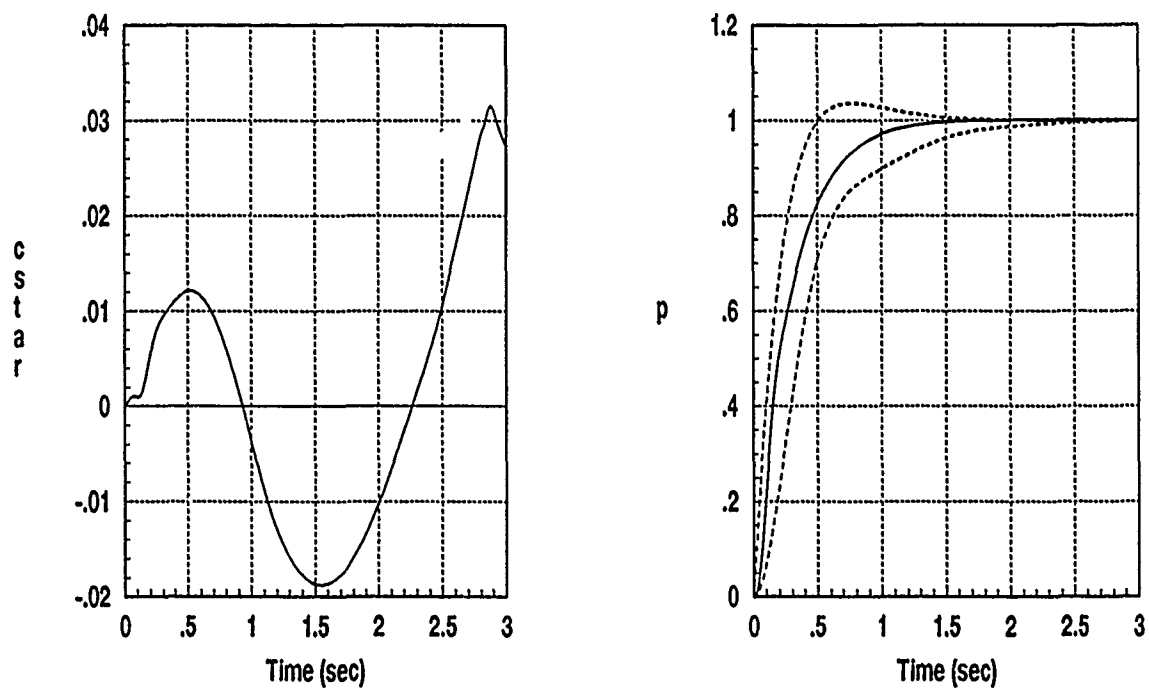


Figure C.3 (a). Commanded Outputs for a $120^\circ/\text{s}$ Roll Rate Command

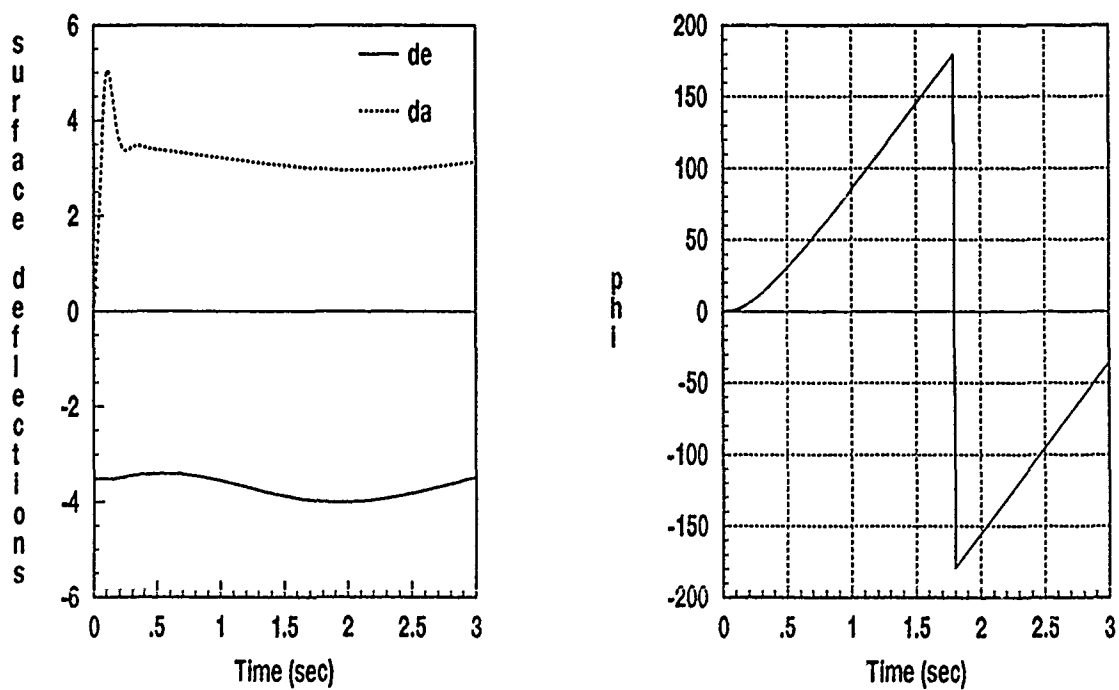


Figure C.3 (b). Surface Deflections and Roll Angle for a $120^\circ/\text{s}$ Roll Rate Command

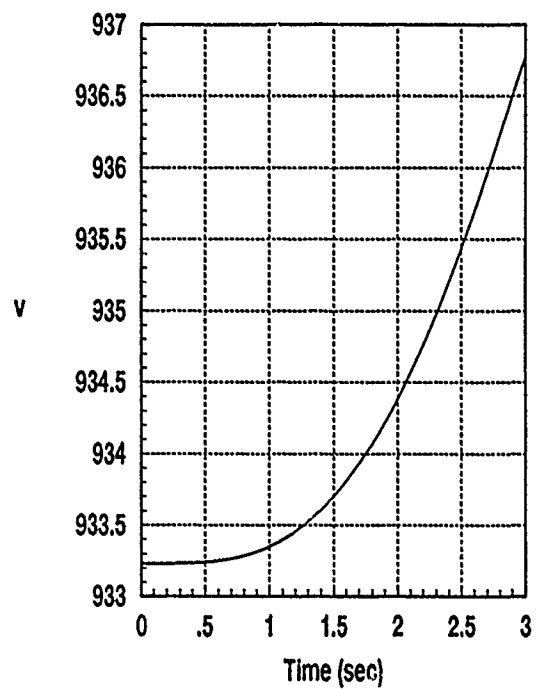
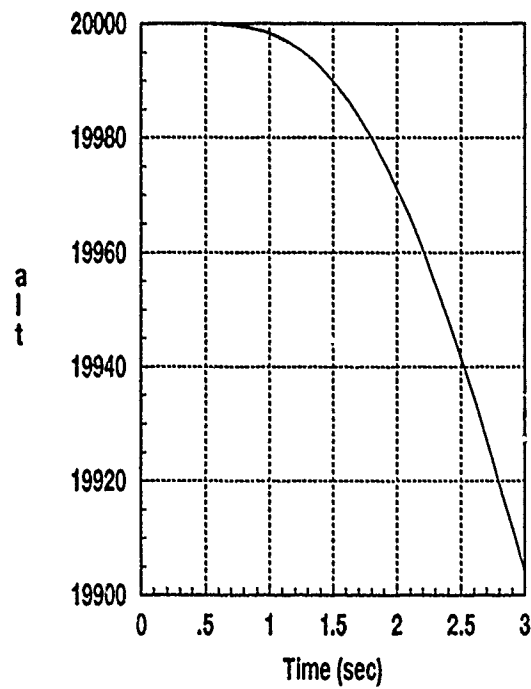


Figure C.3 (c). Altitude and Velocity for a 120°/s Roll Rate Command

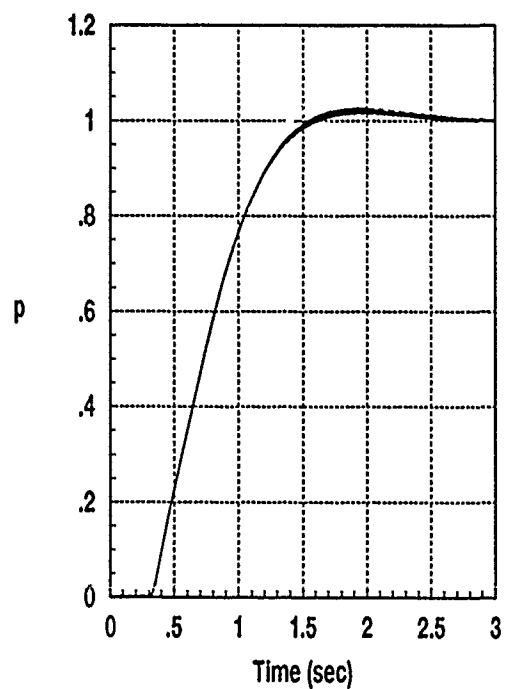
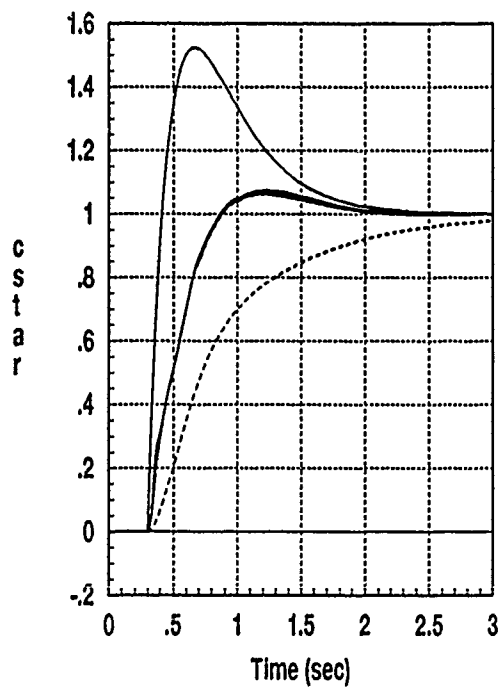


Figure C.4 (a). MIMO Outer loop Simulations at 0.9M, 20K

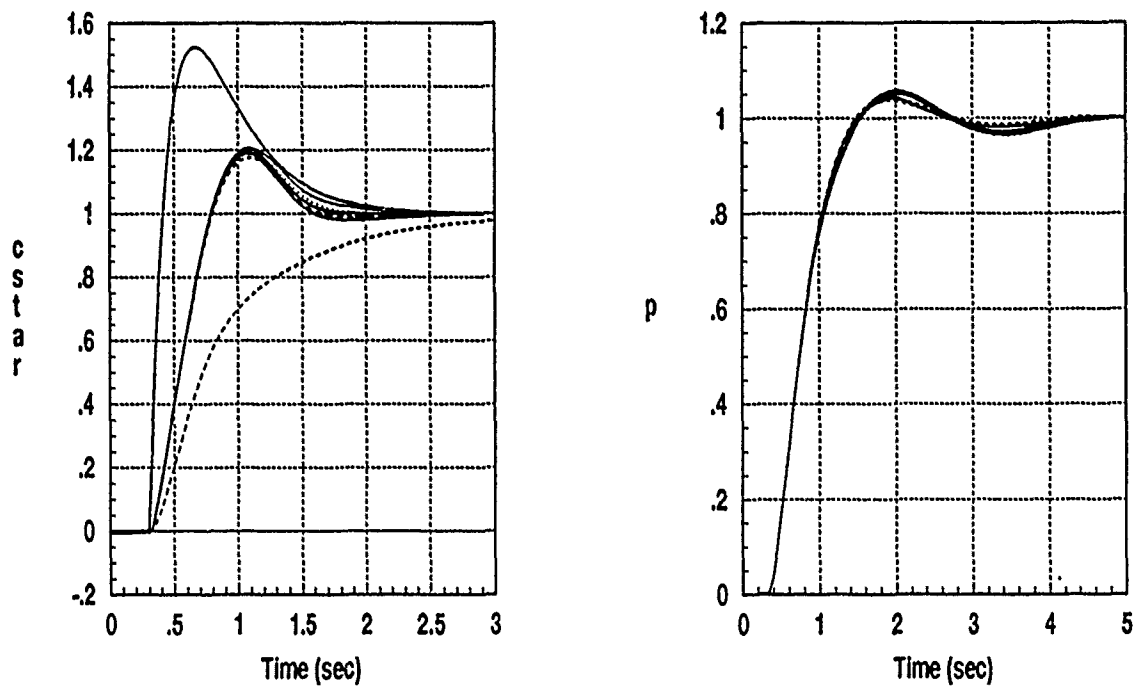


Figure C.4 (b). MIMO Outer Loop Simulations at 0.6M, 30K

The MIMO simulations of the outer loop at the first flight condition are much better than those at the second. Since the outer loop compensation was based on SISO equivalent plants, no consideration was given to coupling between the responses. Therefore, the degraded performance of Figure C.4 (b) is not surprising. As found in the inner loop simulations, the responses are significantly more coupled at 0.6M, 30K than at 0.9M, 20K. If the pilot compensation is designed with MISO equivalent plants as in QFT, these disturbances can be taken into account.

Bibliography

1. Barfield, Finley. Head Control Engineer AFTI/F-16. Personal Interviews. Flight Dynamics Labs, Wright-Patterson AFB, OH January through November 1990.
2. D'Azzo, John J. and Constantine H. Houpis. *Linear Control System Analysis and Design: Conventional and Modern*. New York: McGraw-Hill Book Company, 1988.
3. East, D.J. "A New Approach to Optimal Loop Synthesis," *International Journal of Control*, 34: 731-748 (1981).
4. Horowitz, Issac. Founder of QFT. Personal Interviews. Air Force Institute of Technology, Wright-Patterson AFB OH, January through November 1990.
5. Horowitz, Issac. "The Singular-G Method for Unstable Non-Minimum-Phase Plants," *International Journal of Control*, 44: 533-541 (1986).
6. Horowitz, I.M. *Advanced Control Theory and Applications*, unpublished lecture notes. The Weizmann Institute of Science, Rehovot Israel (1982).
7. Horowitz, I.M. "Nonlinear Uncertain Feedback Systems with Initial State Values," *International Journal of Control*, 34: 749-764 (1981).
8. Horowitz, Isaac and others. *Research in Advanced Flight Control Design*, AFFDL-TR-79-3120, Air Force Wright Aeronautical Laboratories, Wright-Patterson AFB OH, January 1980 (AD-A082424).
9. Horowitz, I.M. "Synthesis of Feedback Systems with Nonlinear Time-Varying Uncertain Plants to Satisfy Quantitative Performance Specifications," *Proceedings of the IEEE*, 64: 123-130 (1976).
10. Horowitz, I.M. and Uri Shaked. "Superiority of Transfer Function Over State-Variable Methods in Linear Time Invariant Feedback System Design," *International Journal of Control*, 20: 84-96 (1975).
11. Houpis, Constantine H. Professor of Electrical Engineering. Personal Interviews. Air Force Institute of Technology, Wright-Patterson AFB OH, January through November 1990.
12. Houpis, Constantine H. *Quantitative Feedback Theory*, AFWAL-TR-86-3107. Dayton OH: AFWAL/FIGL, January 1987.
13. Kobylarz, 1Lt Thomas John. *Flight Controller Design with Nonlinear Aerodynamics, Large Parameter Uncertainty, and Pilot Compensation*. MS thesis, AFIT/GE/ENG/88D-19. School of Engineering, Air Force Institute of Technology (AU), Wright-Patterson AFB Ohio, December 1988 (AD-202 727).
14. Neal, T. Peter, and Rogers E. Smith. *An In-Flight Investigation to Develop Control System Design Criteria for Fighter Airplanes*, AFFDL-TR-70-74, Vol. I, Air Force Flight Dynamics Laboratory: Wright-Patterson AFB Ohio, December 1990.

15. Paschall, Randall N. Class lectures in EENG 641, Automatic Flight Control II. School of Engineering, Air Force Institute of Technology, Wright-Patterson AFB OH, Spring 1990.
16. Roskam, Jan. *Flight Dynamics of Rigid and Elastic Airplanes*. Lawrence KS: Roskam Aviation and Engineering Corp, 1972.
17. Yaniv, O. "Quantitative Design for MIMO Uncertain Plants to Achieve Prescribed Diagonal Dominant Closed-Loop Minimum Phase Tolerances," *International Journal of Control*, 47: 519-528 (1988).
18. Yaniv, O. and I.M. Horowitz. "Quantitative Feedback Theory -- Reply to Criticisms," *International Journal of Control*, 46: 945-962 (1987).
19. Yaniv, O. and I.M. Horowitz. "A Quantitative Design Method for MIMO Linear Feedback Systems Having Uncertain Plants," *International Journal of Control*, 43: 401-421 (1986).

Vita

Lieutenant Russel B. Miller was born on 19 February 1962 in Dallas Texas. He graduated from high school in Alamogordo, New Mexico in 1980. He enlisted in the United States Air Force in 1981, and served as an Avionics Sensor Systems Specialist at Shaw AFB, South Carolina and attended the University of South Carolina part time until he was selected for the Airman's Education and Commissioning Program (AECPP) in 1986. He graduated from New Mexico State University with a BSEE (high honors and 4.0 GPA) in December 1988. After completion of USAF Officer Training School as a distinguished graduate in May 1989, he entered the School of Engineering, Air Force Institute of Technology studying for a Masters Degree in Electrical Engineering. He was awarded a regular commission in April 1990.

After his graduation from AFIT he will be assigned to the Foreign Technology Division at Wright-Patterson AFB, Ohio.

Permanent address: 1409 Arizona
Alamogordo, New Mexico
88310

REPORT DOCUMENTATION PAGE			Form Approved OMB No. 0704-0188	
Public reporting burden for this collection of information is estimated to average 1 hour per response, including the time for reviewing instructions, searching existing data sources, gathering and maintaining the data needed, and completing and reviewing the collection of information. Send comments regarding this burden estimate or any other aspect of this collection of information, including suggestions for reducing this burden, to Washington Headquarters Services, Directorate for Information Operations and Reports, 1215 Jefferson Davis Highway, Suite 1204, Arlington, VA 22202-4302, and to the Office of Management and Budget, Paperwork Reduction Project (0704-0188), Washington, DC 20503.				
1. AGENCY USE ONLY (Leave blank)		2. REPORT DATE December 1990		3. REPORT TYPE AND DATES COVERED Master's Thesis
4. TITLE AND SUBTITLE Multi-Input Multi-Output Flight Control System Design For the YF-16 Using Nonlinear QFT and Pilot Compensation			5. FUNDING NUMBERS	
6. AUTHOR(S) Russel B. Miller, 2 Lt, USAF				
7. PERFORMING ORGANIZATION NAME(S) AND ADDRESS(ES) Air Force Institute of Technology, WPAFB OH 45433-6583			8. PERFORMING ORGANIZATION REPORT NUMBER AFIT/GE/ENG/90D-42	
9. SPONSORING/MONITORING AGENCY NAME(S) AND ADDRESS(ES)			10. SPONSORING/MONITORING AGENCY REPORT NUMBER	
11. SUPPLEMENTARY NOTES				
12a. DISTRIBUTION/AVAILABILITY STATEMENT Approved for public release; distribution unlimited			12b. DISTRIBUTION CODE	
13. ABSTRACT (Maximum 200 words) ➤ Nonlinear Quantitative Feedback Theory (QFT) and pilot compensation techniques are used to design a 2x2 flight control system for the YF-16 aircraft over a large range of plant uncertainty. The design is based on numerical input-output time histories generated with a FORTRAN implemented nonlinear simulation of the YF-16. The first step of the design process is the generation of a set of equivalent linear time-invariant (LTI) plant models to represent the actual nonlinear plant. It has been proven that the solution to the equivalent plant problem is guaranteed to solve the original nonlinear problem. Standard QFT techniques are then used in the design synthesis based on the equivalent plant models. A detailed mathematical development of the method used to develop these equivalent LTI plant models is provided. After this inner loop design, pilot compensation is developed to reduce the pilot's workload. This outer loop design is also based on a set of equivalent LTI plant models. This is accomplished by modelling the pilot with parameters that result in good handling qualities ratings, and developing the necessary compensation to force the desired system responses. ←				
14. SUBJECT TERMS Quantitative Feedback Theory, Nonlinear Systems, Pilot Compensation, Control System Design, YF-16, Flight Control Systems			15. NUMBER OF PAGES 149	
			16. PRICE CODE	
17. SECURITY CLASSIFICATION OF REPORT Unclassified	18. SECURITY CLASSIFICATION OF THIS PAGE Unclassified	19. SECURITY CLASSIFICATION OF ABSTRACT Unclassified	20. LIMITATION OF ABSTRACT UL	